

Uncertainty in reflectance factors measured in the field: Implications for the use of ground targets in remote sensing

Vincent Omondi Odongo
March, 2010

Course Title: Geo-Information Science and Earth Observation
for Environmental Modelling and Management

Level: Master of Science (M.Sc.)

Course Duration: September 2008 - March 2010

Consortium partners: University of Southampton (UK)
Lund University (Sweden)
University of Warsaw (Poland)
International Institute for Geo-Information Science
and Earth Observation (ITC) (The Netherlands)

GEM thesis number: 2010-21

Uncertainty in reflectance factors measured in the field: Implications for the use of
ground targets in remote sensing

by

Vincent Omondi Odongo

Thesis submitted to the International Institute for Geo-information Science and Earth
Observation in partial fulfilment of the requirements for the degree of Master of
Science in Geo-information Science and Earth Observation for Environmental
Modelling and Management

Thesis Assessment Board

Chairman: **Prof. Dr. Ir. A. (Alfred) Stein**

External Examiner: **Prof. Dr. hab. Katarzyna Dąbrowska-Zielińska**

First Supervisor: **Prof. Dr. Edward J. Milton**

Second Supervisor: **Dr. Nicholas Hamm**



UNIVERSITY OF TWENTE.

FACULTY OF GEO-INFORMATION SCIENCE AND EARTH OBSERVATION

Disclaimer

This document describes work undertaken as part of a programme of study at the University of Twente, Faculty of Geo-information Science and Earth Observation. All views and opinions expressed therein remain the sole responsibility of the author, and do not necessarily represent those of the University.

Abstract

Ground calibration targets (GCTs) play a significant role in vicarious calibration (VC) and atmospheric correction (AC). However, assumptions are always made that these targets are dynamically stable and have flat spectra at the time of measurements in the field. Consequently, sources of uncertainty introduced in the data acquisition and methods used are in turn transferred on board the earth observation sensors. Errors from VC and AC campaigns can seriously impact upon the uncertainty associated with products derived from the sensors, compromising the evidence base for decision making. This study developed and tested a framework to characterize the reflectance factor of GCTs to establish best practice guidelines for VC and AC. This entailed evaluating sources of uncertainty arising from method of measurement, changes in archetype GCTs of 100cm x 50cm, effect of sky conditions to dynamic changes on a proposed real test site at a spatial domain. The uncertainty of the method was reported to less than 0.27% across all bands (430nm~949nm) of the spectro-radiometer used. The technique provided a means of disassociating uncertainty due to the instrument and its method of use from that due to changes in the target surface and the environment. Effect of sky conditions on HCRF measurements revealed that sky conditions affected hemispherical conical reflectance (HCRF) measurements variably depending on surface archetype and that solar zenith angle (SZA) and solar azimuth angle (SAA) were significant for smooth and rough surfaces even over the ± 2 hour measurements around solar noon. It was also realized that both smooth and rough archetype surfaces were highly anisotropic under clear sky during the period of normal measurements. This emphasized the need to measure field spectra synchronously with sensor overpass and minimizing the measurements to within a time when SZA and SAA changes are not significant. Local variation in HCRF was evaluated for a proposed VC site in Tuz Gölü, Turkey at a spatial domain using multi-temporal imagery. It was found that variation in HCRF was dependent on spatial uniformity and temporal stability of the surface. Retrieved HCRF from this surface showed uncertainty in the range of 0.01% to 4.05% for Landsat TM bands 1, 2, 3 and 4. These results were in agreement within the range of reported uncertainties of other calibration test sites in the world. This study provides knowledge on the characterization of HCRF in the field and has wider implication on the use GCTs for VC and AC.

Keywords: Uncertainty, Hemispherical Conical Reflectance Factor (HCRF), Ground Calibration Targets (GCTs)

Acknowledgement

I would like to thank the European Union Erasmus Mundus Programme for the award of scholarship into this M.Sc. I thank the GEM consortium directors Professor Andrew Skidmore, ITC, The Netherlands, Prof. Terry Dawson, University of Southampton, UK, Prof. Petter Pilesjö, Lund University, Sweden and Prof. Katarzyna Dąbrowska-Zielińska, University of Warsaw, Poland, the programme secretaries and GEM course coordinator, Andre Kooiman for facilitating the conducive living and learning environment at the respective universities.

It all began with a single essay titled '*The role of ground calibration targets in atmospheric correction of earth observation data*'. And for this I especially want to thank my supervisor Prof. Edward J. Milton for making my interest in this subject a reality. I deeply appreciate his guidance and support during my research while at the University of Southampton. I also thank my supervisor Dr. Nicholas Hamm of ITC for his valuable insight into the project and constructive criticism and ideas all through to the production of this thesis.

Throughout the course of this work, several people contributed significantly towards this work. They are hereby greatly acknowledged; the tramway experimental team Mr. Bill Damon, University of Southampton, did the ingenious design of the automated tramway and provided technical support when there was breakdown during experimental phase; Mr. Robin Wilson, University of Southampton, provided full rights to the use of his RTW IDL™ routine tools and sharing his programming skills. I express my gratitude to Dr. Francesco Vuolo, University of Southampton for helping with the ASD Field spec Lab measurements of the samples. I appreciate the support of Mr. D. G. Anderson, Geodata Institute, with drying of the samples in the lab. Dr. Joanna Nield, University of Southampton, is hereby thanked for sharing insightful knowledge on the geomorphology and dynamics of desert surfaces and playas. Mr. Prasan Pankaew, University of Southampton is appreciated for sharing his insight and knowledge during the research.

I am thankful to the Chilbolton Facility for Atmospheric and Radio Research (CFARR), UK and their staff for providing the ground for setting up the experiment and synchronous met data that facilitated characterization of the sky. Specifically I am grateful for the support of Judith Agnew and Mal Clark who updated us on the status of the tramway.

Finally, I wish to thank my GEM-2008 classmates for their support and a wonderful time well spent.

Table of contents

Abstract	i
Acknowledgements	ii
1. INTRODUCTION	1
1.1. Problem Statement	3
1.2. Rationale	3
1.2.1. Main aim	6
1.2.2. Research objectives	6
1.2.3. Research questions	6
1.2.4. Study context and conceptual framework	6
2. LITERATURE REVIEW	8
2.1. Surface Materials and BRDF	8
2.2. Reflectance factor	11
2.3. Uncertainty in measurement of reflectance factor.....	13
2.4. Spatial uniformity and temporal stability of GCTs	16
3. METHODOLOGY	18
3.1. Site description: CFARR.....	19
3.2. Description of Automated Tramway Spectro-radiometer	20
3.3. Measurement Period	21
3.4. Data Processing & Analysis.....	21
3.5. Selection of GCTs samples	21
3.6. Computing for k_λ value	22
3.7. Selection of data used for analysis	23
3.8. Experiment 1: Uncertainty due to method of measurement.....	27
3.9. Experiment 2: Effect of sky conditions.....	27
3.10. Experiment 3: Effect of local variation in HCRF with time.....	27
3.10.1. Description of test site: Tuz Gölü Lake.....	28
3.10.2. Image Processing.....	29
3.10.3. Analysis of Spatial uniformity.....	31
3.10.4. Analysis of temporal stability.....	32
4. RESULTS	33
4.1. Experiment 1: Uncertainty due to method of measurement.....	33
4.2. Experiment 2: Effect of sky conditions on HCRF measurements.....	35
4.2.1. Temporal variation in HCRF of archetype GCTs (Sand, Gravel and White tile) under stable clear and overcast sky conditions	35
4.2.2. The variation of HCRF measurements with Solar Zenith Angle and Solar Azimuth Angle	40
4.3. Experiment 3: Local variation in HCRF with time	44

4.3.1.	Spatial uniformity	44
4.3.2.	Temporal stability.....	45
4.3.3.	HCRF of proposed site	46
5.	DISCUSSION	49
5.1.	Method of HCRF measurement	49
5.1.1.	Importance of method of measurement to vicarious calibration and atmospheric correction.....	50
5.2.	Illumination conditions and HCRF measurement	52
5.2.1.	Effect of sky conditions on HCRF	52
5.2.2.	Effect of SZA and surface roughness on HCRF measurements	55
5.3.	Effect of local variation on HCRF	57
5.3.1.	Dynamic changes in the surface with time	57
5.3.2.	Spatial uniformity and temporal stability	58
5.3.3.	Local variation in HCRF for proposed site.....	60
6.	CONCLUSIONS AND RECOMMENDATIONS	62
6.1.	Recommendations	63
7.	REFERENCES	65
8.	APPENDICES	73

List of figures

Figure 1.1: Conceptual framework adopted to characterize reflectance factor of GCTs	7
Figure 2.1: Four examples of surface reflectance: (a) Lambertian reflectance (b) non-Lambertian (directional) reflectance (c) specular (mirror-like) reflectance (d) retro-reflection peak (hotspot)	9
Figure 2.2: Conceptual data processing chain of airborne and satellite measurements to convert a reflectance measurement (<i>Case 8</i>) into BHR, BRDF, and DHR, as implemented in the MISR processing scheme	10
Figure 3.1: Flow chart for characterizing method of measurement and HCRF of archetype GCTs	18
Figure 3.2: Location of CFARR in Chilbolton, UK	19
Figure 3.3: Experimental set up at CFARR	20
Figure 3.4: Plot of mean D:G ratio(a) and CV of D:G ratio (b) against radiance of brown tile at 430nm.	25
Figure 3.5: Box plot showing distribution of HCRF at 430nm for the brown tiles ..	26
Figure 3.6: Location map of Tuz Gölü salt lake, Turkey	28
Figure 3.7: Schematic approach used to identify a spatially uniform, temporally invariant site for sampling reflectance for vicarious calibration.....	30
Figure 4.1: Coefficient of variation across the entire spectrum of tramway instrument	34
Figure 4.2: The variation of HCRF measurements under clear and overcast sky for white tile, gravel and sand surfaces	38
Figure 4.3: Temporal change in HCRF measurements for sand at 430nm and 949nm under clear and overcast sky conditions	39
Figure 4.4: Temporal change in HCRF measurements for gravel at 430nm and 949nm under clear and overcast sky conditions	39
Figure 4.5: Temporal change in HCRF measurements for white tile at 430nm and 949nm under clear and overcast sky conditions	40
Figure 4.6: Plots of HCRF measurements (outbound) for sand with SZA and SAA at 430nm and 949nm	41
Figure 4.7: Plots of HCRF measurements (homebound) for gravel with SZA and SAA at 430nm and 949nm	42
Figure 4.8: Plots of HCRF measurements (homebound) for white tile with SZA and SAA at 430nm and 949nm	43
Figure 4.9: Spatially uniform areas in Tuz Gölü	44
Figure 4.10: Spatio-temporal stability map for TG showing a selected proposed calibration site	45

Figure 4.11: Satellite derived HCRF plots of Bands 1, 2, 3 and 4. Error bars show percent standard deviation in HCRF for respective years..... 47

List of Appendices

Appendix 1: HCRF variation with SZA and SAA for the ‘outbound’ measurements 430nm~781nm for sand surface	73
Appendix 2: HCRF variation with SZA and SAA for the ‘outbound’ measurements 820nm~949nm for sand surface	74
Appendix 3: HCRF variation with SZA and SAA for the ‘outbound’ measurements 430nm~781nm for gravel surface.....	75
Appendix 4: HCRF variation with SZA and SAA for the ‘outbound’ measurements 820nm~949nm for gravel surface.....	76
Appendix 5: HCRF variation with SZA and SAA for the ‘outbound’ measurements 430nm~781nm for the white tile surface	77
Appendix 6: HCRF variation with SZA and SAA for the ‘outbound’ measurements 820nm~949nm for the white tile surface	78
Appendix 7: ‘Outbound’ and ‘homebound’ HCRF measurement of the automated tramway spectro-radiometer. The difference in the two was due to positional drift of the instrument.	79
Appendix 8: (a) Spatial uniformity map of current study based on Landsat TM for the month of August for 1984, 1989 (2 images), 1998, 2000, 2003, 2006, 2009 (3 images) integrating bands 1, 2, 3, 4 (b) Spatial uniformity map of NPL based on MODIS (LPDAAC, 2007) satellite images of July and August (2004-2006) for using only red and near infra-red bands (adopted from Pegrum, 2008).....	80
Appendix 9: Gi* index map of Tuz Gölü in bands 1, 2, 3 and 4 for the month of August 1984.....	81
Appendix 10: Gi* index map of Tuz Gölü in bands 1, 2, 3 and 4 for the month of August 1998.....	82
Appendix 11: Gi* index map of Tuz Gölü in bands 1, 2, 3 and 4 for the month of August 2009.....	83
Appendix 12: CV index map of Tuz Gölü in bands 1, 2, 3 and 4 for the month of August 1984.....	84
Appendix 13: CV index map of Tuz Gölü in bands 1, 2, 3 and 4 for the month of August 1998.....	85
Appendix 14: CV index map of Tuz Gölü in bands 1, 2, 3 and 4 for the month of August 2009.....	86

List of tables

Table 2.1: Relation of incoming and reflected radiance terminology used to describe reflectance quantities	13
Table 3.1: k_{λ} values for Brown and White tiles used for computing HCRF	23
Table 3.2: Mean and Coefficient of variation (CV) of D:G ratio at time of measurements and CV of brown tile radiance at 430nm	24
Table 3.3: Landsat TM data used in the study obtained from LPDAAC.....	29
Table 4.1: Uncertainty in measurement of HCRF using single beam method.....	33
Table 4.2: Repeatability of HCRF measurements for brown tile using single beam method	34
Table 4.3: Variation of HCRF measurements for sand under clear sky condition ...	35
Table 4.4: Variation of HCRF measurements for sand under overcast sky condition	36
Table 4.5: Variation of HCRF measurements for gravel under clear sky condition.	36
Table 4.6: Variation of HCRF measurements for gravel under overcast sky condition	37
Table 4.7: Variation of HCRF measurement for white tile under clear sky condition	37
Table 4.8: Variation of HCRF measurements for white tile under overcast sky condition	38
Table 4.9: Long-term HCRF extracted from Landsat TM imagery	46
Table 4.10: Variation of HCRF across the four bands within the proposed site for the years under study	48
Table 5.1: Examples of reported temporal CV for VC test sites	61

List of abbreviations

AC	Atmospheric correction
AERONET	Aerosol Robotic Network
AOT	Aerosol Optical Thickness
ATSR	Along Track Scanning Radiometer
AVHRR	Advanced Very High Resolution Radiometer
BRDF	Bidirectional Distribution Reflectance Function
CEOS	Committee on Earth Observation Satellites
CFARR	Chilbolton Facility for Atmospheric and Radio Research
CV	Coefficient of variation
D:G	Diffuse to Global ratio
FWHM	Full Width Half Maximum
GCTs	Ground Calibration Targets
HCRF	Hemispherical Conical Reflectance Function
IFOV	Instantaneous Field of View
LPDAAC	Land Processes Distributed Active Archive Centre
MERIS	Medium Resolution Imaging Spectrometer
METEOSAT	Meteorological Satellite
MISR	Multi-angle Imaging Spectro-Radiometer
MODIS	Moderate Resolution Imaging Spectro-radiometer
NCAVEO	Network for Calibration and Validation of EO data
NPL	National Physics Laboratory
RTGC	Radiative Transfer Ground Calibration
SAA	Solar Azimuth Angle
SPECNET	Spectral Network
SPOT	Satellite Pour l'Observation de la Terre
SZA	Solar Zenith Angle
TG	Tuz Gölü
TOA	Top of Atmosphere
VC	Vicarious calibration
WGCV	Working Group on Calibration and Validation

1. INTRODUCTION

1.1. Background

Ground calibration targets (GCTs) play an important role in calibration and validation of airborne and space-borne remote sensing sensors. They provide surfaces for vicarious calibration of these sensors and are also used in atmospheric correction (e.g. empirical line and radiative transfer ground calibration (RTGC) methods). Vicarious calibration entails the use of a GCT as test site with ground reflectance reference data to calibrate earth observation satellite sensors. This provides the only independent way of calibrating the sensors post-launch (Bannari et al., 2005) as opposed to the one used for primary calibration of the sensor (NCAVEO, 2005b). Empirical line techniques apply measures of ground targets with different reflectance characteristics recorded using field spectro-radiometers to calculate the reflectance values in an image (Smith and Milton, 1999). On the other hand, *in situ* radiometric measurements of ground targets and the atmosphere are also used to constrain radiative transfer techniques to estimate top-of-atmosphere (TOA) radiance (Schiller, 2003).

Inherent in the use of GCTs is the need to have knowledge on the uncertainties arising from the use of these targets and methods used to acquire *in situ* radiometric measurements of the surface and the atmosphere. Uncertainty refers to a parameter associated with the result of a measurement that characterizes the dispersion of the values that could reasonably be attributed to the measured quantity (Fox, 2001). This can be achieved either by performing a statistical (random) analysis of the measurements describing how measurements are spread about the mean (Fox, 2009). This definition of uncertainty is in accordance with accepted framework of quality assurance for earth observation recommended by the Committee on Earth Observation Satellites Working Group on Calibration and Validation (CEOS WGCV). As a result, reported uncertainties of GCTs have used standard deviation and/or coefficient of variation as a measure of quantitative assessment of uncertainty.

Uncertainty studies of GCTs by Thome (2005) at Ivanpah and Railroad Valley test sites in Nevada, US have shown that the reflectance based approach has uncertainties of less than 3% in visible and near infrared. In addition, works by Slater et al. (1987b) at White sands, New Mexico, US have shows that the expected

uncertainties in the reflectance based approach are less than 5% in the visible and near infrared regions. The primary contributions of these uncertainties have been linked to the determination of aerosol refractive index, aerosol size distribution and largely to the measurements of ground target reflectance (Thome et al., 1998, Biggar et al., 1994). The large contribution in uncertainty due to the measurements of ground target reflectance is closely tied to the assumption that they are always stable and unchanging through time (Anderson and Milton, 2006).

GCTs are often assumed to be stable and unchanging through time. Malla and Helder (2008) describe GCTs as invariant sites, which are well characterized and exhibiting homogeneity in spectra, meaning they are spectrally flat with no spatial and temporal structure. They also assume that GCTs are near-Lambertian to decrease directional reflectance and shadow effects. In particular spatial uniformity and temporal stability of GCTs are of significant importance such that radiometric averaging of imagery acquired by sensors on these surfaces should contain small errors due to spatial variations (Teillet et al., 2007). However, these are rarely tested and there is considerable evidence that even the pseudo-invariant targets are actually highly dynamic (Anderson and Milton, 2006, Kneubuhler et al., 2006, Teillet et al., 1995).

Problems of spatial uniformity and temporal stability of these surfaces pose a serious challenge in establishing accurate quantitative calibration and realizing the long-term characterization of the sensor radiometry (Kneubuhler et al., 2006). Other sources of uncertainty rarely investigated when characterizing GCTs are effect of illumination conditions with time during spectra sampling in the field. Errors arising from inaccurate calibration propagate into earth observation (EO) data used in a wide range of studies. Consequently, decisions related to spatial and multi-temporal analyses, thematic classification and generation of vegetation indices based on these data could be misleading. The dynamic nature of GCTs could be a major source of uncertainty in vicarious calibration.

1.2. Problem Statement

GCTs are normally assumed to have constant reflectance overtime. Hence, agencies using these surfaces for calibration of satellites do not need to take measurements simultaneously with satellite overpass. They are also assumed to be spatially uniform. Hence, when they decide to take the ground measurements, the measurements are located where convenient for access within the assumed site. Sampling of spectra during the field measurements is also usually conducted ± 2 hours around solar noon and it is postulated that uncertainties are introduced during this time period. These assumptions need to be tested. Errors resulting from the use of these surfaces to calibrate sensors can seriously impact upon the uncertainty associated with products derived from the sensors, compromising the evidence base for decision making.

1.3. Rationale

Ground calibration targets (GCTs) are natural earth surfaces extensively used as test sites for post-launch radiometric calibration of satellite sensors (i.e. vicarious calibration (VC)) and atmospheric correction (AC). Lately, artificial surfaces have also been adopted as GCTs. For a surface to qualify as a test site suitable for calibration and atmospheric correction, it has to satisfy the following characteristics (Thome, 2001, Teillet et al., 2007, Kneubuhler et al., 2006):

1. The site should have high spatial uniformity over a large area to minimize mis-registration and adjacency effects due to light scattered from outside the target region.
2. The site should have a reflectance factor¹ greater than 0.3 across all wavelengths averaged over all angles in order to provide higher signal-to-noise ratio (SNR) and reduce uncertainties due to the atmospheric effects.
3. The surface of the site should have flat spectral reflectance to reduce uncertainties due to different spectral response profiles when multiple sensors are involved in cross-calibration.
4. The surface properties of the site (reflectance, BRDF², spectral) should be temporally invariant to reduce BRDF and spectral surface reflectance effects. Otherwise, adequate accuracy would be obtained only if these properties were measured for every calibration. This implies that the site should have no vegetation.

¹ Reflectance factor used in this context is defined according to the nomenclature by Nicodemus (1970). In the present study reflectance factor used was hemispherical conical reflectance factor (HCRF). For detailed explanation refer to section (2.2).

² Bidirectional Reflectance Distribution Function

5. The surface should be horizontal with near-Lambertian reflectance to minimize uncertainties due to different solar illumination and observation geometries. It should also be flat to minimize slope-aspect effects.
6. The site should be located at high altitude (to minimize aerosol loading and the uncertainties due to unknown vertical distribution of aerosols), far from the ocean (to minimize the influence of atmospheric water vapour), and far from urban and industrial areas (to minimize on aerosol loading).
7. The site should be situated in arid regions with low probability of cloudy weather and precipitation that could change the soil moisture and subsequently the surface reflectance. The low probability of cloud coverage also increases the probability of the satellite instruments imaging the test site at the time of overpass.

In reality it is hardly possible that any one test site will have all the stated characteristics but of specific importance are points 1, 3 and 4 since characterization of these surfaces are informed on the uncertainties in spectral measurements in the field. Any significant variation in points 1, 3 and 4 will result to disqualification of the surface as a candidate test site for VC.

Despite the fact that no test site will have all the characteristics stated, there are some standard GCTs which exhibit characteristics close to those stated in points 1, 3 and 4. These are normally used for VC and AC and include dry lake beds or playas, deserts, ice or snow fields, semi-arid range lands, and water bodies. Snow fields, vegetation targets and water bodies are rarely used for calibration. Snow fields, for example, are rarely used because they have very high reflective properties in the visible and near infra-red (Six et al., 2004). This makes them more sensitive to changes in aerosol size distribution (Teillet et al., 2007). Moreover, snow fields that could be used for calibration are located at the poles with very high solar zenith angles (SZA).

Vegetation targets are subject to phenological changes and directional reflectance effects whereas water bodies are mostly avoided because they exhibit sun glint and have low surface reflectance which is more sensitive to atmospheric path radiance. Desert fields and playas are the most preferred GCTs because they are spatially uniform and temporally stable. However, sand dunes and dust blows may introduce errors in deserts when they are used as calibration surfaces (Rao and Chen, 1999). On the other hand, playas and dry lake beds may also experience uncertainties in reflectance introduced by inherent moisture levels in the surfaces caused by seasonal changes (Teillet et al., 1995).

Other levels of uncertainties in reflectance of GCTs may be introduced by the physical nature of the individual surfaces (e.g. surface roughness). This physical nature in turn may cause the surfaces to exhibit some degree of anisotropy in the reflectance measured depending on the illumination conditions at the time of measurement. However, the degree of anisotropy may vary from one type of surface to another depending on the structure of the surface. In view of this, GCTs can be broadly classified into three archetypes, namely smooth (e.g. sand surfaces like deserts, fresh snow and dry lake beds), rough (e.g. gravel) and shiny (e.g. smooth salt pans, wet and refrozen snow).

1.3.1. Main aim

The present study aimed at investigating the uncertainty in reflectance measurements in the field of selected representative GCT surfaces and implications for their use for VC and AC based on three archetypes. The selected surfaces were sand, gravel, and ceramic white tiles representative of smooth, rough and shiny archetypes respectively. Specifically, the study aimed at developing and testing a method for characterizing the reflectance factor of ground calibration targets to establish best practice guidelines for atmospheric correction and vicarious calibration.

1.3.2. Research objectives

The research objectives for this study were;

1. To determine uncertainty in HCRF resulting from method of measurement.
2. To investigate the effect of sky conditions on HCRF measurements of archetype GCTs.
3. To investigate the local variation of HCRF at a spatio-temporal scale on a spatially uniform and temporally stable site.

1.3.3. Research questions

Based on the above research objectives the following questions were developed to realize the objectives;

1. What is the repeatability of the single beam method of measurement using an automated tramway spectro-radiometer?
2. How do HCRF measurements vary between clear sky and overcast sky conditions for the different archetype surfaces?
3. Does the reflectance of archetype GCT surfaces remain invariant under stable skies over the time period of measurements (± 2 hours around solar noon)?
4. How does satellite retrieved HCRF of a spatially uniform and temporally stable site vary from year to year?

1.3.4. Study context and conceptual framework

The prime focus of this study was to investigate sources of uncertainty in reflectance factor measurements and develop a robust framework for characterizing them with implications on the use of GCTs. The ultimate goal was to come up with best practice guidelines for characterizing the GCT surfaces for VC and AC. Initial steps involved distinguishing uncertainty from instrument and method of its use. Further, uncertainties introduced by inherent surface response and apparent effects due to sky

illumination were also investigated. In summary, uncertainty was documented based on the;

1. Method of measurement
2. Sky conditions and its interaction with different archetype surfaces and
3. Dynamic changes in the surface with time

Figure (1.1) shows the conceptual approach adopted in this study.

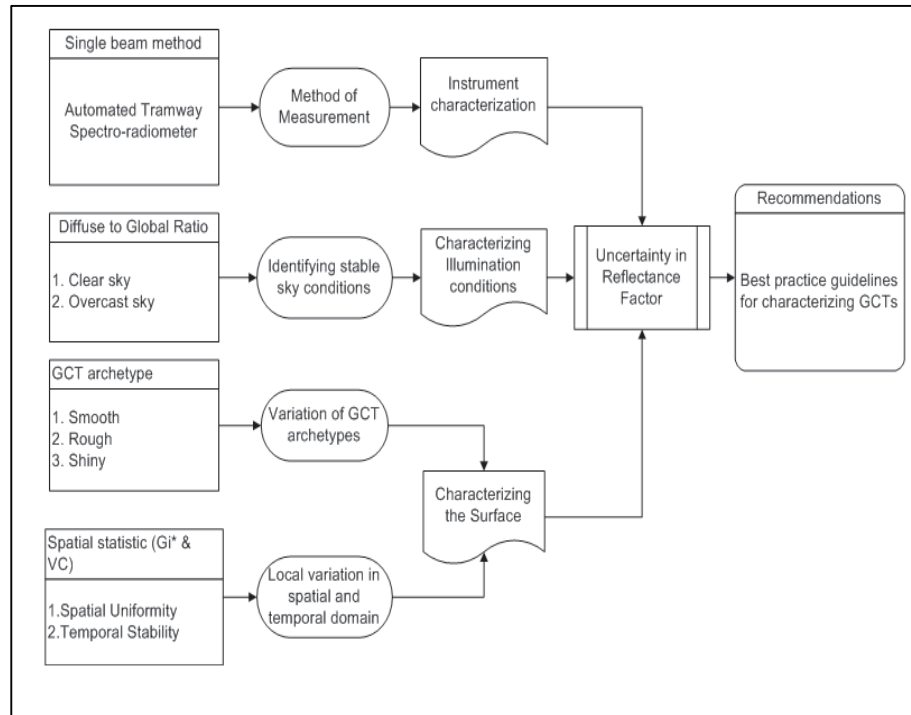


Figure 1.1: Conceptual framework adopted to characterize reflectance factor of GCTs

2. LITERATURE REVIEW

2.1. Surface Materials and BRDF

Natural earth surface materials are known to be generally non-Lambertian in nature i.e. they do not reflect irradiance equally in all directions and tend to be anisotropic (exhibit reflectance directionality) (Abdou et al., 2001, Diner et al., 1998). The degree of anisotropy depends on the nature of the surface being measured, spectral and the directional nature of irradiance. In addition, the measured reflectance will vary depending on the view, the illumination and the solar zenith angles of the surface under clear sky conditions (Anderson and Milton, 2005, Kriebel, 1976).

The factors that determine the degree of anisotropy of a surface include: (i) density and arrangement of surface objects (surface structure), which in turn introduce shadows under clear skies with varying illumination zenith and azimuth angles; and (ii) transmittance and absorption properties of the surface. Figure (2.1) illustrates the different directional nature of surface reflectance of different surfaces.

The anisotropic nature (non-Lambertian) of Earth surface materials introduced by the presence of surface structure has provided opportunities to study and derive information on structures useful for purposes such as biophysical modelling (e.g. canopy reflectance modelling) based on the evaluation of reflectance measurements on these surfaces (Disney, 2001, Diner et al., 1998). On the other hand, the non-Lambertian property of the Earth surface materials has been a limitation in using such surfaces for calibration of Earth Observation (EO) sensors. Calibration of EO sensors requires that a surface used for calibration of the sensors be near-Lambertian and that the reflectance measured should be spectrally flat with change in time.

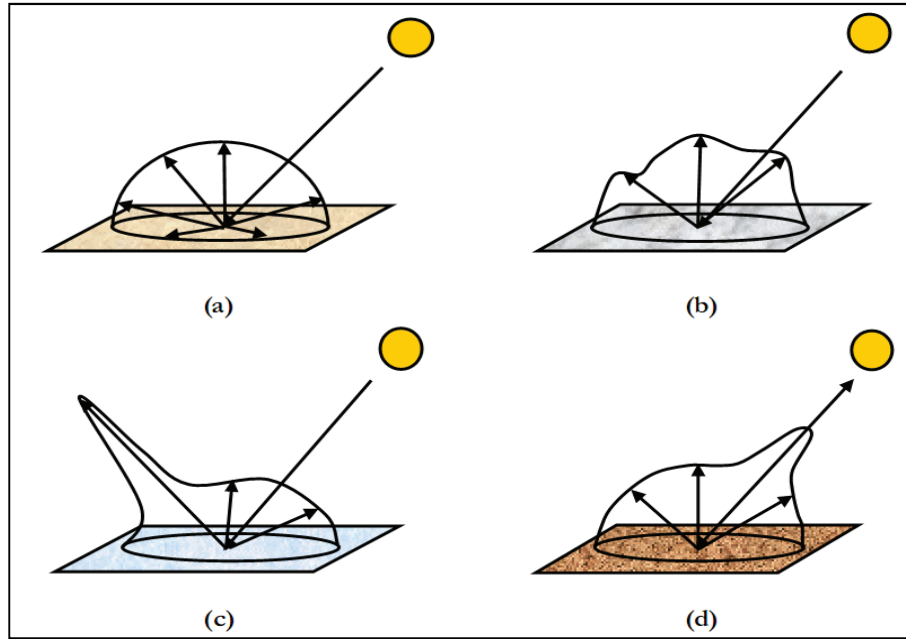


Figure 2.1: Four examples of surface reflectance: (a) Lambertian reflectance (b) non-Lambertian (directional) reflectance (c) specular (mirror-like) reflectance (d) retro-reflection peak (hotspot)
Source: Disney (2001)

Surface reflectance anisotropy is best described by the bidirectional reflectance distribution function (BRDF). BRDF as defined by Nicodemus et al.(1977) “is a derivative, a distribution function, relating the irradiance incident from one given direction to its contribution to the reflected radiance in another direction”. It is a conceptual quantity defined only for infinitesimal view and illumination angles and thus cannot be measured in the field. Instead, HCRF measurements from spectro-radiometers have been used in models such as Rahman-Pinty-Verstraete (RPV) model (Engelsen et al., 1998) to produce BRDF and other related directional reflectance approximations (Schaepman-Strub et al., 2006). A conceptual data processing chain of airborne and satellite measurement to convert reflectance measurement into BHR, BRDF and DHR is shown in Figure (2.2).

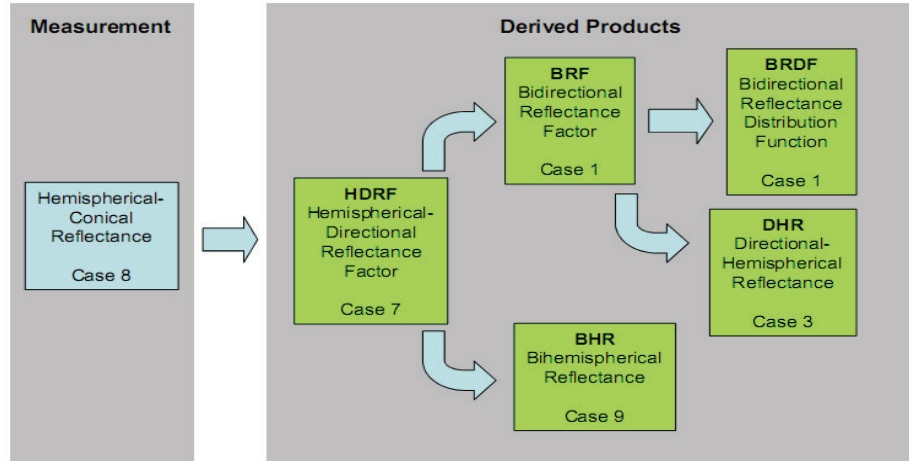


Figure 2.2: Conceptual data processing chain of airborne and satellite measurements to convert a reflectance measurement (Case 8) into BHR, BRDF, and DHR, as implemented in the MISR processing scheme.

Source: Schaepman-Strub (2006)

Specifically, the magnitude of anisotropic behaviour of earth surfaces is controlled by spectral and structural properties of the surface (Li and Strahler, 1985, Kimes, 1983, Gao et al., 2003). A BRDF model is well placed to establish a relationship between these spectral and structural features and the bidirectional reflectance such that the BRDF can be determined by specifying parameters of the surface, the viewing and illumination geometries (Gao et al., 2003). Commonly used BRDF models are the kernel-driven models which have a simple linear form as shown in Equation (1) (Roujean et al., 1992).

$$BRDF = f_{iso} + f_{vol} \times k_{vol}(\theta_i, \theta_v, \varphi) + f_{geo} \times k_{geo}(\theta_i, \theta_v, \varphi) \quad (1)$$

Where k_{vol} , a function of illumination θ_i and view zenith θ_v and relative azimuth φ , describes the volume scattering from a surface and k_{geo} , describes the surface scattering from a surface (Roujean et al., 1992). These functions are called volumetric and geometric kernels respectively. f_{iso} is a constant corresponding to isotropic reflectance. The geometric kernel describes the shadowing effect introduced as a result of surface structures whereas the volumetric kernel is responsible for the scattering component of the surface (Gao et al., 2003). The isotropic component is a constant describing the degree of diffuse scattering of the surface and it accounts for multi-scattering effects because the kernel-driven BRDF models assume single scatter (Disney, 2001).

2.2. Reflectance factor

Field measurements of reflectance represented as reflectance factors were first documented by Nicodemus et al.(1977). Reflectance measurements have been used to support vicarious calibration (e.g. (Thome, 2001, Doherty and Warren, 1998, Six et al., 2004, Slater et al., 1987a, Slater, 1987), atmospheric correction (Moran et al., 2001) and scaling-up measurements to match with satellite derived reflectance (Milton et al., 2009, Gamon et al., 2006b). Reflectance measurements have also been used to develop and validate surface reflectance models ((Maignan et al., 2004) and have been incorporated in process-based modelling and validating biophysical models (Goel and Reynolds (1989), Strahler (1997), Kuusk et al. (2009).

Despite the wide application of reflectance measurements, different reflectance terminologies have been used to inform on spectral measurements in the field by the remote sensing community, a fact that has raised suggestions to the proper use of the terminology (Martonchik et al., 2000, Schaepman-Strub et al., 2006, Milton et al., 2009). Schaepman-Strub et al. (2006) argues that to keep in line with advances in spectroscopy, radiometric calibration, atmospheric correction and product development there is need to standardise reflectance terminology and products thereof. This is because the confusion may lead to insurmountable uncertainties. Also, not all of the documented reflectance nomenclature by Nicodemus et al.(1977) can be measured in the natural environment and some remain conceptual (Martonchik et al., 2000, Milton et al., 2009) (See Table 1). Nicodemus et al.(1977) further states that under natural conditions in the field, single direction incident light measurement is not achievable. This is because diffuse irradiance is highly influenced by the atmosphere and the surface hence directional incidence and reflection will unlikely be estimated as required.

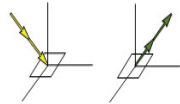
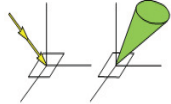
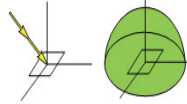
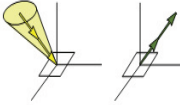
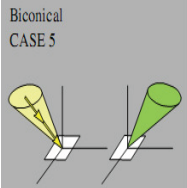
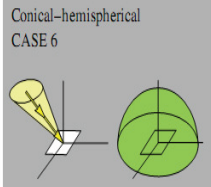
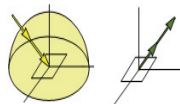
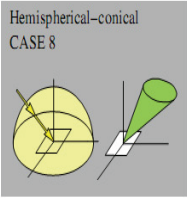
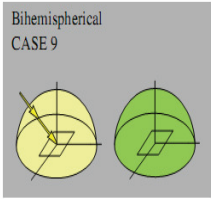
Nonetheless, Martonchik et al. (2000), Schaepman-Strub et al.(2006) and Milton et al. (2009) argue that a number of reflectance measurements in literature have been documented as bidirectional reflectance (BRF) and hemispherical directional reflectance factor (HDRF) whereas in essence they should be termed as hemispherical conical reflectance (HCRF). Single directional spectral measurements require infinitesimally solid angles of incidence and reflectance. However, all field spectro-radiometers have a finite field of view (IFOV) and will always measure HCRF (Milton et al., 2009). Milton et al. (2009) explains that approximations of HDRF may be valid if the instrument has a narrow instantaneous field of view (IFOV) (3° or less) and that there are no directional effects within the FOV. This means that the presumed HDRF measurement will not vary within the FOV for it to qualify as HDRF as opposed to HCRF. Furthermore, the target surface should be homogenous. In view of this, it is reasonable that documentation be made

describing; (i) the IFOV of instrumentation used in spectral measurements; (ii) homogeneity of target surfaces measured; and (iii) characterization of sky conditions at the time of measurements. This would help to support the correct inference and usage of reflectance products.

Documentation will not only ensure proper standardization of reflectance terminologies as stated by Nicodemus (1977), Martonchik et al (2000) and (Schaepman-Strub et al., 2006), but also raise awareness of the uncertainties associated with the different reflectance products. For example, climate models have been found sensitive to specification of surface albedo, with accuracies ranging from ± 0.02 to ± 0.05 , regarded as suitable (Oleson et al., 2003, Henderson-Sellers and Wilson, 1983, Sellers, 1995). In this regard, standardization of the reflectance quantities and products will ensure that the right choice of reflectance products are integrated in modelling approaches and that users are aware of uncertainties existing where there is need to fuse or compare different reflectance products from different sensors (e.g. MODIS BRDF/albedo product MOD43B, MISR reflectance products). Gutman (1994) suggested that before reflectance measurements of varying sun zenith angles can be compared, they should be normalised to a standard view and illumination equivalent reflectance. On the contrary, Privette et al. (1997) argues that reflectance measurements conducted under different view and illumination angles cannot be compared directly.

Hence in the present study, the spectro-radiometer instrument used measured HCRF as proposed by Martonchik et al.(2000), Schaepman-Strub et al.(2006) and Milton et al. (2009) because it had an IFOV greater than 3° and the fact that irradiance was contributed both directly and diffusely even though the measured targets were homogenous. Specifically, the study sought to investigate the uncertainty in reflectance measurements in the field associated with the selected GCT archetypes.

Table 2.1: Relation of incoming and reflected radiance terminology used to describe reflectance quantities

<i>Incoming/Reflected</i>	Directional	Conical	Hemispherical
<i>Directional</i>	Bidirectional CASE 1 	Directional-conical CASE 2 	Directional-hemispherical CASE 3 
<i>Conical</i>	Conical-directional CASE 4 	Biconical CASE 5 	Conical-hemispherical CASE 6 
<i>Hemispherical</i>	Hemispherical-directional CASE 7 	Hemispherical-conical CASE 8 	Bihemispherical CASE 9 

Relation of incoming and reflected radiance terminology used to describe reflectance quantities. The labelling with 'Case' corresponds to the nomenclature of Nicodemus et al. (1977). Grey fields correspond to measurable quantities (Cases 5, 6, 8 and 9), the others (Cases 1–3, 4 and 7) denote conceptual quantities

Source: Schaepman-Strub et al. (2006)

2.3. Uncertainty in measurement of reflectance factor

Previous sections have explained details of how reflectance measurements should be better informed when measured in the natural environment and also how it interacts with different kinds of natural surfaces. Most importantly, it is necessary also to evaluate variation (herein referred to as uncertainty) in measurements of reflectance as this gives confidence in the measured value. Fox (2001) defines uncertainty as “A parameter associated with the result of a measurement that characterizes the dispersion of the values that could reasonably be attributed to the measurand (i.e. quantity)”. Uncertainty should characterize the range of values within which the true value is speculated to lie. This can be realized by accounting for all possible effects, both random and systematic (Fox, 2009).

As reported by Ungar et al.(2008), uncertainty in measurement as well as accuracy reports are necessary accompaniments to assure on the product quality in terms of consistency or when comparing or combining different products. This argument is also emphasised in the Working Group on Calibration and Validation (WGCV) vision which states that;

“Empower the climate, environmental and weather analyses and prediction community with sustained high quality observations and associated error characteristics, *“in order to improve monitoring of the state of the Earth, increase understanding of Earth processes and enhance prediction of the behaviour of the Earth system” (GEOSS 10 year Implementation Plan)*”

This implies that delivered EO products should have documentation of uncertainty stating their confidence levels and traceability to a reference standard. In the case of reflectance measurements in the field, the white Spectralon™ panel is normally used to anchor traceability of measurements to national and/or international standards.

Quantitative studies of uncertainty associated with reflectance measurements of surfaces in the field has been the foundation of evaluating the quality of EO products acquired simultaneously from space-borne and air-borne sensors. Earlier studies by Kriebel (1976) makes two distinctions on how uncertainty of reflected radiation is introduced in the natural environment. These are: (i) reflected target radiance recorded at sensor is combined with the reflected radiation by the air mass and (ii) angular anisotropy inherent in natural surfaces. Anderson and Milton (2005) also emphasized this distinction in uncertainty and classified them as those arising from inherent surface response and those from apparent illumination and viewing conditions. The inherent properties here refers to uncertainty due to the structure of the surface and their spectral-dependent properties (Gao et al., 2003) whereas apparent illumination and viewing conditions are due to the changes in the distribution of hemispherical irradiance (Kriebel, 1976).

Anderson (2005) summarised causes of uncertainty due to inherent surface response as surface moisture variations, growth of plant and other biological material on the surface, weathering and erosion of the surface. These factors have been known to influence the optical properties, uniformity and stability of ground calibration test site (Bannari et al., 2005, Kneubuhler et al., 2006). Of significance to the study of playas and dry lake beds used as ground targets for sensor calibration is soil moisture which normally varies seasonally from year to year (Kneubuhler et al., 2006).

Other studies have focused in quantifying the uncertainty in reflectance measurements associated with instrument design (such as quantization of the measured data by the instrument and changes in the gain and offset of the sensor during subsequent measurements) (e.g. Manoochchri et al., 1999, Gu et al., 1992). Gu et al. (1992) evaluated uncertainties in ground reflectance measurements introduced by a SPOT simulating radiometer detectors and quantified them separately from those due to inherent surface response and apparent illumination conditions for La Crau calibration test site in France. Instrumental uncertainty is equally important as the uncertainties caused by inherent surface response and apparent illumination and view conditions in order to monitor the instrumental drift.

The methods of measurement of reflectance in the field (i.e. single or dual beam) have also been evaluated in other studies (e.g. Milton, 1981, Duggin and Cunia, 1983, Anderson et al., 2006). These entail combined uncertainties inherent in the instrument design and the method itself with other factors held constant. However, the instrumental uncertainties can be budgeted for separately as shown by Gu et al. (1992). The use of dual beam method uses two sensor heads simultaneously taking measurements, one viewing the target and the other viewing a reference reflector (Duggin and Cunia, 1983). This is opposed to single beam method which measures the target, reference reflector, then back to the target sequentially (Duggin, 1980). The dual beam approach has been reported to produce the most accurate means of sampling spectra in the field (Milton, 1981, Duggin and Cunia, 1983, Duggin, 1980) because it restricts error effects of passing sub-visual clouds and haze to changes in reflectance properties of the target under the varying illumination conditions. However, single beam measurements will lump such effects consequently increasing the error term. Anderson and Milton (2006) reported uncertainties in reflectance measurements of $\pm 0.26\%$ at 700nm wavelength associated with dual beam method for a concrete surface.

Despite this advantage, the dual beam method is expensive because of the cost of an extra sensor or mechanism for providing simultaneous view. Also, there is the rigour of deriving and maintaining the inter-calibration between the two sensor heads (Anderson et al., 2006, Milton and Rollin, 2006). For these reasons the single beam method is widely adopted for sampling reflectance in the field (Milton et al., 2009). The limitation with single beam method is that illumination conditions are assumed not to change between successive measurements between the target and the reference reflector despite the lag in acquiring the measurements. Milton et al. (2009) explains that this assumption is usually addressed by taking sandwiched measurements of reference surface before and after those from the target surface and interpolating for the reference panel. This assumes that the irradiance is changing

predictably or smoothly as would be the case with solar zenith angle (SZA) which might not be the case if there is a cloud overpass (Milton et al., 2009). Hence to overcome this, single beam measurements are much better scheduled when the sky conditions are stable.

2.4. Spatial uniformity and temporal stability of GCTs

Spatial uniformity and temporal stability are important properties that should be evaluated when using GCTs for sensor calibration (de Vries et al., 2007, Thome et al., 2004, Thome, 2001, Thome et al., 1998, Teillet et al., 2007, Scott et al., 1996, Rondeaux et al., 1998). Rondeaux et al. (1998) describes GCTs as flat surfaces that are uniform over an extended area of several pixels in all directions. Spatial uniformity in this context means that the surface should be invariant in measured spectra across space. This is important especially for cross-calibration between sensors because it minimizes the effects of mis-registration (Teillet et al., 2007). This means that surface-retrieved-reflectance from imagery of one sensor may not correspond well with that retrieved from another sensor for the same surface (Scott et al., 1996). On the other hand, temporal stability means that the surface should be invariant in measured spectra over time. Large temporal variation of the surface would require that spectral measurements be carried synchronously with sensor overpass every time calibration is performed to achieve sufficient calibration (Scott et al., 1996, Teillet et al., 2007).

Spatial uniformity and temporal stability of a test site can be affected by different factors such as surface moisture, variation in topography, which in turn create shade effects, and vegetation causing spectral changes (Kneubuhler et al., 2006). These factors introduce uncertainties into the characterization of GCTs. Guoyong et al. (1999) states that uncertainties introduced by spatial and temporal variability have a great impact on aerosol optical thickness retrieval for atmospheric correction activities. The authors explain that as the size of spatial uniformity increases, the adjacency effects become less pronounced and the uncertainty level of mean aerosol optical thickness reduces. In addition, the authors reported uncertainties in aerosol optical thickness retrieval to about 5-20 times the uncertainty of surface reflectance.

The most common statistic used to quantify both spatial and temporal variability of GCTs is the coefficient of variation (CV) (de Vries et al., 2007). In imagery, CV is computed within a predefined local window that is convolved over the entire image. A surface with a CV of 3% or less is considered to be uniform and temporally stable within the computed window (Kneubuhler et al., 2006, Cosnefroy et al., 1996, Bannari et al., 2004, Bannari et al., 2005). However, CV computation can be

misleading in determining a spatially uniform and temporally stable surface in that two or more connected surfaces may be considered to have same CV meaning that they are spatially uniform, but may not exhibit homogeneity. Hence, other robust spatial indices which could adequately characterize spatial uniformity and temporal stability should be explored to enhance characterization of GCTs.

3. METHODOLOGY

This section presents the methodology used in the study. Two sites were used each with a unique role. The first site was Chilbolton Facility for Atmospheric and Radio Research (CFARR). The second site was a proposed VC site, Tuz Gölü, Turkey. CFARR provided ground to set up experiment for studying uncertainty in measuring HCRF of archetype GCTs under changing sky conditions. It also provided instrumentation to monitor and characterize the sky conditions suitable for spectral sampling. Tuz Gölü site in Turkey was used to study the temporal variation in HCRF of a real VC site at a spatial domain. This was important to enable characterization of expected uncertainty in HCRF due to local dynamic changes of a real VC surface. The output of the two study sites were then used to draw guidelines on best practice for characterizing HCRF in the field and their implication for use of GCTs in remote sensing.

Figure (3.1) illustrates a summary of the documented method and process for characterizing method of measurement and HCRF of archetype GCTs at CFARR.

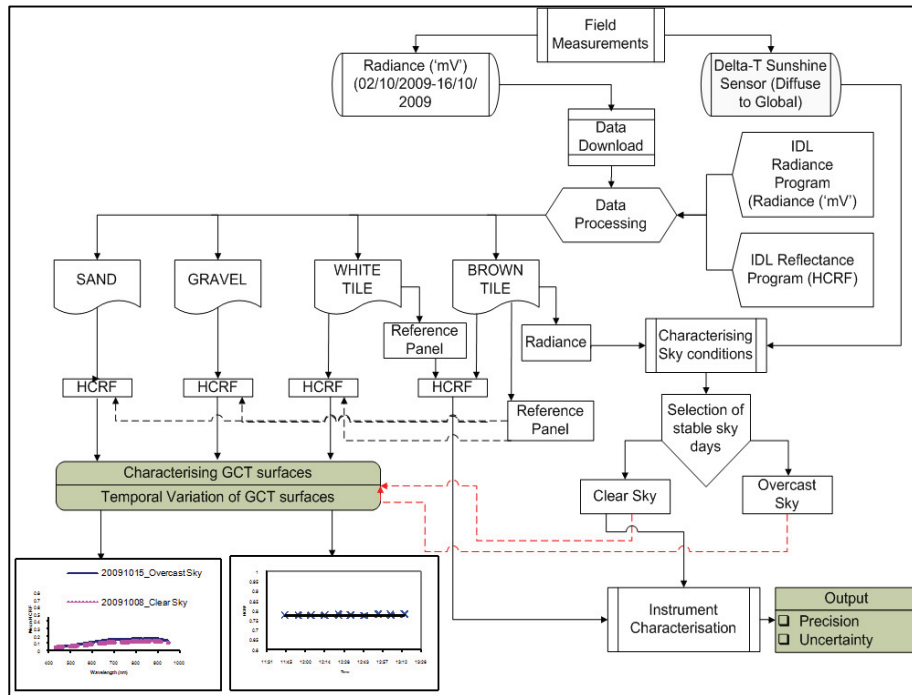


Figure 3.1: Flow chart for characterizing method of measurement and HCRF of archetype GCTs

3.1. Site description: CFARR

The calibration test site used in setting up this study was located at Chilbolton Facility for Atmospheric and Radio Research (CFARR) situated in Chilbolton, Andover, UK. The site is relatively flat at an altitude of approximately 81m above mean sea level at latitude 51° 09' N and longitude 01° 26' W. Figure (3.2) shows the location map of CFARR site.

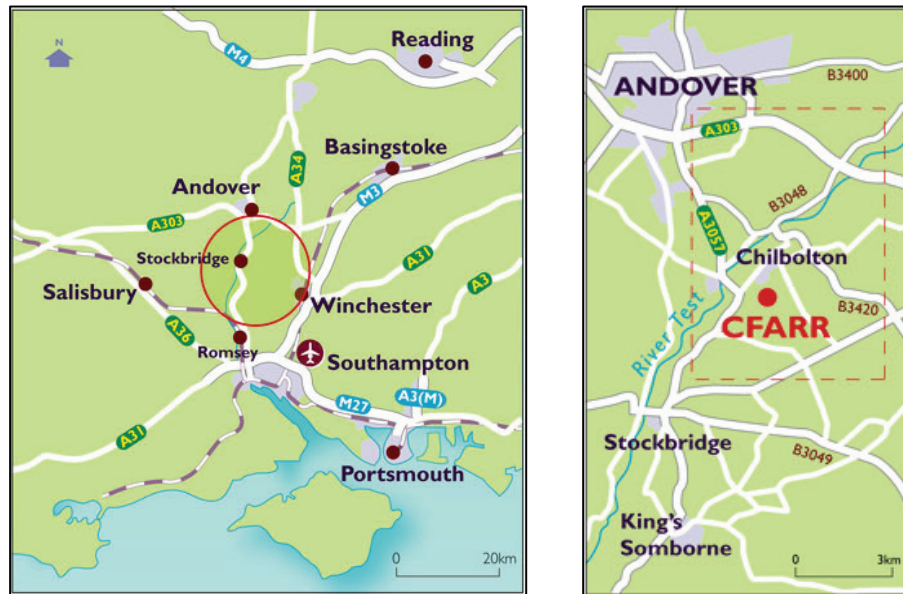


Figure 3.2: Location of CFARR in Chilbolton, UK
Source: NCAVEO (2009)

The experimental setup was oriented approximately in the north-south direction away from tall and obstructing structures that may introduce adjacency reflectance and shadow effects on the laid out archetype GCT surfaces. The orientation was also laid such that there were no self-shadowing effects from the instrument at the time of sampling spectra.

3.2. Description of Automated Tramway Spectro-radiometer

The concept of automated tramway spectro-radiometer approach adopted in this study was similar to that developed by Gamon et al. (2006a) for Spectral Network (SPECNET). The automated spectro-radiometer measured hemispherical conical reflectance factor (HCRF) using a single beam approach in eight bands (430nm~949nm). These bands were chosen specifically because they are known to be sensitive to changes in sky conditions. It was mounted on a motorised sled travelling along an elevated tramway raised at 1.5m above the ground and 8m long. The system has a logger for storing spectral measurements sampled at predefined time intervals controlled by a timing device, which triggers the sled to make runs. The sled stops at magnetic sensors fixed on the tramway right above the central locations of the ground targets to be sampled and records the measurements. It takes approximately one minute for the sled to complete one run of measurements. In each run, the spectro-radiometer measures four targets with the first three being measured twice and the last target measured only once. Simultaneous measurements of diffuse and total irradiation were also measured on-site and logged after every five minutes using a Delta-T sunshine sensor. A rain sensor was also installed at the site and linked to switch off the tramway from taking measurements during rainy events. Figure (3.3) shows the experimental set up at CFARR.

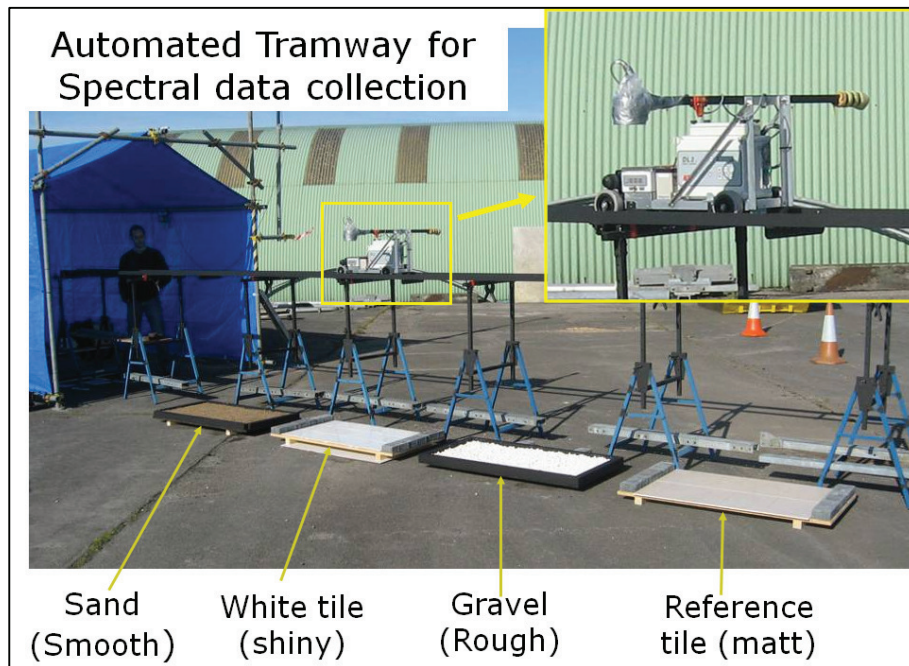


Figure 3.3: Experimental set up at CFARR

3.3. Measurement Period

The tramway measurements were conducted from 02/10/2009 to 16/10/2009 between 11:00GMT \pm 1hr. This was based on the knowledge that most Earth observation satellites normally acquire data around this time. Within this period the instrument took measurements after every 10 minutes. This was determined by the available memory of the data logger. The measurements recorded by the instrument were in millivolt (mV) for each wave band and corresponded to each target. The measurements were used to compute the HCRF using Equation (2). The solar zenith angle at the time of measurements varied from 57.4° to 61.8°.

3.4. Data Processing & Analysis

Interactive Data Language (IDL™) programs were written to process data downloaded from both the tramway spectro-radiometer and the Delta-T™ sunshine sensor. Afterwards analysis of the data was then performed in SPSS™ and graphs and charts plotted using Gnuplot© (Williams and Kelley, 1986-1993,1998, 2004) and Microsoft™ Excel.

3.5. Selection of GCTs samples

Four GCTs samples were selected (sand, gravel, white tile, brown tiles) as representative of Bidirectional Reflectance Distribution Function (BRDF) archetypes exhibiting diffuse reflection, backscatter and forward scatter. The brown tile was of ceramic origin and assumed to have invariant reflectance in all spectra, unchanging in structure and near-Lambertian under all sky conditions. It was used as the 'standard' reference surface for computing reflectance of the other target surfaces. It was also used as a control surface to characterize reflectance associated with the instrument and method of measurement, and separate it from uncertainties affecting the GCT samples. The white tile surface was also of ceramic nature with a uniform glossy structure and was used as a 'standard' reference surface for computing the reflectance of the brown tile which was then used to characterize the instrument.

Sand and gravel surfaces were selected for two major reasons; (i) most surfaces used for calibration of sensors consist either of these surfaces; and (ii) the two samples represented different geomorphologic properties which are of interest to the understanding of reflectance properties of GCTs. Sand had particle size distribution

in the range of 125 μm ~1000 μm whereas the gravel particle size ranged from 0.5cm~3.5cm.

All GCT samples were then each spread uniformly on wooden platforms of 100cm by 50cm and raised 5cm from the ground. The white and brown tiles were glued separately on the individual wooden panels as shown in Figure (3.3).

Separate identical samples of the surfaces used in the field measurements were also taken and measured for reflectance in the laboratory against a standard SpectralonTM white panel (Sample Identification Number, SRT-99-100) using an ASDTM spectro-radiometer. This was done to ensure traceability to a referenced standard. Sand and gravel were first dried in the oven at 105°C for 24 hours to remove moisture content and cooled before measuring their reflectance.

The ASDTM spectro-radiometer instrument consisted of a tungsten halogen quartz lamp illuminating on the targets and recording reflectance in the bandwidth range of 350nm~1050nm. The instrument was set to white reference mode with bare fibre and reflectance computed against a standard white SpectralonTM as the reference panel. Measurements in the laboratory were important to establish the dry reflectance of the surfaces and also to obtain the correction factor, k_λ , for correcting the brown and white tile reflectance used in the field as reference surfaces.

3.6. Computing for k_λ value

The white and brown tile reflectance measurements in the laboratory were then built into separate spectral library files in ENVITM. These were then resampled using user defined filter functions. The filter functions were created in separate text files by assigning the centre wavelength (CWL) of each spectro-radiometer band a value of 1 and half wavelengths on either side of the waveform assigned 0.5. Manufacturer's information for each band of the spectro-radiometer was used to refine the filter functions. The rest of the bands were assigned zeros.

The brown and white tile kernels were also converted into spectral library files and convolved respectively with the brown and white tile spectral files obtained from laboratory measurements to obtain the correction factor, k_λ values for each band. The HCRF was then computed using Equation (2)

$$HCRF = \frac{V_{gct} - V_o}{V_r - V_o} \times k_\lambda \quad (2)$$

Where HCRF is the hemispherical conical reflectance factor, V_{gct} is the spectro-radiometer output for the target, V_r is the spectro-radiometer output of the white tiles used in the field, V_o is the dark voltage of spectro-radiometer computed for each band and k_λ is the correction factor for white tiles used in the field relative to the Spectralon™ panel for each band.

Brown tile HCRF was computed using the k_λ values obtained from the white tile and the brown tile k_λ values were later used to compute the HCRF for the sand, gravel and white target surfaces. Table (3.1) summarizes the output results of the k_λ values used to compute HCRF for each wavelength.

Table 3.1: k_λ values for Brown and White tiles used for computing HCRF

Wavelength (nm)	Brown tile k_λ	White tile k_λ
430	0.42	0.74
500	0.49	0.75
670	0.65	0.76
781	0.70	0.76
820	0.71	0.75
831	0.71	0.75
882	0.72	0.75
949	0.72	0.74

Dark current, V_o measurements were performed in the field for the spectro-radiometer by shutting the aperture using a dark cloth. This was important so as to account for any stray light within the instrument.

3.7. Selection of data used for analysis

Data used in the analysis was selected for the days with low coefficient of variation in measured radiance in all the bands with diffuse to global ratio (D:G) being constant at the time of measurements. These data was further tested for normality using Shapiro-Wilk normality test. The brown tile radiance at 430nm measurements were used to establish this criterion because it was assumed to be invariant in nature. Hence, it was able to discriminate between uncertainty due to instrument and its method of use as well as uncertainty introduced by the environment. The contrary of

which would have been difficult to discriminate between the two levels of uncertainties. The variation of radiance at 430nm waveband complimented the selection of stable days because it is more sensitive to atmospheric changes than the other bands.

The combination of low mean D:G ratio with low coefficient of variation (CV) in both D:G ratio and brown tile radiance at the time of measurements indicated a stable clear sky condition. As a result, this particular day was used to evaluate the method of measurement used in the study (i.e. single beam).

A high mean D:G ratio with low coefficient of variation (CV) in both D:G ratio and brown tile radiance at the time of measurements was indicative of a stable overcast sky condition. Measurements conducted under this condition together with the stable clear sky condition were used to investigate the effect of sky conditions on HCRF measurements. The identified days were the 08/10/2009 and 15/10/2009, which was clear sky and overcast sky, respectively. These are highlighted in Table (3.2) and Figures (3.4) and (3.5). Measurements under these two conditions provided suitable data for evaluating the method of measurement as well as investigating the effect of sky conditions on reflectance measurements of the GCT surfaces. Table (3.2) shows computed descriptive statistic for the days measurement were conducted. Figure (3.4a) and (3.4b) shows plot of mean D:G ratio against individual radiance measurements of brown tile at 430nm.

Table 3.2: Mean and Coefficient of variation (CV) of D:G ratio at time of measurements and CV of brown tile radiance at 430nm

Date	mean D:G ratio	CoV of D:G ratio (%)	CoV of Brown Tile radiance (%)
20091002	0.37	54.92	24.10
20091003	0.99	8.49	24.20
20091008	0.21	5.03	2.47
20091009	1.00	0.11	15.19
20091010	0.54	34.09	44.01
20091011	1.00	0.22	39.23
20091012	0.25	33.54	18.12
20091013	0.23	10.57	4.14
20091014	0.67	40.45	14.50
20091015	1.00	0.09	19.99
20091016	0.55	47.97	28.07

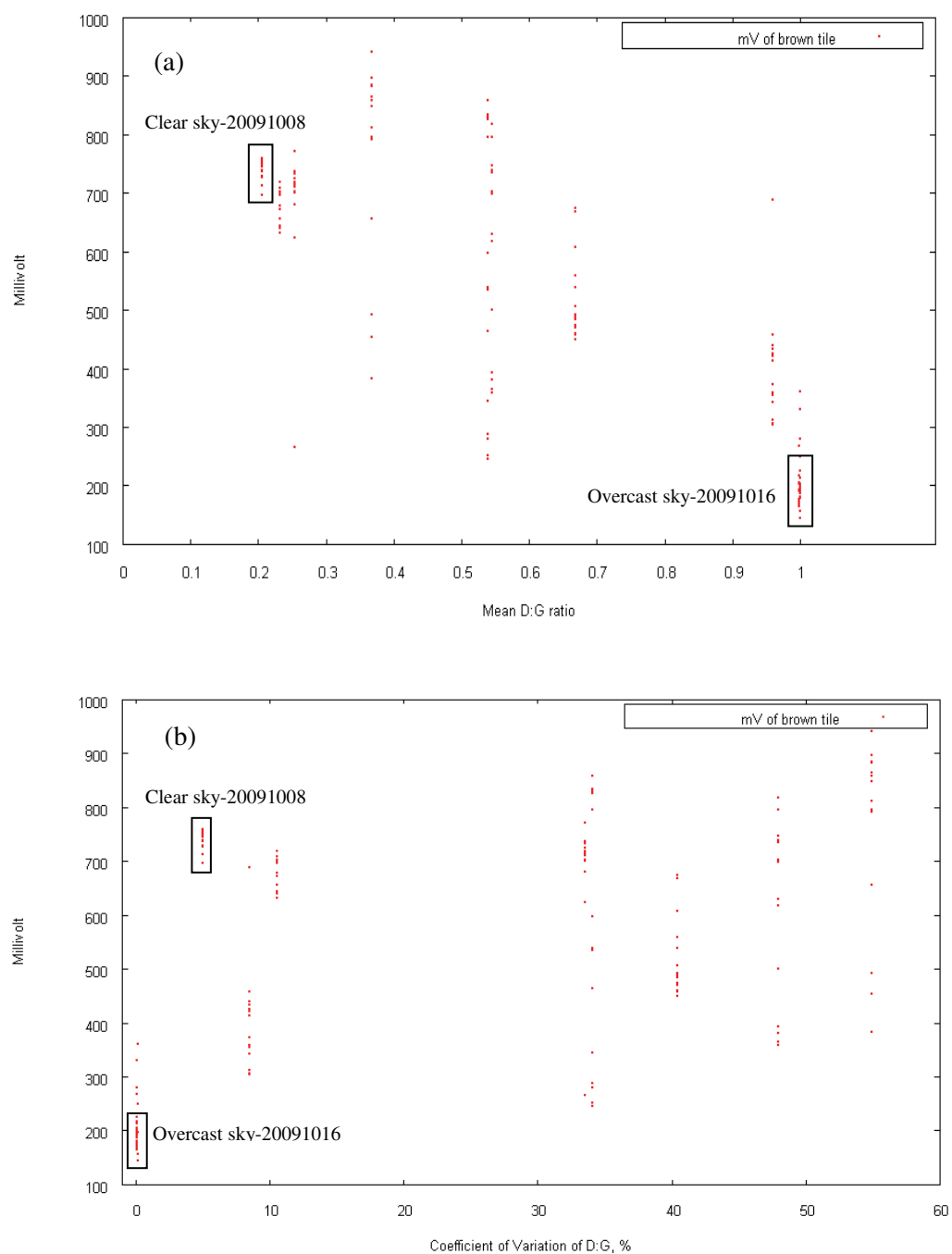


Figure 3.4: Plot of mean D:G ratio(a) and CV of D:G ratio (b) against radiance of brown tile at 430nm.

The two days also showed minimal distribution of outliers in HCRF at 430nm as depicted from the box plot in Figure (3.5) and passed the Shapiro-Wilk normality test at $p=0.01$. These provided two extreme weather conditions in which to test the precision of the automated tramway instrument.

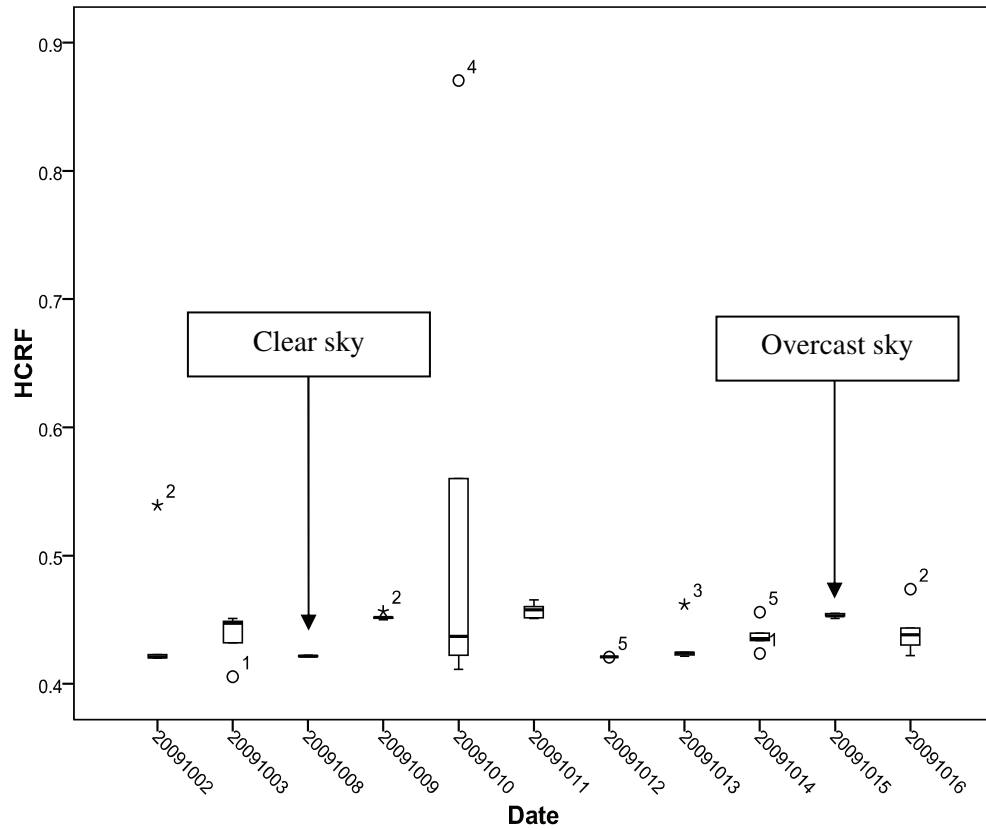


Figure 3.5: Box plot showing distribution of HCRF at 430nm for the brown tiles

3.8. Experiment 1: Uncertainty due to method of measurement

To evaluate the uncertainty due to the method of measurement (i.e. single beam), the stable clear sky day (08/10/2009) was used. Evaluation of uncertainty in the method of measurement was indicative of the repeatability of sampling spectral measurements using the automated tramway, with respect to the invariant brown tile surface used. Repeatability describes the closeness of agreement between the results of successive measurements of same physical parameter, carried out under same conditions of measurements (Fox, 2001). Under stable atmospheric conditions and the surface being invariant, variation in measurements was envisaged to occur due to sensor variation, positional variation and its method of use. Uncertainty was evaluated using coefficient of variation (CV) as shown in Equation (3) and standard deviation in absolute reflectance of the brown tiles.

$$CV = \frac{s}{\bar{x}} \quad (3)$$

Where CV is the coefficient of variation in percent, s is the standard deviation of the spectral measurements and \bar{x} is the mean of the spectral measurements. Uncertainty in the measurements was computed for each bandwidth of the instrument.

3.9. Experiment 2: Effect of sky conditions

The two stable sky conditions (clear and overcast) were used to investigate how HCRF varied for the selected surfaces within the two hour window of measurements. Measurements under these two conditions were used to investigate how sky conditions affect the HCRF measurements of different surfaces. Coefficient of variation (CV) shown in Equation (3) was used for this evaluation. A correlation coefficient between solar zenith angle (SZA) and HCRF measurements was computed to determine the wavelength dependency of the relationship between the two. The significance of SZA at the time of measurements was investigated using Pearson's correlation coefficient for each surface in all the bands.

3.10. Experiment 3: Effect of local variation in HCRF with time

This part of the study was focused on examining real changes in HCRF over time in a spatial domain for a potential vicarious calibration test site in Tuz Gölü, Turkey. The automated tramway spectro-radiometer tested in the previous section does provide a suitable approach for sampling HCRF measurements for a VC test site considering the low level of uncertainty associated with it. Moreover, it can be scheduled to take simultaneous measurements with satellite overpass. This will

ensure reduced time and manpower required in sampling spectra for vicarious campaigns.

Multiple measurements acquired from the tramway could be used to sufficiently characterize the surface over normal sampling time (± 2 hours within solar noon). However, the tramway was not used to test the surface in this study because the site is an ephemeral salt lake that is only dry and accessible in the month of August. The study site is a prime candidate being investigated as a potential test site. Therefore, the results of this work provide a scoping study for a scheduled field campaign in August 2010.

3.10.1. Description of test site: Tuz Gölü Lake

Tuz Gölü Lake shown in Figure (3.6) is the second biggest lake in Turkey. It is located in central Anatolian region, 105 km North East of Konya and 150 km South East of Ankara (capital of Turkey) at an altitude of about 905 m above mean sea level. For most of the year, this very shallow and saline lake has an area of 1,500 km² at its peak. The lake is approximately 80 km long and 50 km wide. Atmospheric conditions of the area are sunny and cloud-free in the dry season (July-August) suitable for VC and AC campaigns (Gurol et al., 2008).

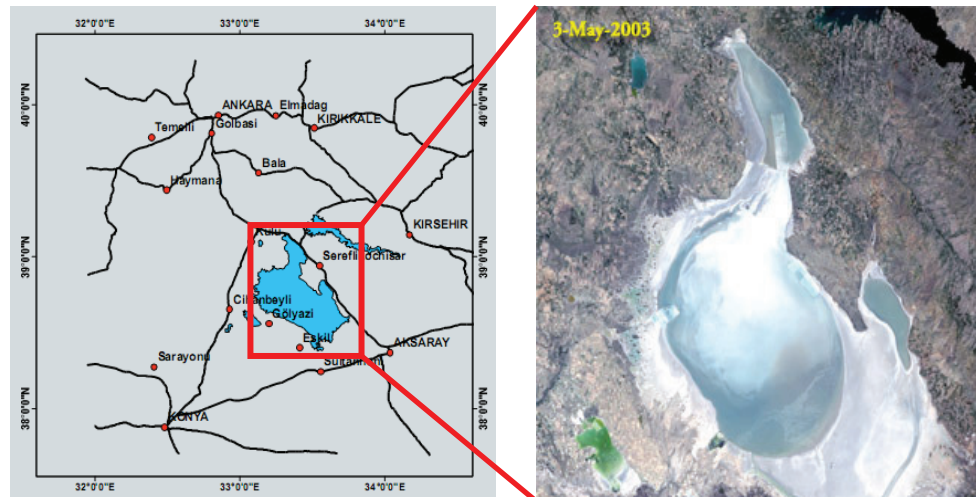


Figure 3.6: Location map of Tuz Gölü salt lake, Turkey
Source: (USGS, 2009)

3.10.2. Image Processing

Time series of pre-existing Landsat TM satellite images of the site were obtained from Land Processes Distributed Active Archive Centre (LPDAAC). The images were selected for retrieval of HCRF to investigate the variation of the site. The selection of images was based on the following factors: (i) metadata on percentage cloud cover provided by the data for the months of July and August. Images with no cloud cover covering the lake were selected (See Table 3.3). Landsat TM provided ample pre-existing data covering the study area to investigate the temporal pattern in stability of the surface; (ii) resolution was a compromise between high and medium resolution sensors to investigate the local variation in HCRF over time; (iii) Landsat images covering the lake for months of July and August were available over a long period of time compared with other newly launched satellites.

The images were radiometrically and atmospherically corrected based on standard estimates of atmospheric profiles using Atmospheric and Topographic Correction software (ATCOR-2) to obtain surface reflectance of the Tuz Gölü.

Table 3.3: Landsat TM data used in the study obtained from LPDAAC

Date (YY-MM-DD)	Time (GMT)	Cloud (%)	SZA (degrees)
1984-08-03	7:50:51	0	33.39
1989-08-16	8:01:06	0	35.28
1998-08-26	8:00:04	0	36.77
2000-08-15	7:59:06	0	34.51
2003-08-08	7:58:19	0	33.03
2006-07-31	8:14:43	0	29.04
2006-08-16	8:14:54	0	32.31
2009-07-30	8:16:43	0	29.55
2009-08-15	8:16:57	0	32.73
2009-08-31	8:17:12	4	36.38

Having retrieved HCRF from the imagery, the spatial uniformity was then computed to determine most homogenous areas. The homogenous areas were then assessed to establish their temporal variation in HCRF. Figure (3.7) summarises the methodological approach used in this part of the study.

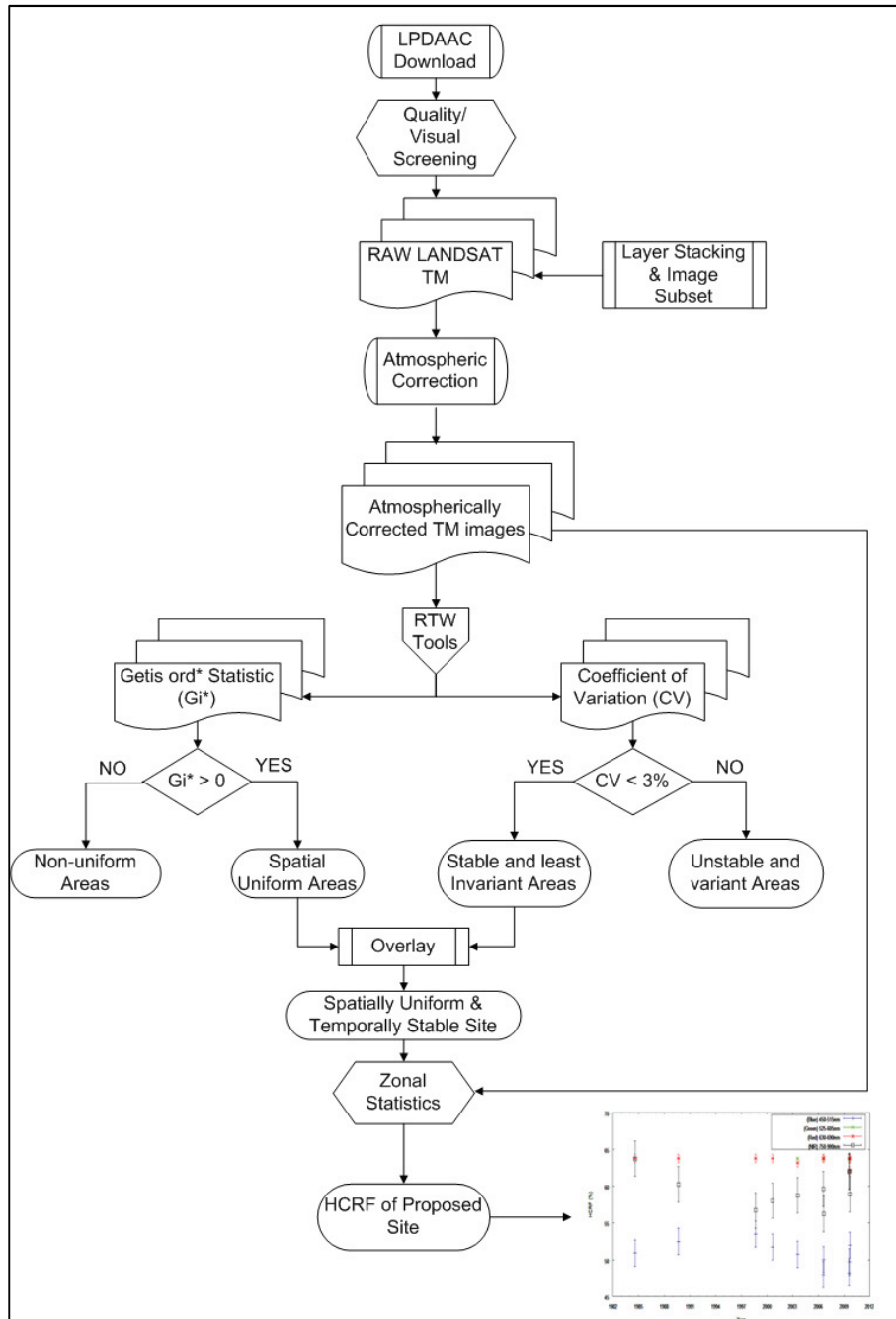


Figure 3.7: Schematic approach used to identify a spatially uniform, temporally invariant site for sampling reflectance for vicarious calibration

3.10.3. Analysis of Spatial uniformity

Spatial uniformity also referred to as spatial homogeneity refers to the characteristic of a surface to constitute same kind of elements or be similar in nature (i.e. exhibiting similar spatial structure) in space. A homogenous surface has uniform composition of elements or structure. With regard to GCT surfaces, spatial homogeneity is important because it determines the spatial uniformity of the surfaces. A spatially homogenous surface is envisaged to exhibit spatial uniformity.

Getis ord* statistic (G_i^*) developed by Ord and Getis (1995) was used to identify areas, which have consistent spatial uniformity throughout the years. In remotely sensed imagery, G_i^* computes positive values for pixels surrounded by clusters of high reflectance while negative values are surrounded by clusters of low reflectance. This ability to highlight brighter pixels makes the G_i^* superior and particularly useful in characterizing GCTs. Brighter pixels are of significance to vicarious calibration and atmospheric correction. According to Bannari et al. (2005) and Wulder and Boots (1998) positive G_i^* values are indicative of pixel reflectance values above the mean reflectance (Bright pixels) and negative G_i^* values indicate reflectance values below the mean reflectance (Dark pixels).

In summary, G_i^* has the ability to combine spatial association and relative spectral response from imagery compared to other local indicators of spatial autocorrelation (LISA) such as Geary's c and Moran's I . The G_i^* was computed using Equation (4) within a local distance predefined using a kernel using an IDL™ routine code in RTW tools written by Wilson (2009).

$$G_i^*(d) = \frac{\sum w_{ij}(d)x_j - W_i^* \bar{x}}{s[W_i^*(n - W_i^*)/(n-1)]^{1/2}} \quad (4)$$

Where $w_{ij}(d)$ is a matrix of spectral weights with binary and symmetric weight equal to unity ($w_{ij} = 1$) for all pixels found within distance d of pixel i considered and a weight equal to zero ($w_{ij} = 0$) for all pixels found outside d . $\sum w_{ij}(d)x_j$ is the sum of varying values X (i.e. reflectance of the imagery) within distance d of pixel i (i included), W_i^* is the number of pixels within the distance d (i included).

The G_i^* distance d was determined at a scale of 1 (3x3 window). This provides a compromise for small to medium resolution sensors. Higher values of d resulted in smoothened surface and compromised on the local variation. G_i^* was computed for each imagery in Table (3.3) for band 1, 2, 3 and 4 corresponding to the spectral range of the automated tramway spectro-radiometer.

Gi* values greater than zero representing positive reflectance values (Brighter pixels) were then extracted by overlaying all the Gi* output maps for bands 1, 2, 3 and 4 for all the years represented in Table (3.3). This was important since it ensured the extraction of areas within Tuz Gölü that have remained spatially uniform throughout the years. Spatial Analyst™ in ESRI ArcGIS™ provided the platform for this analysis. The output was a single map showing the areas of spatial uniformity.

3.10.4. Analysis of temporal stability

Having identified spatially uniform areas in the previous section, it was important to investigate how reflectance in those areas varied over yearly time-scale. Variation in HCRF was computed using coefficient of variation (CV) given in Equation (5).

$$CV = \frac{s}{\bar{x}} \quad (5)$$

Where s is the standard deviation of the spectral measurements and \bar{x} is the mean of the spectral measurements. Variation in HCRF was also computed in a local window of 3x3 using RTW Tools written by Wilson (2009) for bands 1, 2, 3 and 4. This was done for all the images shown in Table (3.3).

CV has been used to estimate spatial uniformity of VC sites like Rail Road Playa, US (Scott et al., 1996, Kneubuhler et al., 2006, Bannari et al., 2005), Saharan and Arabian Desert sites (Cosnefroy et al., 1996), La Crau, France (Gu et al., 1990) and Western Queensland, Australia (de Vries et al., 2007). A surface with a CV of 3% or less in all the bands was considered temporally stable as recommended by Teillet et al. (2007). This was done for each of the selected bands and for all the years considered within a 3x3 window. Though it has been widely used as a measure of uniformity, CV computation can mislead in determining a spatially homogenous surface in that two or more connected surfaces may have different means and standard deviations yet have same CV. This may lead to inferring those surfaces as spatially uniform whereas there maybe some significant differences.

Areas matching less than 3% local variation within the 3x3 window were extracted for all the bands using ESRI spatial analyst™ and overlaid on the spatially uniform areas. Areas with CV less than 3% that lied over the spatially uniform areas were then envisaged to be temporally stable with minimal subtle variations in HCRF across the 3x3 window. Finally, a large extent of the area was identified that was invariant in time and space. This area was oriented coincidence with the satellite path to avoid any mis-alignment of pixels within the area. This area was proposed as the most suitable for vicarious calibration and atmospheric correction activities.

4. RESULTS

4.1. Experiment 1: Uncertainty due to method of measurement

Uncertainty of method used in the measurement was evaluated using coefficient of variation (CV). It was found to vary in the order of 0.09% at 430nm after which it increased to a maximum of 0.27% at 949nm. The increase in uncertainty with wavelength was typically due to a decrease in signal to noise ratio of the instrument (Anderson et al., 2003). However, there was some decline in uncertainty in the region beyond 670nm through to 830nm before it increased to the peak. This trend was similar to the obtained by Anderson et al (2003) conducted using a dual beam approach. The authors estimated the uncertainty in dual beam approach to be 0.5% within 400nm-1000nm wavelength range of the instrument. In the present study the overall uncertainty associated with the single beam method of measurement was estimated at 0.27% within the usable range of the automated tramway spectroradiometer. Table (4.1) and Figure (4.1) present the uncertainty in HCRF measurements using single beam method across the entire spectrum of the tramway instrument.

Table 4.1: Uncertainty in measurement of HCRF using single beam method

Band(nm)	Mean	Standard Deviation	Coefficient of variation (%)
430	0.4216	0.00038	0.091
500	0.4787	0.00048	0.099
670	0.6293	0.00107	0.170
781	0.6778	0.00063	0.093
820	0.6846	0.00066	0.096
831	0.6817	0.00063	0.092
882	0.6917	0.00103	0.149
949	0.6955	0.00188	0.271

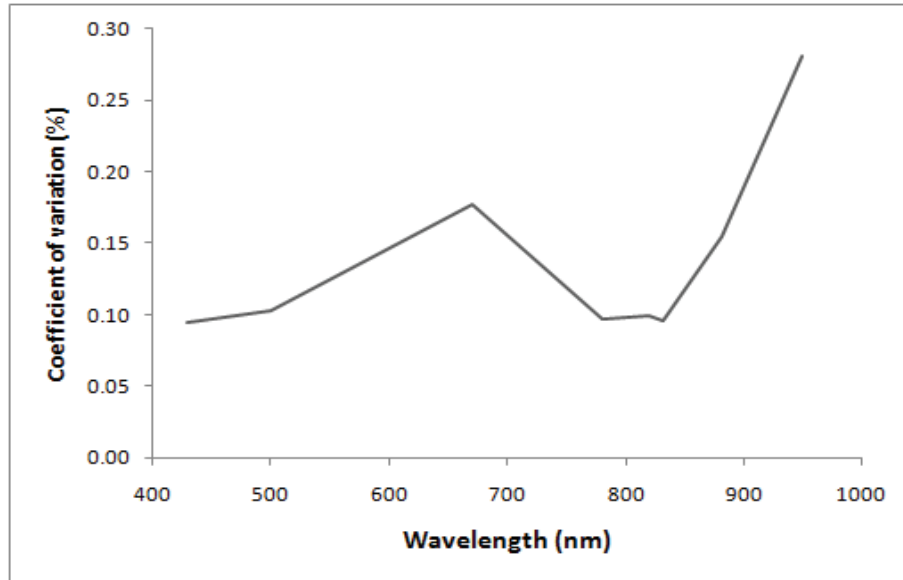


Figure 4.1: Coefficient of variation across the entire spectrum of tramway instrument

Repeatability of measurement using the tramway spectro-radiometer was evaluated using standard deviation in absolute reflectance across all bands of the instrument. Table (4.2) shows the repeatability of measurements across the usable range of the instrument. Repeatability was estimated to decline with increase in wavelength indicating increasing uncertainty across the bandwidth of the instrument. In summary repeatability of method was better than $\pm 0.19\%$ within 1 standard deviation in all bands of the instrument. This was based on the highest standard deviation computed.

Table 4.2: Repeatability of HCRF measurements for brown tile using single beam method

Band (nm)	Precision (%)
430	42.16 ± 0.04
500	47.87 ± 0.05
670	62.93 ± 0.11
781	67.78 ± 0.06
820	68.46 ± 0.07
831	68.17 ± 0.06
882	69.17 ± 0.10
949	69.55 ± 0.19

4.2. Experiment 2: Effect of sky conditions on HCRF measurements

4.2.1. Temporal variation in HCRF of archetype GCTs (Sand, Gravel and White tile) under stable clear and overcast sky conditions

The HCRF measurements for selected GCT surfaces were computed using Equation (2) with the brown tile as a 'standard' reference panel. The brown tile was used as a reference panel because it had no glossiness to cause any specular reflection. Under clear sky condition, sand surface showed more variation in HCRF measurements across all bands compared to overcast sky condition. This variation of HCRF measurement is shown in Tables (4.3) and (4.4). Moreover, HCRF measurements for sand surface under clear sky conditions in the visible bands (430nm and 500nm) showed lower variability compared to measurements under overcast conditions for same visible bands. On the other hand, the infra-red bands (781nm, 820nm, 831nm, 882nm, 949nm) for sand and gravel measurements showed higher variability under clear sky compared to similar bands under overcast conditions (Tables 4.5 & 4.6). This was attributed to the increase in uncertainty with wavelength as signal to noise ratio declined with increase in spectral range of the instrument (Figure 4.1). White tile surface behaved differently from the other surfaces under both clear and overcast conditions. It showed higher variation under overcast than under clear sky condition (Tables 4.7 & 4.8).

The HCRF measurement of sand under overcast was higher than under clear sky as shown in Figure (4.2). This significant difference ($p=0.05$) could be attributed to apparent moisture retained in the sand surface after rain events over the past five days before clear sky measurement was done.

Table 4.3: Variation of HCRF measurements for sand under clear sky condition

Band (nm)	Mean	Standard Deviation	Coefficient of variation (%)
430	0.0456	0.0009	1.9339
500	0.0591	0.0013	2.1825
670	0.1039	0.0021	1.9823
781	0.1237	0.0026	2.0706
820	0.1295	0.0027	2.0694
831	0.1301	0.0027	2.0451
882	0.1322	0.0028	2.1101
949	0.1377	0.0030	2.2072

Table 4.4: Variation of HCRF measurements for sand under overcast sky condition

Band (nm)	Mean	Standard Deviation	Coefficient of variation (%)
430	0.0511	0.0017	3.2736
500	0.0704	0.0016	2.2397
670	0.1308	0.0022	1.6814
781	0.1592	0.0024	1.4786
820	0.1666	0.0025	1.5288
831	0.1672	0.0025	1.5050
882	0.1723	0.0021	1.2311
949	0.1792	0.0031	1.7044

The gravel measurements had higher variability under clear sky conditions than measurements carried under overcast sky conditions (Tables 4.5 & 4.6). Gravel HCRF was lower under clear sky than under overcast sky condition (Figure 4.2). The variation of solar angle during clear sky was likely to be the cause of this because gravel particles had angular structure, which introduced shadowing effect. As a result, the HCRF measurements under clear sky were considerably lower than under overcast sky.

Table 4.5: Variation of HCRF measurements for gravel under clear sky condition

Band (nm)	Mean	Standard Deviation	Coefficient of variation (%)
430	0.4964	0.0122	2.4651
500	0.5409	0.0106	1.9599
670	0.6364	0.0139	2.1850
781	0.6564	0.0098	1.4998
820	0.6580	0.0096	1.4625
831	0.6583	0.0104	1.5841
882	0.6634	0.0127	1.9130
949	0.6647	0.0145	2.1748

Table 4.6: Variation of HCRF measurements for gravel under overcast sky condition

Band (nm)	Mean	Standard Deviation	Coefficient of variation (%)
430	0.5349	0.0075	1.4018
500	0.5773	0.0076	1.3120
670	0.6612	0.0082	1.2421
781	0.6849	0.0079	1.1528
820	0.6841	0.0076	1.1061
831	0.6858	0.0073	1.0688
882	0.6918	0.0077	1.1147
949	0.6870	0.0086	1.2484

White tile surface exhibited low variability in HCRF measurements under clear sky than under overcast sky conditions. White tile reflectance under clear sky was significantly higher (at $p=0.05$) than under overcast sky. The white tile surface was smooth and did not have any surface structure hence its temporal reflectance varied less compared to sand and gravel (Figure 4.5).

Table 4.7: Variation of HCRF measurement for white tile under clear sky condition

Band (nm)	Mean	Standard Deviation	Coefficient of variation (%)
430	0.7431	0.0033	0.4451
500	0.7685	0.0022	0.2863
670	0.7721	0.0022	0.2822
781	0.7869	0.0013	0.1677
820	0.7849	0.0020	0.2544
831	0.7844	0.0022	0.2777
882	0.7811	0.0022	0.2753
949	0.7775	0.0024	0.3141

Table 4.8: Variation of HCRF measurements for white tile under overcast sky condition

Band (nm)	Mean	Standard Deviation	Coefficient of variation (%)
430	0.6902	0.0056	0.8084
500	0.7187	0.0060	0.8327
670	0.7344	0.0062	0.8468
781	0.7485	0.0056	0.7456
820	0.7460	0.0059	0.7904
831	0.7449	0.0056	0.7547
882	0.7420	0.0056	0.7540
949	0.7388	0.0081	1.1015

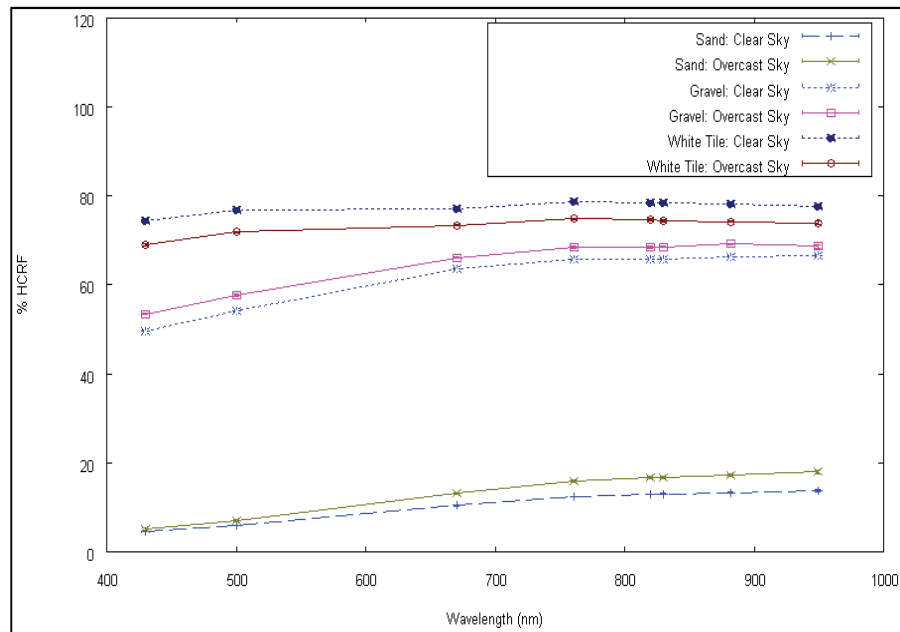


Figure 4.2: The variation of HCRF measurements under clear and overcast sky for white tile, gravel and sand surfaces

Figures (4.3), (4.4) and (4.5) show the temporal change of HCRF measurements for sand, gravel and white tile surfaces under overcast and clear sky.

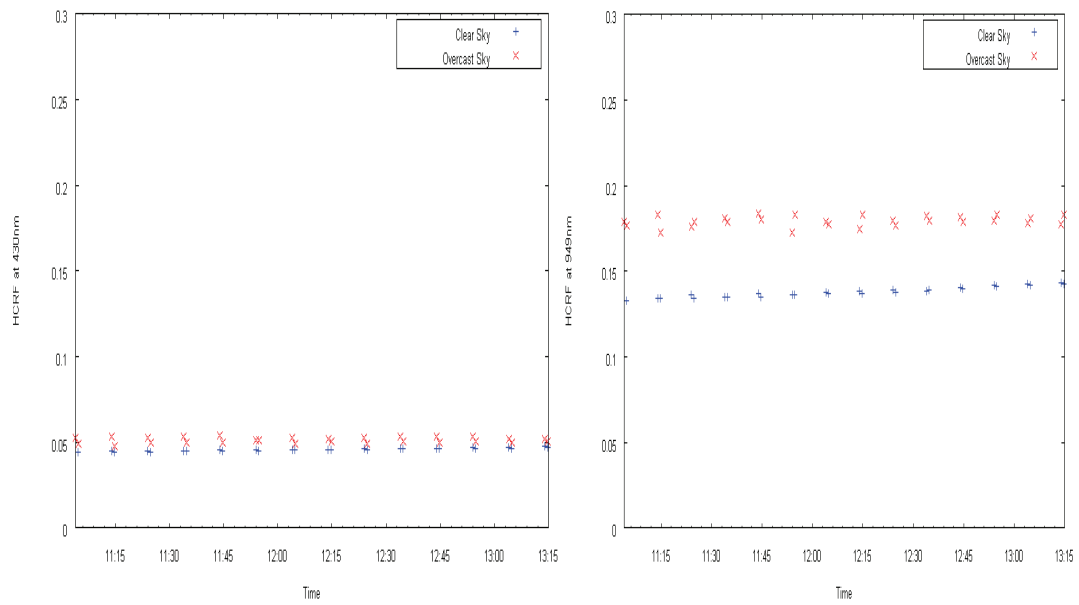


Figure 4.3: Temporal change in HCRF measurements for sand at 430nm and 949nm under clear and overcast sky conditions

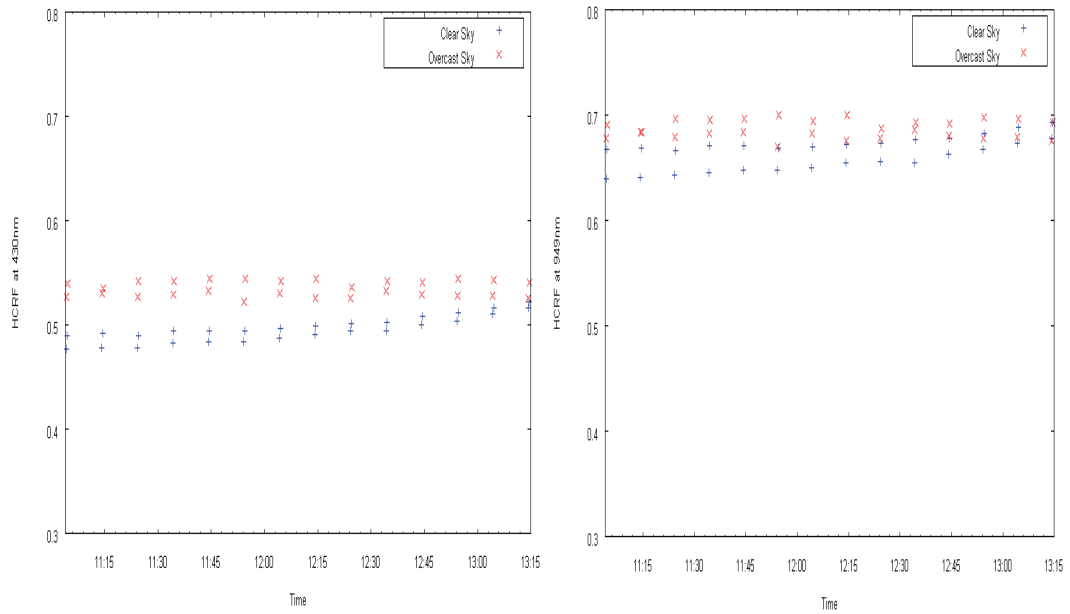


Figure 4.4: Temporal change in HCRF measurements for gravel at 430nm and 949nm under clear and overcast sky conditions

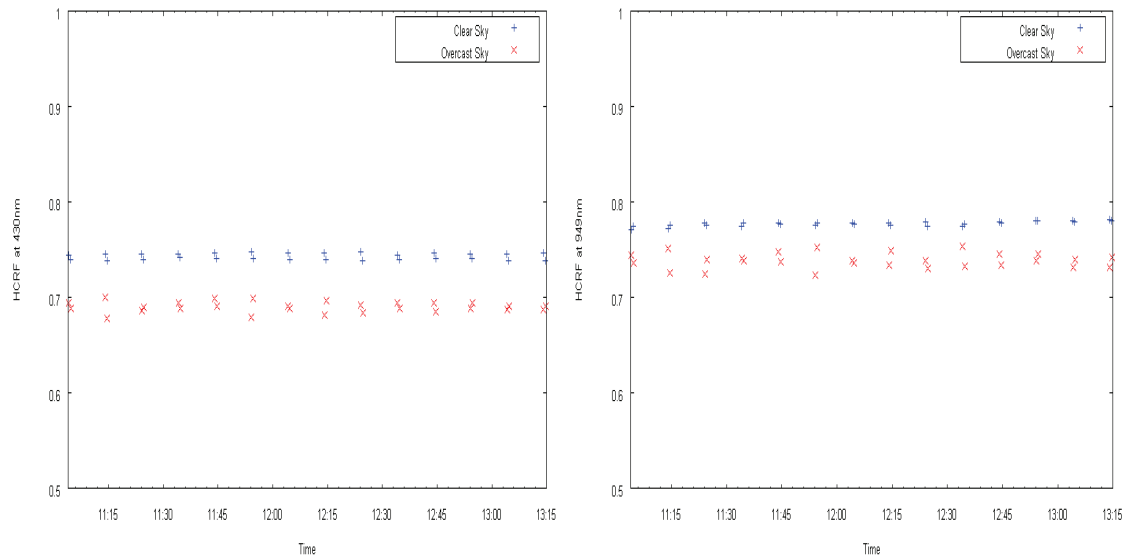


Figure 4.5: Temporal change in HCRF measurements for white tile at 430nm and 949nm under clear and overcast sky conditions

4.2.2. The variation of HCRF measurements with Solar Zenith Angle and Solar Azimuth Angle

The solar zenith angle (SZA) varied from 57.4° to 61.8° and solar azimuth angle (SAA) varied from 149.0° to 186.3° at the time of measurements. The HCRF measurements for sand and gravel showed a significant ($p=0.01$) correlation with SZA and SAA within the two hour period. However, white tile was not significantly ($p=0.01$) correlated with SZA and SAA except at 949nm. This was indicative that the measurements of the white tile did not change with the sun angles at shorter wavelengths. Due to positional displacement of the spectro-radiometer at sequential measurements for each surface, HCRF plots of the measurements with the solar angles appeared as a reflection of each other (Appendix 7). For this reason the measurements were split and plotted for the ‘outbound³’ and ‘homebound⁴’ measurements with respect to SZA and SAA. The plots of outbound and homebound are shown in Figures (4.6) through (4.8) and Appendix (1), (2), (3), (4), (5) and (6) .

The average drift in position of the instrument was measured by marking the positions of each sequential stop using a masking tape and the difference in distance measured using a

³ ‘Outbound’ refers 1st measurement taken per run for each sample target

⁴ ‘Homebound’ refers 2nd measurement taken per run for each sample target

tape measure. A displacement of 22cm was recorded and found to introduce some level of uncertainty in the measurements though it was not significant ($p=0.01$) across all the bands for the sand surface. This was expected because instantaneous field of view (IFOV) of the instrument was 35cm and buffered the effect of the positional displacements. However, for gravel surface, the measurements were significant at $p=0.01$ across all bands. This was due to varying self-shadowing effects due to angular property of gravel particles. For white tile surface the, measurements were significant at $p=0.01$ for all bands except at 949nm. This was speculated to be caused by the specular reflection behaviour of the shiny white tile surface which may have varied across the surface.

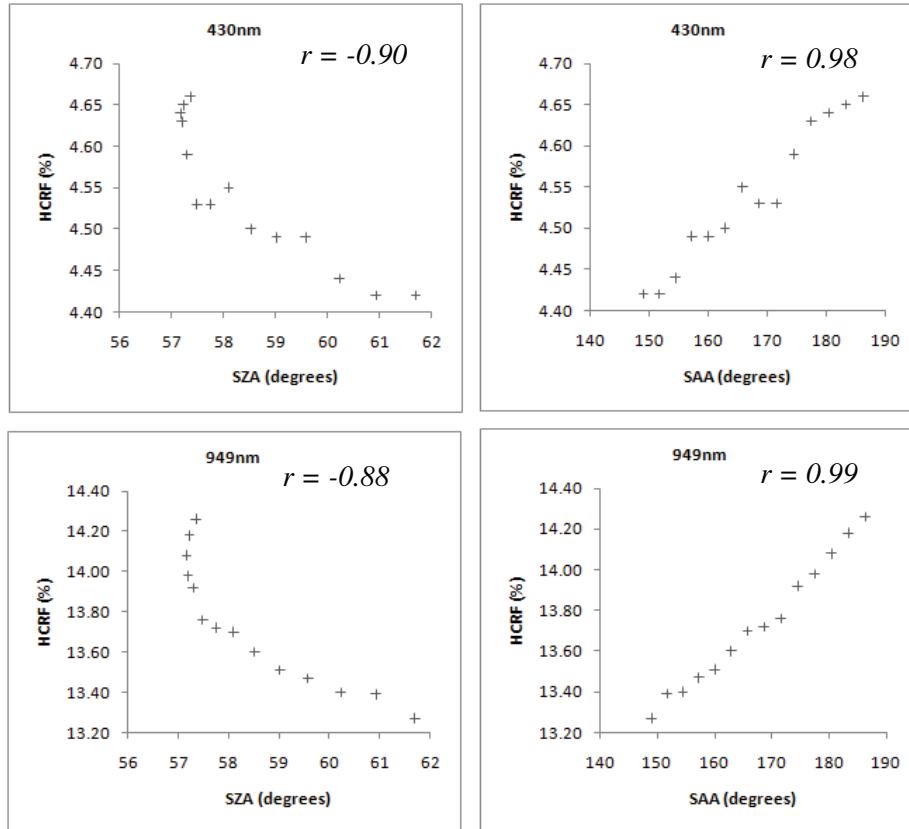


Figure 4.6: Plots of HCRF measurements (outbound) for sand with SZA and SAA at 430nm and 949nm

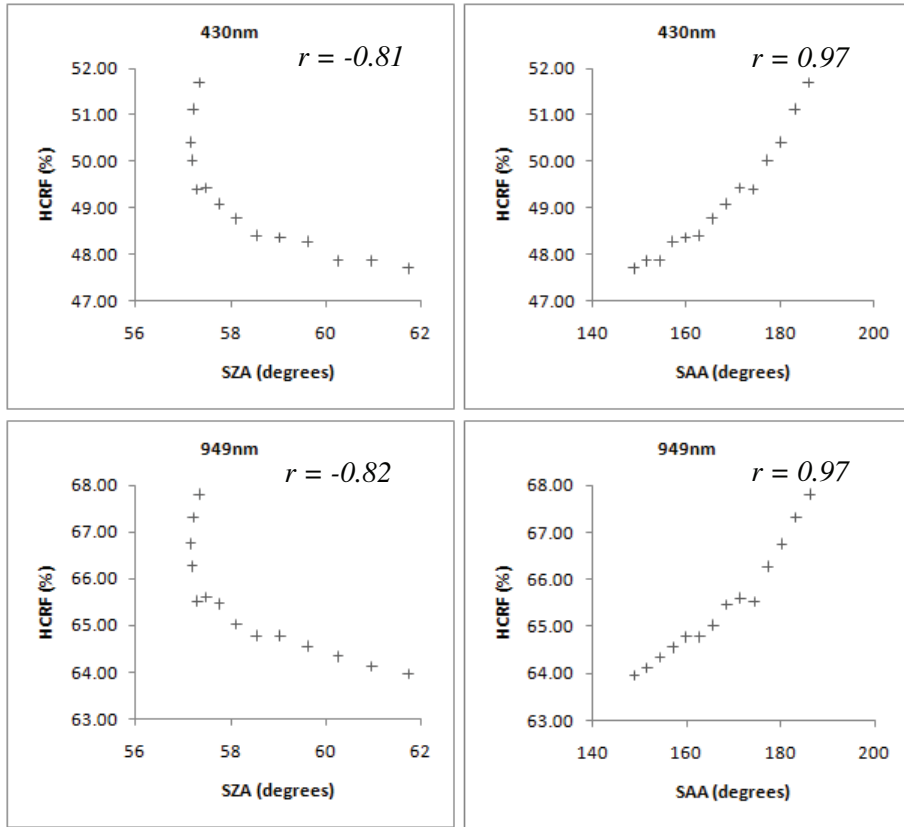


Figure 4.7: Plots of HCRF measurements (homebound) for gravel with SZA and SAA at 430nm and 949nm

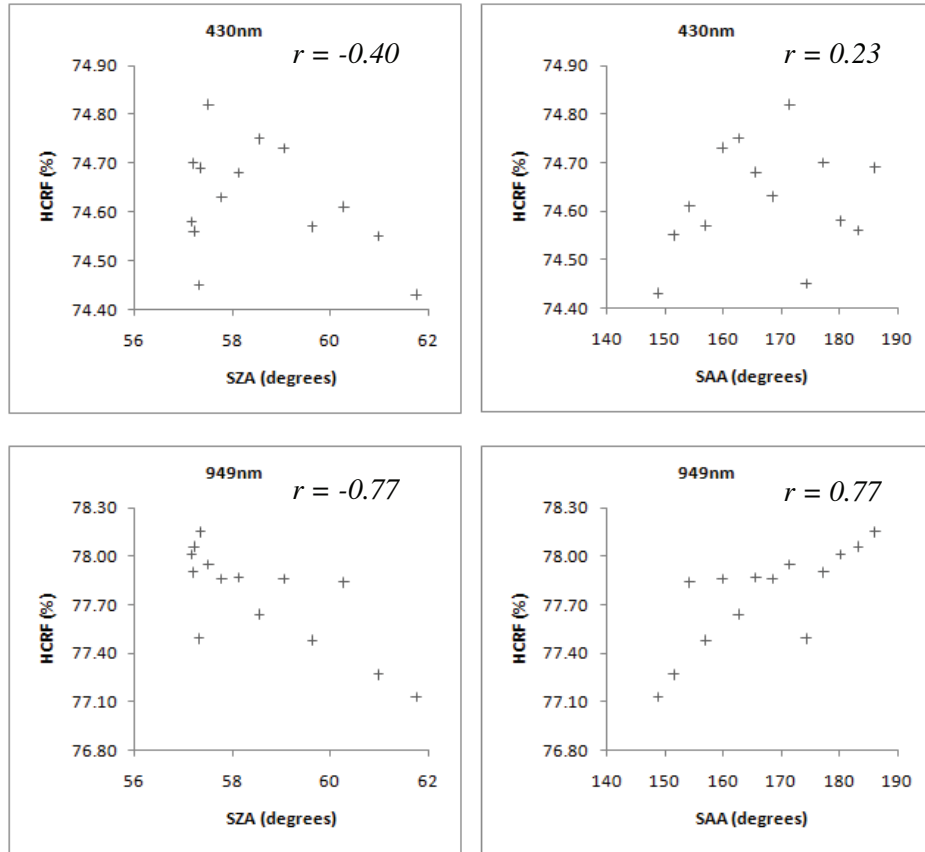


Figure 4.8: Plots of HCRF measurements (homebound) for white tile with SZA and SAA at 430nm and 949nm

4.3. Experiment 3: Local variation in HCRF with time

4.3.1. Spatial uniformity

Spatial uniformity based on G_i^* statistic for Tuz Gölü (TG) shows that there is an expansive fairly uniform area concentrated at the centre of upper half of the lake (Figure 4.9). This area was approximated to be 275 km² and constituted about 25% of the whole area.

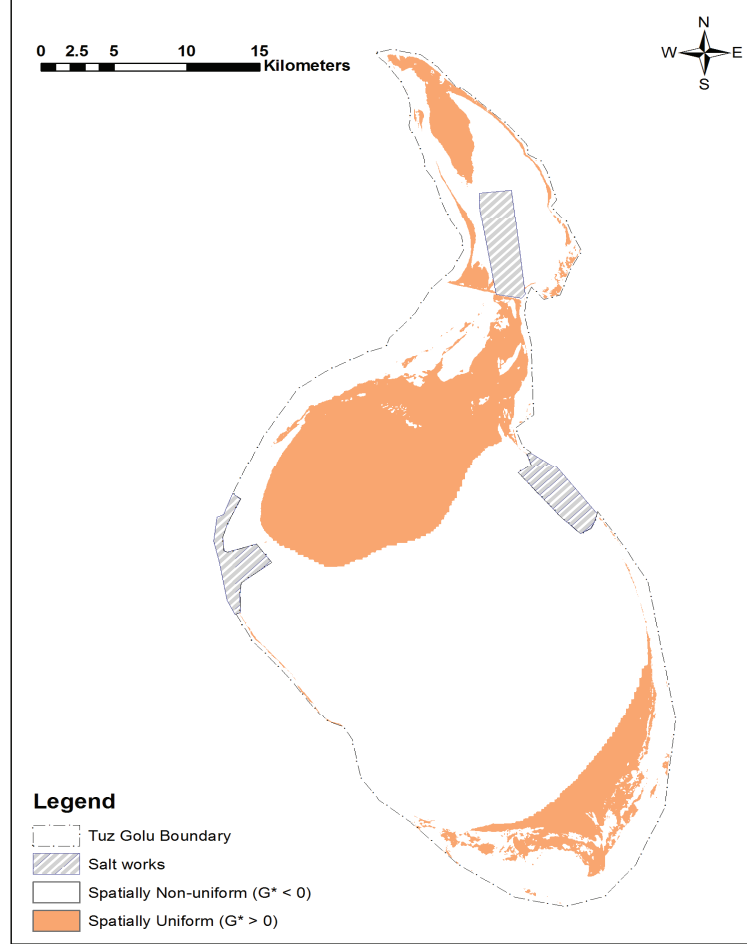


Figure 4.9: Spatially uniform areas in Tuz Gölü

Smaller uniform areas were also found in the southern and northern parts at the fringes of the lake but they were of lesser extent compared to the upper middle part. The result shows that there are areas, which are consistently uniform year-by-year in

TG. These uniform patches were characteristically clustered in zonations typical of salt pans and playas (Earl, 1990). Possibly, these zonations could be due to sub-environments identifiable as facies which are an aggregation of salt crusts usually formed in the centre of playas (Magee, 1991).

It was also evident that much of the area within TG (approximately 75%) is more variable and not all of it is stable year after year. This is highly possible considering that TG is a seasonal salt lake that experiences intra-annual and inter-annual variations in the surface. These variations could be responsible for the modification of the surface structure properties.

4.3.2. Temporal stability

A surface was considered temporally stable when the CV within the local window (3x3) was within 3% as recommended by Teillet et al. (2007) and Bannari et al. (2004) for vicarious calibration sites. Temporal stable areas within the spatially uniform areas of TG based on CV computations showed that a majority (approximately 80%) of stable areas fall within the spatially uniform area as shown in Figure (4.10).

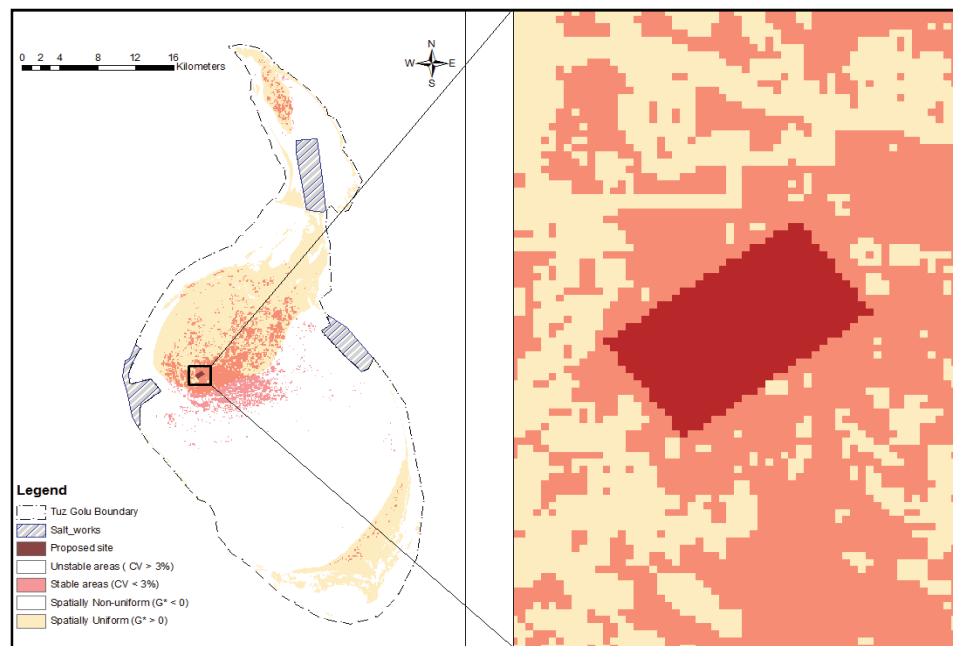


Figure 4.10: Spatio-temporal stability map for TG showing a selected proposed calibration site

Having identified the temporally stable areas over the spatially uniform area, an expanse proportion of an area that could be sampled on the ground for spectra was then visually identified. This area (Figure 4.10) was approximately 885m x 440m in size, twice as much as the size of La Crau test site in France and Rail Road Playa Valley (RRPV) in US.

4.3.3. HCRF of proposed site

The mean HCRF of the proposed site was extracted from the radiometrically and atmospherically corrected images. This was accomplished by computation of zonal statistics using ESRI Spatial Analyst™ tool. This was done for the 885m x 440m selected area. The results are summarised in Table (4.9) and illustrated in Figure (4.10). The results show that Bands 2 and 3 reflect in equal proportions and the trend is similar over the years investigated. This means that both one of these bands could explain information contained by the other in this particular site and therefore, calibration coefficients estimated for band 2 could be used to calibrate for band 3. This is on the assumption that Landsat TM sensor was well calibrated at the time of acquisition of the images used in this study and that the two bands do not saturate at sensor due to target brightness. *In situ* measurements are best placed to investigate and confirm this.

Table 4.9: Long-term HCRF extracted from Landsat TM imagery

Date	Band1	Band2	Band3	Band4
1984-08-03	50.94	63.75	63.75	63.74
1989-08-16	52.50	63.75	63.75	60.23
1998-08-26	53.50	63.75	63.75	56.70
2000-08-15	51.75	63.75	63.75	58.03
2003-08-08	50.75	63.75	63.14	58.76
2006-07-31	48.00	63.75	63.75	59.62
2006-08-16	50.05	63.74	63.75	56.23
2009-07-30	48.25	63.75	63.75	61.96
2009-08-15	49.72	63.75	62.05	62.06
2009-08-31	52.00	63.75	63.74	58.91

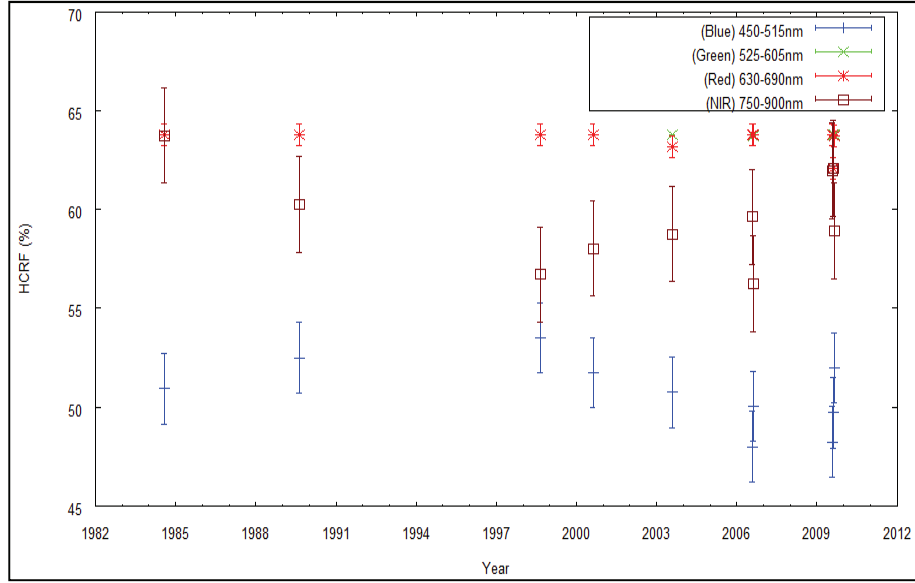


Figure 4.11: Satellite derived HCRF plots of Bands 1, 2, 3 and 4. Error bars show percent standard deviation in HCRF for respective years

Variation in HCRF for the proposed area was computed using Equation (5) for the all the years in the study. Bands 2 and 3 had minimal variations below 3%. However, Band 1 and 4 had slightly high variations above 3%. This high variation was associated to the increase in window (in this case the whole area of the proposed site 885m x 440m) during the CV estimation. Subtle variations at smaller window scales (e.g. 3x3 (90m x 90m)) window were normally expected to be much minimal compared to larger scale windows. Also, Band 1 is highly sensitive to aerosols and hence, the high uncertainty could be attributed to errors when approximating atmospheric aerosols used within ATCOR-2. Band 4 is sensitive to water absorption and thus the increased uncertainty in this region could be as a result of strong water absorption. However, the results were well within 5% uncertainty reported by Thome (2001) based on a vicarious calibration campaign in Rail Road Playa for Landsat ETM+ calibration campaign. Table (4.10) shows the results of variation computed for the proposed calibration site for the years under study.

Table 4.10: Variation of HCRF across the four bands within the proposed site for the years under study

Band	Mean	Standard deviation	CV (%)
1	50.75	1.78	3.51
2	63.75	0.00	0.01
3	63.52	0.55	0.86
4	59.62	2.42	4.05

5. DISCUSSION

5.1. Method of HCRF measurement

Experimental results on the use of the automated single beam method reveal that the method gives highly precise measurements of HCRF for a brown tile. This was better than uncertainty results reported from single beam method in other studies (e.g. Milton and Rollin, 2006, Duggin and Cunia, 1983). Milton and Rollin (2006) report uncertainty levels of upto 7% associated with single beam method under clear sky condition for simulated HCRF measurements on green vegetation. Duggin and Cunia (1983) also states that uncertainty in the method could be more than 10%. The results of these authors show high levels of uncertainties nearly equal in magnitude because their measurements were both conducted on vegetative canopies. Inherently, vegetation canopies are highly non-Lambertian and they exhibit scattering properties which lower precision of spectral measurements in the field. Anderson and Dungan (2009) argue that such variations in vegetation canopy are primarily due to varying biochemical concentrations in the leaves that take place even on fine spatial scales, background soil variation and movement of leaves caused by winds during measurements. Consequently, these variations increase levels of uncertainty in HCRF measurements.

In the present study, uncertainty of the method used was evaluated using a brown tile, which was tested for variability in HCRF. There was insufficient evidence to reject the null hypothesis of no variability in HCRF ($p = 0.05$) across the entire bandwidth of the instrument under varying conditions of multi-date HCRF measurements. This invariant property of the brown tile coupled with stable sky characterisation provided a better technique of quantifying uncertainty of the method than reported techniques of similar method discussed above. The technique provided a means of accounting for uncertainty due to the instrument from that due to changes in the target surface, the environment and its method of use. It is further demonstrated that single beam measurements could provide sufficiently high precision $\pm 0.19\%$ (within 1 standard deviation).

The common assumptions in uncertainty estimation using the single beam approach are that the target surfaces and the instrument remain stable and only illumination conditions affect measurements. Hence, discriminating uncertainty introduced by the instrument from those introduced by the environment and changes in the target surfaces themselves become hardly possible. Moreover, the results of the automated

single beam method showed low levels of uncertainty when compared to reported dual beam methods (e.g. Milton and Rollin, 2006, Gu et al., 1992, Duggin and Cunia, 1983, Anderson et al., 2003, Anderson and Milton, 2005) which are usually preferred because of their ability to account for instantaneous short-term changes in irradiance. Although, this was a significant result, it would be incorrect to deduce that single beam approach gives more precise results with low uncertainty than dual beam approach.

The ability of dual beam approach to account for uncertainty caused by time delay in sampling HCRF between the target and reference surface, which single beam does not, provides additional value to the system. Despite this advantage, the dual beam approach introduces additional uncertainty in that it requires the need to intercalibrate the spectro-radiometer and maintain this throughout the measurement period in the field (Milton et al., 2009, Duggin and Cunia, 1983, Duggin, 1980, Anderson et al., 2006). In addition, the common assumptions of the target being invariant, the instrument being stable during HCRF measurements in the field and that only the sky conditions are changing prevails in most studies even when dual beam approach is used. This has resulted in considerable high uncertainties reported in those studies compared to the findings of the present study. For example, Anderson et al.(2003) reported uncertainties in the order of $\pm 0.5\%$ using a dual beam approach when investigating on the temporal stability of a concrete surface. The concrete surface investigated by the authors was found to show evidence of seasonal growth of biological materials suggesting that it was changing not stable.

In summary, the results have shown that in order to evaluate uncertainty of HCRF measurements in the field, it is imperative to account for changes in the instrument, the target surface and the atmospheric state. The present study was able to attain low levels of uncertainty under 1% using the single beam approach because all three factors were accounted for. Essentially the dual beam method would equally attain such high precision if all three factors are accounted for other than only accounting for short-term episodic changes in atmospheric state.

5.1.1. Importance of method of measurement to vicarious calibration and atmospheric correction

Vicarious calibration and atmospheric correction play a very important role in ensuring that data products from Earth observation (EO) sensors are of high quality. Hence, these activities require that measurements of inputs (i.e. reflectance of ground calibration targets and environmental variables such as aerosol loadings) used in these activities be of high precision and high accuracy. Inherent uncertainties while estimating these inputs on grounds used for VC and AC are eventually

transferred to the sensor and consequently to the earth observation (EO) products thereof. This has been shown by Biggar et al (1994) and Thome et al. (1998) at Lunar Lake Playa, Nevada, US. They found out that, uncertainty in the at-sensor radiance were similar to uncertainty measured *in situ* at the playa (i.e. 2%). These levels of uncertainty have wider implication on the use of EO products in applications such as studies of climate change (Pinty et al., 2005). Climate change models are sensitive to retrieved surface albedo, with accuracies ranging from ± 0.02 to ± 0.05 regarded as suitable (Oleson et al., 2003, Henderson-Sellers and Wilson, 1983, Sellers, 1995). Retrieval of aerosol optical thickness (AOT) for AC algorithms has also been found to be sensitive to measured surface HCRF (Guoyong et al., 1999). Guoyong et al.(1999) explains that uncertainties associated with measurement of HCRF may increase the errors associated with AOT retrieval. Consequently, this has a huge impact on AC algorithms, which in turn are used to correct for atmospheric effect and retrieve at-sensor reflectance products.

Low uncertainty associated with the single beam method reported here suggests that the method is applicable for use in VC and AC studies on condition that: (i) the sky is characterized as stable during measurements; and (ii) the technique of measuring HCRF of an invariant target concurrently with the site being sampled is maintained. This ensures that uncertainties due to positional drift of instrument and its method of use are not lumped into uncertainties resulting from changes of the site. The disadvantage of the method is that the sky conditions ought to be stable during the measurement period. Obviously, under instantaneous changing sky conditions the dual beam approach will prove superior as discussed in previous studies (Anderson and Milton, 2006, Anderson et al., 2003, Duggin, 1980, Duggin and Cunia, 1983, Milton, 1981, Milton et al., 2006). Nevertheless, VC and AC activities are usually conducted under stable clear sky conditions.

The enhanced automatic mechanism of measuring HCRF using the tramway approach ensured that the measurements were taken at user-defined time intervals. This approach means that the instrument could be precisely synchronised to acquire HCRF measurements simultaneously at the time of EO satellite overpass on the targeted site. In addition, this will reduce the time required to sample HCRF for VC and AC, subsequently decreasing uncertainties in HCRF measurements due to changing solar zenith angles (SZA) and changes in illumination conditions. Thome et al. (1994) tested uncertainty in measuring reflectance in the field using a Modular Multispectral 8-channel radiometer (MMR) mounted on a trailer that was then towed within a VC site. The uncertainty from this mobile device dubbed 'reflectomobile' was compared with uncertainty arising from sampling HCRF using a backpack

mounted MMR radiometer. The authors found out that the difference in uncertainty between the two methods was less than 6%.

In essence, the rigour of VC and AC campaigns requires a fast method of sampling HCRF in the field at high precision and low uncertainty. The automated tramway spectro-radiometer used in this study does provide such a robust method suitable for these kinds of activities. Furthermore, the automation mechanism will reduce the manpower requirements usually associated with VC and AC campaigns. Finally, the results of the present study concurred with Biggar et al. (1994) who postulated that improvements in techniques and methods of measurement of HCRF for VC studies could bring the total uncertainty to less than 3.5%.

5.2. Illumination conditions and HCRF measurement

HCRF measurements are usually performed under stable sky conditions specifically during clear skies. The reasons for these are normally to match up these measurements with at-sensor retrieved measurements and minimize on uncertainties introduced by cloudy and overcast conditions. Moreover, matching up of field spectral measurements with at-sensor measurements requires that atmospheric attenuation be corrected for airborne and spaceborne acquired imagery. This is usually achieved by models that have been developed and validated under clear sky conditions (NCAVEO, 2005a). Also specifically, most measurements of bidirectional reflectance (BRF) require that clear sky conditions be considered to minimize influence of diffuse radiation (Cierniewski et al., 2004). In this study, it was important to characterize HCRF for the two extreme sky conditions and how they affect HCRF of the archetype GCT surfaces. The results of these outcomes are discussed in the following sections.

5.2.1. Effect of sky conditions on HCRF

The results of analysing HCRF variation for two selected stable ‘golden days’ i.e. clear sky (08/10/2009) and overcast sky (15/10/2009) showed that sky conditions do affect HCRF measurements variably depending on archetype GCT surfaces. For smooth archetype represented by sand, variation was higher under clear sky conditions than under overcast skies. The outcome was similar for rough archetype surface represented by gravel. However, for shiny archetype represented by the white tile, the converse was true.

Relatively, few studies have been conducted investigating HCRF measurements on surfaces under overcast conditions. Li and Zhou (2002) have used overcast

conditions to model for snow surface albedo, which is an important variable for snow melt budget. The authors argue that clear sky days are rare in temperate countries where snow occurs and solar incident angles hamper the establishment of these data. Hence, they used snow spectral reflectance measurements under overcast conditions to derive surface direct spectral albedo to within 2% uncertainty. The result of their study agrees with findings of the present work under overcast conditions for smooth archetype surfaces represented by sand. The uncertainty for sand was found to be within 3% at 430nm and within 2% for 500nm~949nm. This was not coincidence finding since it has been reported that sand and snow exhibit near similarity in their modelled bidirectional reflectance functions (Liang, 2004). These similarities include the fact that they are both characterized by dense particulate matter with close surface roughness though their spectral patterns are quite different.

Other HCRF measurements conducted by Moore et al. (1998) under overcast skies have shown levels of uncertainty in the range of 0.0025 standard deviation (1 standard deviation) for an invariant white Spectralon™ plaque. For the white tile used in the present study, variation under overcast sky conditions was 0.0081 standard deviation (within 1 standard deviation) across all wavelengths. Typically, this was due to the fact that the white tile was not as Lambertian compared to a white Spectralon™. Considering that the white tile was shiny and glossy, it was postulated that it may have exhibited specular and/or spurious reflection properties. The behaviour of the surface under diffuse conditions was uncertain.

The variation across individual spectral bands for sand emulated the trend of uncertainty of instrument detectors with high variations found at the edges of the spectrum. This trend was also similar for the rough archetype surface represented by gravel. However, the white tile exhibited a different uncertainty pattern under overcast conditions with the lower bands having lower variations compared to higher bands. The reasons for this were unclear and could not be clearly explained within the framework of the present study. Since the white tile represented shiny archetype surfaces, probably it would have been better understood if was tested under the same conditions with a natural shiny surface such as a salt pan.

Nevertheless, illumination conditions under clear sky measurements for both sand and gravel were found to be significantly ($p=0.05$) lower than measurements under overcast conditions. For sand, this was associated to effect of moisture from previous precipitation that made the sand wet. Many studies (e.g. Lobell and Asner, 2002, Matthias et al., 2000, Bowers and Hanks, 1965) of wet and dry sandy soils have shown that wet sandy soils generally will show lower HCRF values than when

they are dry. Addition of moisture through precipitation increases the refractive index (Twomey et al., 1986) and thus, more light will interact and be absorbed with increased moisture before being reflected. This causes exiting light to be of less intensity that leads to reduced HCRF of wet sand compared to dry sand. However, in between the clear sky and the overcast day the sand dried out progressively causing HCRF to be significantly high.

On the other hand, gravel HCRF measurements were lower under clear sky conditions compared to overcast conditions. This was typically the effect of shadowing introduced by illumination of the direct solar beam on the larger angular microrelief of the gravel particles (Cierniewski et al., 2004). Under overcast skies there were no shadows and all illumination was from the diffuse sky illuminated in all angles hemispherically.

Further, results from sand and gravel indicate that HCRF measurements under overcast sky introduced less variation in HCRF measurements than during clear sky. The reason for this was attributed to the influence of illumination geometries which varies with time under clear sky. These findings are in agreement with those investigated by Moore et al. (1998) who evaluated uncertainty for a white Spectralon™ plaque under clear and overcast sky conditions and found that there was more variation under clear sky (standard deviation = 0.0028, 1 standard deviation) than overcast sky (standard deviation = 0.0025, 1 standard deviation). This is evidence that HCRF measurements carried under clear sky condition have higher levels of uncertainties compared to measurements under overcast conditions.

Of significance to the investigation of the effect of illumination conditions on HCRF under overcast skies, was to examine the possibility of whether HCRF measurements can be precisely collected under these conditions better than under clear sky conditions. The levels of uncertainty under overcast conditions were significantly ($p=0.05$) lower than uncertainties reported for clear skies for smooth and rough archetypes. These findings are significant for vicarious calibration of airborne sensors when clear sky days are elusive. Most important, was the near-Lambertian behaviour of the archetype surfaces under overcast sky. Schiller et al. (n.d.) argue that bidirectional effects are normally reduced by increased diffuse to global ratio. Consequently, this makes surfaces behave near-Lambertian under overcast skies as evidenced in this study. This means that many flat spectral measurements can be sampled under overcast to fully characterize surfaces and matched to airborne-at-sensor measurements without the worry of anisotropic effects and at low levels of uncertainty as well. However, this might be met with confounding challenges of correcting for atmospheric effect on the resulting airborne

images considering that most atmospheric correction algorithms were developed and validated under clear skies (NCAVEO, 2005a).

5.2.2. Effect of SZA and surface roughness on HCRF measurements

Natural surfaces are known to be non-Lambertian, meaning that the magnitude of the reflected irradiance is normally not equal in all directions (i.e. anisotropic). They show variation in measured HCRF due to changes in irradiance and the direction in which the irradiance is reflected. The non-Lambertian property of natural surfaces has also been found to be dependent on surface roughness coupled with the incidence angle of the solar beam (Cierniewski and Verbrugghe, 1997). The surface archetypes used in this study represented different roughness properties, and HCRF measurements for the surfaces were measured at nadir with solar zenith angle (SZA) varying from 57.4° to 61.8° during the clear sky day.

The results showed that SZA significantly ($p=0.01$) correlated with HCRF measurements of sand and gravel surfaces. However, SZA correlations for sand surface measurements were stronger than the correlation for gravel surfaces in all bands. The strong relationship of sand and SZA is typical characteristic of surfaces with small grains. This was due to little self-shadowing effect of the sand particles. Hence, trapping of incident light was less as opposed to gravel particles, which had larger shadows and trapped more light within.

Inherently, the scatter of light within the gravel particles and eventual trapping of the light will vary with increasing solar angles. But, this was not a smooth variation because the gravel particles were not of equal shapes and size distribution. This introduced larger random shadows as the solar angle changed and thus, it would not have been expected to smoothly vary with the SZA compared to the sand granules.

Studies by Cierniewski and Verbrugghe (1997), and further by Matthias et al. (2000) found out that a decrease in roughness of soil particles and spacing between the particles caused the hemispherical directional reflectance to increase. This does not mean that small particles do have higher HCRF than rougher surfaces. Instead, it seeks to explain that there is indeed some significant reduction in measured HCRF for rougher surfaces and vice versa. By how much the HCRF increases relative to particle size depends on the nature and type of the surface and illumination conditions.

The gravel HCRF were higher compared to the sand HCRF possibly because they were brighter and reflected more as opposed to the sand particles which were darker. Ogilvy and Merklinge (1991) also noted that the albedos of rough soil surfaces tend

to decrease with increasing solar angle. The gravel particles were rougher and had wider spacing between them relative to sand particles. This may have led to incidence light to be scattered more within the particles before exiting and caused a general reduction in the reflected radiance. Earlier studies by Coulson and Reynolds (1971) expanded this argument when they suggested that trapped light between soil particles reappear readily at high zenith angles and consequently, minimizes albedo at these angles. Though their study was on soil particles, the combination of arguments by Coulson and Reynolds (1971), Ogilvy and Merklings (1991), Cierniewski and Verbrugghe (1997) and Matthias et al. (2000) seek to explain the present results specifically for the gravel surfaces which had large particle sizes relative to sand.

Comparison in HCRF measurements between gravel and sand surface showed that gravel generally had lower uncertainties across all wavelengths compared to sand. Generally, smooth surfaces are expected to exhibit lower variation than rougher surfaces which was not the case in the present findings. However, a geometric model by Cierniewski and Verbrugghe (1997) predicted that rougher surfaces with minimal aggregate spacing could show lower variation in HCRF at high SZAs compared to less rougher surfaces. The SZA at which HCRF measurements for the present study were conducted ranged from 57.4° to 61.8°. Possibly, this SZA was sufficiently high to permit lower variations in measurements for gravel compared to sand.

Interestingly, HCRF of the white tile surface showed no significant correlation with SZA and SAA in all the bands except at 949nm. The HCRF of the surface was flat for bands 430nm~882nm regardless of increase of SZA and SAA. This showed that the surface was near-Lambertian with some specular reflection as discussed in section 5.2.1. However, at 949nm, the white tile showed anisotropic behaviour with SZA and SAA. This was characteristic finding similar to compacted snow as reported by Knap and Reijmer (1998) and Giardino and Brivio (2003) who found out that the snow anisotropy increased with wavelength. This behaviour ought to be compared with natural shiny surfaces like salt playas and compacted snow in future to generalize on its behaviour, relative to natural shiny surfaces used for vicarious and atmospheric correction.

Though there was a significant negative correlation between SZA and HCRF measurements for sand and gravel, it was discernible that at around solar noon when SZA was near stable, the HCRF continued to increase. This behaviour was similar to a study by Cosnefroy et al. (1996) who investigated satellite sensor calibration over desert surfaces. SZA alone could not explain this change of directionality with HCRF measured in the field. This change of direction of measurements around solar

noon was hypothesized to be the influence of the solar azimuth angle (SAA) which continued to increase even though the SZA varied minimally at solar noon. The results of this showed significant positive correlations of SAA and HCRF across all bands for the archetype surfaces. Hence, SZA and SAA helped to explain the variation of HCRF for the archetype surfaces. The Walthal model (Walthall et al., 1985) is best suited to model for such variation in nadir HCRF measurements. As a result, it has been used (e.g. Nilson and Kuusk, 1989, Anderson and Milton, 2005) to model for HCRF variation of surfaces since it accounts for changes in solar angles. However, the present study accounted for few a HCRF measurements to warrant the use of the Walthall model.

Normally, during VC campaigns spectra are collected ± 1 hour around solar noon in which case SZA and SAA will continue affecting the behaviour of HCRF of smooth and rough archetype surfaces. The impact of the solar angles on HCRF variation may cause significant uncertainty in the field measurements of HCRF, which eventually may be transferred to EO sensor calibration and consequently to the products. A method that will allow for systematic sampling of spectra before solar noon and reduce the time of sampling spectra would greatly reduce these apparent uncertainties introduced by changing sun angles. The automated tramway system was envisaged to provide such a system as a proof of concept. This was with consideration that it was robust in design and the automation mechanism would allow for mobility to rapidly sample HCRF in the field, before any significant changes in apparent solar angles can occur.

5.3. Effect of local variation on HCRF

5.3.1. Dynamic changes in the surface with time

Having evaluated uncertainties associated with instrumentation and changing of sky conditions, the other dimension of evaluating uncertainty was on a spatial domain. Spatial dynamic changes in ground calibration target surfaces arise due to changes in surface moisture, deposition of metals such as iron, gypsum and magnesium on the surface, presence of vegetation and other artefacts that may possibly introduce variation on the surface. These changes may vary seasonally and cause significant variation of spectra and therefore, render those surfaces less worthwhile for VC or AC campaigns. Hence, characterization of GCTs both on the ground and from imagery is of paramount importance to minimize on the uncertainty of HCRF measured and derived from satellite imagery.

The results of this part of the study were tailored to examine real changes in HCRF over time in a spatial domain for a potential vicarious calibration test site in Tuz

Gölü, Turkey. The lake is an ephemeral salt lake, which undergoes intra-annual and inter-annual seasonal changes typical of salt lakes. This provided for the study of temporal dynamics of the lake by identifying a spatially uniform and stable area from pre-existing imagery by evaluating the variation in HCRF across bands 1, 2, 3, 4 of Landsat TM. It was important that an area that is spatially uniform and temporally stable in all these bands be identified for this evaluation. The results of this part are discussed in the next section and followed by discussion on the variation of satellite retrieved HCRF in bands 1, 2, 3 and 4.

5.3.2. Spatial uniformity and temporal stability

Spatial uniformity and temporal stability of a test site can be affected by different factors such as surface moisture, variation in topography, which in turn create shade effects, and vegetation causing spectral changes (Kneubuhler et al., 2006). For the case of Tuz Gölü, it was expected that moisture conditions in the lake do vary year after year thus affecting spatial uniformity and temporal stability. Many studies involving the characterization of these two properties of a GCT surface have used only coefficient of variation (CV) as a measure of the two properties (e.g. Scott et al., 1996, Cosnefroy et al., 1996, Kneubuhler et al., 2006). Consequently, the impression created is that they are one and the same thing. A fact that Cosnefroy et al. (1996) recognizes and states that “...for reasons of practicability, we have chosen to privilege the spatial uniformity criterion, conjecturing that if a site is repeatedly very uniform over a large period of time, it is quite likely that it should satisfy the other criterion as well”. The “other criterion” herein meaning temporal stability.

In the current study the two surface properties were defined and evaluated separately. First, the spatial uniformity was evaluated using G_i^* statistic on yearly basis from acquired images for each band. These were then intersected to obtain the areas that were consistently uniform year after year. The results showed that there was a consistently spatially uniform area located at the upper central part of Tuz Gölü year after year (Figure 4.9). Not only has this part been consistently uniform but it has brighter pixels which are significant for vicarious calibration and atmospheric correction campaigns.

CV computed within a local window can be misleading interpretation of spatial uniformity because two connected surfaces may have equal CV but have different means and standard deviations altogether. Also, a CV computed within a local window may itself vary across years for the same local window. Hence, an index that best evaluates change in spatial uniformity of a VC site was adopted (i.e. Getis ord* (G^*)) to first characterize for spatial uniformity. Spatial uniformity has some

temporal dimension in that there may be areas, which progressively shift from being homogenous to heterogeneous and vice versa from year to year (LeDrew et al., 2004, LeDrew and Lim, 2005).

For VC campaigns it is necessary that uniformity be upheld across all bands of the sensor and from year to year. Only then can CV be used to check for temporal stability by computing the variability in spectra retrieved from imagery to assure for a full spatial and temporal integrity of a test site. This technique inherently provided for the use of spatial statistics as a quality metric for characterizing HCRF of GCTs on a spatial scale.

Furthermore, the results of temporal stability highlighted areas within Tuz Gölü that were actually spatially uniform but temporally not stable. This suggests that application of the CV alone to account for both spatial uniformity and temporal stability as argued by Cosnefroy et al. (1996) could misinform on the true characterization of the surface. A preliminary campaign to characterize Tuz Gölü by National Physics Laboratory (NPL) of United Kingdom used Getis ord* (G_i^*) statistic as a measure to inform on both the spatial uniformity and temporal stability of the site (Pegrum, 2008, Gurol et al., 2008). Not only did they not compute the variation in HCRF to identify temporally stable areas but used only red and near infra bands of MODIS imagery from 2006 to 2008 for the months of July and August to characterize for spatial uniformity. Their spatial uniformity map was quite different from the output of the present work (Appendix 8). This was due to their methodological approach, which was different from that outlined in the present study.

The current study defined homogenous and bright pixels ($G_i^* > 0$) of the study area from ten Landsat TM imagery dataset for bands 1, 2, 3 and 4. Then temporally stable ($CV < 3\%$) areas were identified from ten satellite imagery datasets, which were overlaid on the homogenous and bright pixels layer. The output was a map representative of areas which were spatially uniform and temporally stable to within 3% (Figure 4.10) as recommended for vicarious calibration test sites (Dingirard and Slater, 1999, Thome et al., 1997, Biggar et al., 1994).

G_i^* statistic has been widely used in applications such as vegetation cover classification (e.g. Wulder and Boots, 1998, Lees, 2006), coral reef stress (e.g. LeDrew et al., 2004, LeDrew and Lim, 2005) and lately it has been applied on vicarious calibration sites (Bannari et al., 2005). Bannari et al. (2005) applied G_i^* and CV as a synergistic approach to characterize the spatial uniformity and stability of Lunar lake playa in Nevada, US. The authors used SPOT HRV spectral bands 1,

2, and 3 for March 1997, June 1997 and June 1998. In their analysis, the authors assumed that both indices are a measure of spatial uniformity hence, could be conjectured for temporal stability as well. Furthermore, their results indicated that, temporal CV between 1997 and 1998 changed beyond 3% for bands 2 and 3. This would imply that part of that area would not meet the criteria of being temporally stable considering the practical containment of uncertainty to within 3% (Dingirard and Slater, 1999, Thome et al., 1997, Biggar et al., 1994). Nevertheless, Bannari et al. (2005) showed that the two indices complimented each other and provide a new approach to the use of spatial statistics as a quality metric to characterize vicarious calibration test sites.

5.3.3. Local variation in HCRF for proposed site

Having selected a spatially uniform ($G_i^* > 0$) and temporally stable ($CV < 3\%$) areas within the 3×3 local window, an area fulfilling these criterion approximately $885m \times 440m$ in size was identified. This area was oriented coincident with the satellite path to avoid any mis-alignment of pixels within the area. Satellite retrieved HCRF from this proposed site for bands 1, 2, 3 and 4 showed satisfactory results to within the acceptable uncertainties. Uncertainty in HCRF was less than 4% across all the bands. Noticeable in these results was the 'high' CV for Band 1 (3.5%) and Band 4 (4%) yet the areas selected had CV to within 3% on a 3×3 local window (i.e. $90m \times 90m$). This can be explained by the fact that the CV was computed for the whole proposed site i.e. mean of HCRF for the $885m \times 440m$ against the standard deviation of HCRF within this site. By enlarging the window to the extent of the site, Bands 1 and 4 exhibited more variation at the global level ($885m \times 440m$) than was expected at the local level ($90m \times 90m$).

The temporal CV of the site for all the bands was within the range of 0.01% to 4.05%. These figures compare favourably with reported temporal CV based on reflectance measurements at other VC test sites as shown in Table (5.1). Cosnefroy et al. (1996) recorded lower temporal variation for the Saharan and Arabian Deserts with a CV in the order of 1% to 2% because the authors corrected for anisotropic effects.

Table 5.1: Examples of reported temporal CV for VC test sites

	Test Site	CV	Sensor	Authors
1.	La Crau, France	5 to 10%	SPOT	Gu et al.(1990)
2.	La Crau, France	10 to 15%	ASTR-2	Rondeaux et al. (1998)
3.	Rail Road Playa, US	1.2% to 2.5%	SPOT	Scott et al. (1996)
4.	Rail Road Playa, US	3%	SPOT, AVHRR and LANDSAT TM	Bannari et al. (2004)
5.	Rail Road Playa, US	4.31%	MERIS	Kneubuhler et al. (2006)
6.	Western Queensland, Australia	1.2% to 5.2%	LANDSAT ETM+ & TM	de Vries et al.(2007)
7.	Saharan & Arabian Deserts	1% to 2%	METEOSAT	Cosnefroy et al. (1996)

This study reports high variations for Bands 1 (Blue) and 4 (Near Infra Red (NIR)). The high variation noted in Band 1 could be attributed to atmospheric effects which are known to significantly affect this region (Thome et al., 2004). Band 4 showed high variation because of water absorption in the salt lake. Studies by Pengau et al. (1997) and Ruddick et al. (2005) have shown that NIR is highly affected by water absorption. Hence, the results for Band 4 could be explained by the fact that Tuz Gölü being a seasonal salt lake that dries up in the months of July and August every year, was envisaged to hold substantial amounts of moisture in the surface likely to cause water absorption effect in NIR. Also, the band 4 HCRF was lower than HCRF for bands 2 and 3. This result conforms with field measurements for Tuz Gölü reported by Pegrum (2008) linked to the speculated inherent water on the lake.

6. CONCLUSIONS AND RECOMMENDATIONS

Ground calibration targets play a significant role in vicarious calibration (VC) and atmospheric correction (AC). In reality, however, accurate VC and AC using ground targets can present many technological and scientific challenges due to many sources of uncertainty introduced in the data and methods used. Errors resulting from VC and AC campaigns throughout the life of a sensor can seriously impact upon the uncertainty associated with products derived from the sensors, compromising the evidence base for decision making. The dynamic nature of many apparently stable surfaces is a major source of uncertainty due to the spatial heterogeneity of surfaces that appear uniform to the eye.

This study sought to investigate different sources of uncertainty arising from: (i) the method of measurement of HCRF in the field; (ii) the apparent changes in sky conditions relative to archetype surfaces normally used for VC and AC campaigns; and (iii) dynamic changes in HCRF at a local scale of a proposed VC site. It is apparent, from this study, that a robust methodology of sampling precise spectral ground measurements, characterization of the atmosphere and the surface (i.e. spatial uniformity and temporal stability) are crucial to VC and AC campaigns.

The method of measurement used an automated single beam spectro-radiometer which was evaluated against an invariant brown tile. The precision of the method was better than $\pm 0.19\%$ (1 standard deviation) across all the bands of the spectro-radiometer for the invariant brown tile surface within the normal ± 2 hour measurements around solar noon. The uncertainty of the method was reported to be less than 0.27% in all the bands. The technique provided a means of disassociating uncertainty due to the instrument and its method of use from that due to changes in the target surface and the environment.

Effect of sky conditions on HCRF measurements revealed that sky conditions affected HCRF measurements variably depending on the surface archetype. Moreover, SZA and SAA were significant for smooth and rough surfaces even over the ± 2 hour measurements around solar noon. Furthermore, it was realized that the smooth archetype surface represented by sand, and rough archetype represented by gravel surface, were highly anisotropic under clear sky during the period of normal measurements. This emphasized the need to measure field spectra synchronously with sensor overpass and within a time when SZA and SAA changes are not significant.

Local variation of HCRF measurements was found to be dependent on the spatial uniformity and temporal stability of a surface. These two properties are known to be affected by surface conditions (e.g. moisture, weathering and wind action on the surface and also vegetation growth) driven by intra-annual and inter-annual variations. The study employed the use of spatial statistic as a quality metric to characterize the spatial uniformity and temporal stability using multi-temporal imagery datasets. From this, an area that was spatially uniform, temporally stable and exhibited normal distribution in all spectra (approximately 885m x 440m) was identified from a proposed VC site in Tuz Gölü, Turkey, which is a salt lake that dries up every July and August. Retrieved HCRF from this surface showed uncertainty in the range of 0.01% to 4.05% for Landsat bands 1, 2, 3 and 4. These results fit well within the range of other reported uncertainties of calibration test sites in the world.

In summary, this study has highlighted the various sources of uncertainties arising from measuring HCRF in the field and implications of those uncertainties on the use of ground calibration targets. Further, the study evaluated uncertainty due to local variations on a prime candidate test site being investigated as a potential test site. The results of this work thereof provided a scoping study for a field campaign in Tuz Gölü, Turkey scheduled for August 2010. Finally, the study recommends the need for proper characterization of HCRF in the field, with a robust method of characterizing GCTs. These results have a wider implication for those using GCTs for VC and AC.

6.1. Recommendations

The following recommendations highlight specifically on best practice guidelines that should be adopted when characterizing GCTs for VC and AC.

1. Sampling ground HCRF measurements for characterizing GCTs should be confined to within shorter time scales under stable, clear sky conditions. This will minimize on the directional effects caused by changing illumination geometry. Specifically, sampling spectra around solar noon should be avoided. Spectral measurements changed direction and continued to increase even though change in SZA was minimal at solar noon as discussed in section 5.2.2. This has wider implication not only for GCT characterization but also to the wider field spectroscopy practitioners who sample spectra ± 2 hours around solar noon. Alternatively, anisotropic effects of surfaces can be modelled and corrected for after measurements, in which case other orders of uncertainty might be introduced.

2. Stable overcast skies provided the potential of sampling spectra with low uncertainties and near-Lambertian surface behaviour hence there is need to investigate the potential of these conditions using airborne sensors for VC and AC activities.
3. The automated approach of instrumentation applied in this study will be of additional value in sampling spectra in the field within short-time scales at high precision with low levels of uncertainty under stable sky conditions. Coupling a dual beam approach to the instrumentation will add value.
4. Spatial uniformity and temporal stability of GCTs are two different properties of a surface and one should not be conjectured to infer the other. The general assumption that they are the same need to be tested to better inform on the nature of surfaces. The use of a combination of spatial statistic indices (e.g. G_i^* and CV) as a quality metric will greatly enhance these characterization.
5. There is need to investigate the effect of moisture on natural GCTs HCRF measurements. Specifically, testing for a hypothesis on how soon the targets regain their actual HCRF after a rainfall event.
6. Beyond characterizing spatial uniformity and temporal stability of a GCT surface, there is need for interdisciplinary approach to fully understand the dynamic nature of GCTs. This should involve remote sensing scientists, spatio-temporal statisticians, environmental modellers, atmospheric scientists, physicists, geomorphologists, geomatic engineers and many more who can add input towards characterizing GCTs. This is because calibration and validation is not just about products but also about methods-developing and disseminating best practice guidelines through knowledge exchange.

7. REFERENCES

- ABDOU, W. A., HELMLINGER, M. C., CONEL, J. E., BRUEGGE, C. J., PILORZ, S. H., MARTONCHIK, J. V. & GAITLEY, B. J. 2001. Ground measurements of surface BRF and HDRF using PARABOLA III. *Journal of Geophysical Research*, 106, 11967-76.
- ANDERSON, K. 2005. Temporal variability in calibration target reflectance: Methods, models and applications Unpublished PhD thesis, University of Southampton, UK, 30 pp.
- ANDERSON, K. & DUNGAN, J. 2009. Uncertainty in Proximal Measurements of Vegetation Reflectance Factors Measured in the Field. *Proceedings of RSPSoc 2009 Annual Conference, Leicester, UK*, 112-117.
- ANDERSON, K. & MILTON, E. J. 2005. Characterisation of the apparent reflectance of a concrete calibration surface over different time scales. In, *Proceedings of the 9th International Symposium on Physical Measurements and Signatures in Remote Sensing (ISPMSRS). Institute of Geographic Sciences and Natural Resources Research, CAS*.
- ANDERSON, K. & MILTON, E. J. 2006. On the temporal stability of ground calibration targets: implications for the reproducibility of remote sensing methodologies. *International Journal of Remote Sensing*, 27, 3365-3374.
- ANDERSON, K., MILTON, E. J. & ROLLIN, E. M. 2003. The temporal dynamics of calibration target reflectance. In, *Scales and Dynamics in Observing the Environment*, Nottingham, UK, 10-12 Sep 2003. *Remote Sensing and Photogrammetry Society*, 14.
- ANDERSON, K., MILTON, E. J. & ROLLIN, E. M. 2006. Calibration of dual-beam spectroradiometric data. *International Journal of Remote Sensing*, 27, 975-986.
- BANNARI, A., OMARI, K., TEILLET, P. M. & FEDOSEJEVS, G. 2005. Potential of Getis statistics to characterize the radiometric uniformity and stability of test sites used for the calibration of Earth observation sensors. *Geoscience and Remote Sensing, IEEE Transactions*, 43, 2918- 2926.
- BANNARI, A. A., OMARI, K., TEILLET, P. M. & FEDOSEJEVS, G. Year. Multisensor and multiscale survey and characterization for radiometric spatial uniformity and temporal stability of Railroad Valley Playa (Nevada) test site used for optical sensor calibration. In: *Sensors, Systems, and Next-Generation Satellites VII*, 2004 Barcelona, Spain. SPIE, 590-604.
- BIGGAR, S. F., SLATER, P. N. & GELLMAN, D. I. 1994. Uncertainties in the in-flight calibration of sensors with reference to measured ground sites in the 0.4-1.1 m range. *Remote Sensing of Environment*, 48, 245-252.
- BOWERS, S. A. & HANKS, R. J. 1965. Reflection of Radiant Energy From Soils. *Soil Science*, 100, 130-138.
- CIERNIEWSKI, J., GDALA, T. & KARNIELI, A. 2004. A hemispherical-directional reflectance model as a tool for understanding image distinctions between cultivated and uncultivated bare surfaces. *Remote Sensing of Environment*, 90, 505-523.

- CIERNIEWSKI, J. & VERBRUGGHE, M. 1997. Influence of soil surface roughness on soil bidirectional reflectance. *International Journal of Remote Sensing*, 18, 1277-1288.
- COSNEFROY, H., LEROY, M. & BRIOTTET, X. 1996. Selection and Characterization of Saharan and Arabian Desert Sites for the Calibration of Optical Satellite Sensors. *Remote Sensing of Environment*, 58, 101-114.
- COULSON, K. L. & REYNOLDS, D. W. 1971. The Spectral Reflectance of Natural Surfaces. *Journal of Applied Meteorology*, 10, 1285-1295.
- DE VRIES, C., DANAHER, T., DENHAM, R., SCARTH, P. & PHINN, S. 2007. An operational radiometric calibration procedure for the Landsat sensors based on pseudo-invariant target sites. *Remote Sensing of Environment*, 107, 414-429.
- DINER, D. J., BECKERT, J. C., REILLY, T. H., BRUEGGE, C. J., CONEL, J. E., KAHN, R. A., MARTONCHIK, J. V., ACKERMAN, T. P., DAVIES, R., GERSTL, S. A. W., GORDON, H. R., MULLER, J. P., MYNENI, R. B., SELLERS, P. J., PINTY, B. & VERSTRAETE, M. M. 1998. Multi-angle Imaging SpectroRadiometer (MISR) instrument description and experiment overview. *IEEE Transactions on Geoscience and Remote Sensing*, 36, 1072-87.
- DINGUIRARD, M. & SLATER, P. N. 1999. Calibration of Space-Multispectral Imaging Sensors: A Review. *Remote Sensing of Environment*, 68, 194-205.
- DISNEY, M. 2001. Improved estimation of surface biophysical parameters through inversion of linear BRDF models, PhD thesis, University College London, UK.
- DOHERTY, S. J. & WARREN, S. G. Year. The Antarctic and Greenland snow surfaces as calibration targets for the visible channel of the Advanced Very High Resolution Radiometer. *In*, 1998 New York, NY, USA. IEEE, 2267-9.
- DUGGIN, M. J. 1980. The field measurement of reflectance factors. *Photogrammetric Engineering & Remote Sensing*, 46, 643-647.
- DUGGIN, M. J. & CUNIA, T. 1983. Ground reflectance measurement techniques: a comparison. *Applied Optics*, 22, 3771-7.
- EARL, R. A. 1990. Arid zone geomorphology edited by D. S. G. Thomas, Belhaven, London, 1989. No. of pages: 372. ISBN 0470 21341 8. *Earth Surface Processes and Landforms*, 15, 761-762.
- ENGELSEN, O., PINTY, B., VERSTRAETE, M. M. & MARTONCHIK, J. V. Year. Parametric surface bidirectional reflectance factor models for atmospheric radiative transfer modeling. *In*, 1998 New York, NY, USA. IEEE, 713-15.
- FOX, N. 2001. Traceability to SI for EO measurements. CEOS WGCV Cal/Val Newsletter 9, January 2001, pp. 1-9, Available online at: http://wgcv.ceos.org/docs/newsletters/wgcv_newsletter_issue9.pdf (accessed 02 August 2009).
- FOX, N. 2009. A guide to expression of uncertainty of measurements GEO, Quality Assurance for Earth Observation Guide: 23rd May 2009, Available online

at: http://qa4eo.org/docs/QA4EO-QAEO-GEN-DQK-006_v3.0.pdf
(accessed 10 December 2009).

- GAMON, J. A., CHENG, Y., CLAUDIO, H., MACKINNEY, L. & SIMS, D. A. 2006a. A mobile tram system for systematic sampling of ecosystem optical properties. *Remote Sensing of Environment*, 103, 246-254.
- GAMON, J. A., RAHMAN, A. F., DUNGAN, J. L., SCHILDHAUER, M. & HUENNRICH, K. F. 2006b. Spectral Network (SpecNet)--What is it and why do we need it? *Remote Sensing of Environment*, 103, 227-235.
- GAO, F., SCHAAF, C. B., STRAHLER, A. H., JIN, Y. & LI, X. 2003. Detecting vegetation structure using a kernel-based BRDF model. *Remote Sensing of Environment*, 86, 198-205.
- GIARDINO, C. & BRIVIO, P. A. 2003. The application of a dedicated device to acquire bidirectional reflectance factors over natural surfaces. *International Journal of Remote Sensing*, 24, 2989-2995.
- GOEL, N. S. & REYNOLDS, N. E. 1989. Bidirectional canopy reflectance and its relationship to vegetation characteristics. *International Journal of Remote Sensing*, 10, 107-132.
- GU, X., GUYOT, G. & VERBRUGGHE, M. 1990. Analysis of the spatial variability of a test-site: the example of the Crau (France). *Photo Interpretation: Images Aeriennes et Spatiales*, 90, 39-52.
- GU, X. F., GUYOT, G. & VERBRUGGHE, M. 1992. Evaluation of measurement errors in ground surface reflectance for satellite calibration. *International Journal of Remote Sensing*, 13, 2531-2546.
- GUOYONG, W., SI-CHEE, T., CAHALAN, R. F. & OREOPOULOS, L. 1999. Path radiance technique for retrieving aerosol optical thickness over land. *Journal of Geophysical Research*, 104, 31321-32.
- GUROL, S., OZEN, H., LELOGLU, U. M. & TUNALI, E. 2008. Tuz Gölü: New Absolute Radiometric Calibration Test Site. *THE INTERNATIONAL ARCHIVES OF THE PHOTOGRAMMETRY, REMOTE SENSING AND SPATIAL INFORMATION SCIENCES ISPRS Congress Beijing, China, ISPRS*, XXXVII, 35-39.
- HENDERSON-SELLERS, A. & WILSON, M. F. 1983. Surface albedo data for climatic modeling. *Reviews of Geophysics and Space Physics*, 21, 1743-78.
- KIMES, D. S. 1983. DYNAMICS OF DIRECTIONAL REFLECTANCE FACTOR DISTRIBUTIONS FOR VEGETATION CANOPIES. *Applied Optics*, 22, 1364-1372.
- KNAP, W. H. & REIJMER, C. H. 1998. Anisotropy of the Reflected Radiation Field Over Melting Glacier Ice: Measurements in Landsat TM Bands 2 and 4. *Remote Sensing of Environment*, 65, 93-104.
- KNEUBUHLER, M., SCHAEPMAN, M. & THOME, K. Year. Long-term vicarious calibration efforts of MERIS at railroad valley playa (NV) - An update. In, 2006 Frascati, Italy. European Space Agency, European Space Agency.
- KRIEBEL, K. T. 1976. ON THE VARIABILITY OF THE REFLECTED RADIATION FIELD DUE TO DIFFERING DISTRIBUTIONS OF THE IRRADIATION. *Remote Sensing of Environment*, 4, 257-264.

- KUUSK, A., KUUSK, J. & LANG, M. 2009. A dataset for the validation of reflectance models. *Remote Sensing of Environment*, 113, 889-92.
- LEDREW, E. & LIM, A. Year. The application of the Getis statistic to high resolution imagery to detect change in the spatial structure of submerged tropical corals between image dates. *In: 2005 International Workshop on the Analysis of Multi-Temporal Remote Sensing Images*, 16-18 May 2005, 2005 Piscataway, NJ, USA. IEEE, 217-19.
- LEDREW, E. F., HOLDEN, H., WULDER, M. A., DERKSEN, C. & NEWMAN, C. 2004. A spatial statistical operator applied to multirate satellite imagery for identification of coral reef stress. *Remote Sensing of Environment*, 91, 271-279.
- LEES, B. 2006. The spatial analysis of spectral data: Extracting the neglected data. *Applied GIS*, 2, 14.1-14.13.
- LI, X. & STRAHLER, A. H. 1985. GEOMETRIC-OPTICAL BIDIRECTIONAL REFLECTANCE MODELING OF A CONIFER FOREST CANOPY. *IEEE Transactions on Geoscience and Remote Sensing*, GE-24.
- LIANG, S. 2004. *Quantitative Remote Sensing of Land Surfaces*, New Jersey, John Wiley & Sons.
- LOBELL, D. B. & ASNER, G. P. 2002. Moisture Effects on Soil Reflectance. *Soil Sci Soc Am J*, 66, 722-727.
- MAGEE, J. W. 1991. Late quaternary lacustrine, groundwater, aeolian and pedogenic gypsum in the Prungle Lakes, southeastern Australia. *Palaeogeography, Palaeoclimatology, Palaeoecology*, 84, 3-42.
- MAIGNAN, F., BREON, F. M. & LACAZE, R. 2004. Bidirectional reflectance of Earth targets: Evaluation of analytical models using a large set of spaceborne measurements with emphasis on the Hot Spot. *Remote Sensing of Environment*, 90, 210-220.
- MALLA, R. & HELDER, D. L. 2008. Radiometric calibration of reflective bands of landsat 4 thematic mapper using pseudo-invariant site technique. *International Geoscience and Remote Sensing Symposium (IGARSS)*, 4, IV1344-IV1347.
- MANOOCHHEHRI, F., KÄRHÄ, P., PALVA, L., TOIVANEN, P., HAAPALINNA, A. & IKONEN, E. 1999. Characterisation of optical detectors using high-accuracy instruments. *Analytica Chimica Acta*, 380, 327-337.
- MARTONCHIK, J. V., BRUEGGE, C. J. & STRAHLER, A. H. 2000. A review of reflectance nomenclature used in remote sensing. *Remote Sensing Reviews*, 19, 9-20.
- MATTHIAS, A. D., FIMBRES, A., SANO, E. E., POST, D. F., ACCIOLY, L., BATCHILY, A. K. & FERREIRA, L. G. 2000. Surface Roughness Effects on Soil Albedo. *Soil Sci Soc Am J*, 64, 1035-1041.
- MILTON, E. J. 1981. DOES THE USE OF TWO RADIOMETERS CORRECT FOR IRRADIANCE CHANGES DURING MEASUREMENTS? *Photogrammetric Engineering and Remote Sensing*, 47, 1223-1225.
- MILTON, E. J., FOX, N. P. & SCHAEPMAN, M. E. Year. Progress in field spectroscopy. *In, 2006 Piscataway, NJ, USA. IEEE*, 2018-20.

- MILTON, E. J. & ROLLIN, E. M. 2006. Estimating the irradiance spectrum from measurements in a limited number of spectral bands. *Remote Sensing of Environment*, 100, 348-355.
- MILTON, E. J., SCHAEPMAN, M. E., ANDERSON, K., KNEUBUHLER, M. & FOX, N. 2009. Progress in field spectroscopy. *Remote Sensing of Environment*, 113, S92-S109.
- MOORE, K. D., VOSS, K. J. & GORDON, H. R. 1998. Spectral reflectance of whitecaps: Instrumentation, calibration, and performance in coastal waters. *Journal of Atmospheric and Oceanic Technology*, 15, 496-509.
- MORAN, M. S., BRYANT, R., THOME, K., NI, W., NOUVELLON, Y., GONZALEZ-DUGO, M. P., QI, J. & CLARKE, T. R. 2001. A refined empirical line approach for reflectance factor retrieval from Landsat-5 TM and Landsat-7 ETM+. *Remote Sensing of Environment*, 78, 71-82.
- NCAVEO. 2005a. *Atmospheric correction* [Online]. Available: http://www.ncaveo.ac.uk/special_topics/atmospheric_correction/ [Accessed 24/01/ 2010].
- NCAVEO. 2005b. *Calibration* [Online]. Available: <http://www.ncaveo.ac.uk/calibration/radiometry/in-flight/> [Accessed 29/09/ 2009].
- NCAVEO 2009. Chilbolton.
- NICODEMUS, F. E., RICHMOND, J. C., HSIA, J. J., GINSBERG, I. W. & LIMPERIS, T. 1977. Geometrical considerations and nomenclature for reflectance. USA: Nat. Bur. Stand., Washington, DC, USA.
- NILSON, T. & KUUSK, A. 1989. A reflectance model for the homogeneous plant canopy and its inversion. *Remote Sensing of Environment*, 27, 157-167.
- OGILVY, J. A. & MERKLINGER, H. M. 1991. Theory of Wave Scattering from Random Rough Surfaces. *The Journal of the Acoustical Society of America*, 90, 3382-3382.
- OLESON, K. W., BONAN, G. B., SCHAAF, C., GAO, F., JIN, Y. & STRAHLER, A. 2003. Assessment of global climate model land surface albedo using MODIS data. *Geophysical Research Letters*, 30, 26-1.
- PEGAU, W. S., GRAY, D. & ZANEVELD, J. R. V. 1997. Absorption and attenuation of visible and near-infrared light in water: dependence on temperature and salinity. *Appl. Opt.*, 36, 6035-6046.
- PEGRUM, H. 2008. Tuz Gölü Salt Lake Test Site Characterisation Technical Report, Univesity of Southampton
- PINTY, B., LATTANZIO, A., MARTONCHIK, J. V., VERSTRAETE, M. M., GOBRON, N., TABERNER, M., WIDLOWSKI, J. L., DICKINSON, R. E. & GOVAERTS, Y. 2005. Coupling diffuse sky radiation and surface albedo. *Journal of the Atmospheric Sciences*, 62, 2580-91.
- RAO, C. R. N. & CHEN, J. 1999. Revised post-launch calibration of the visible and near-infrared channels of the Advanced Very High Resolution Radiometer (AVHRR) on the NOAA-14 spacecraft. *International Journal of Remote Sensing*, 20, 3485 - 3491.

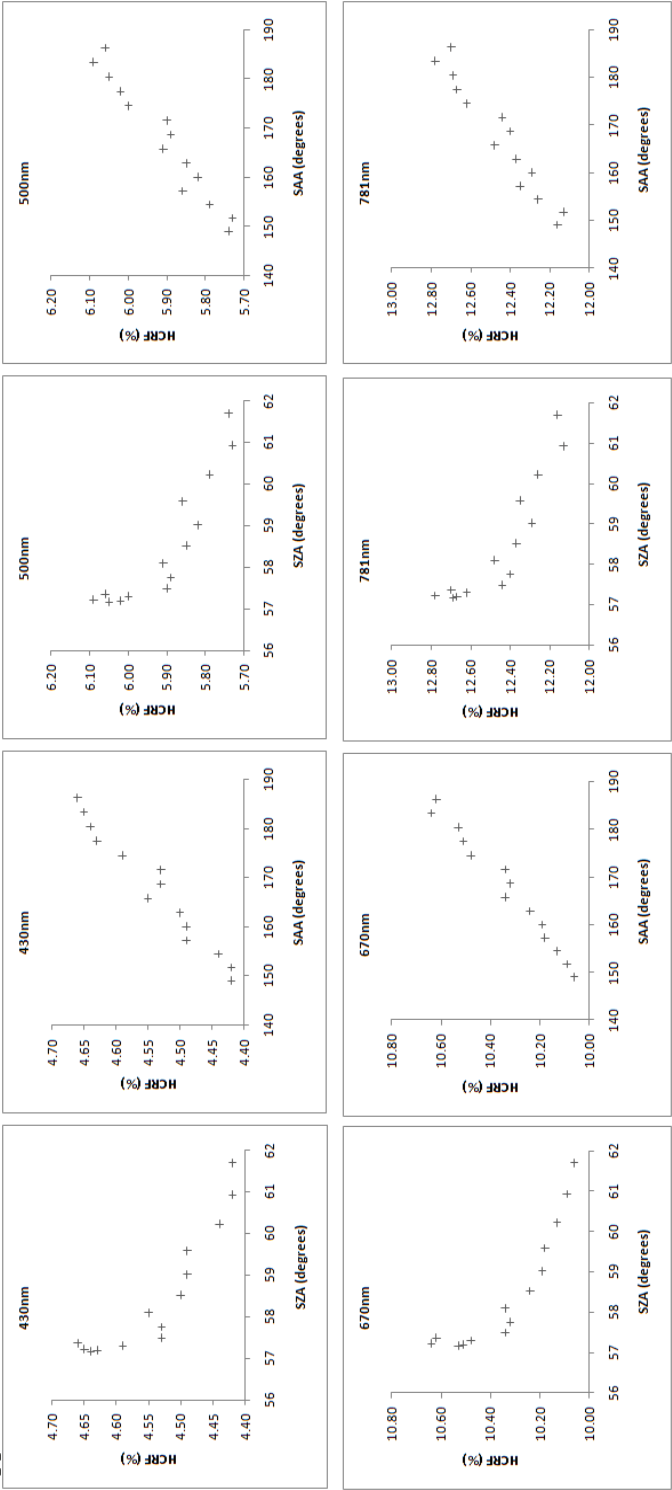
- RONDEAUX, G., STEVEN, M. D., CLARK, J. A. & MACKAY, G. 1998. La Crau: a European test site for remote sensing validation. *International Journal of Remote Sensing*, 19, 2775 - 2788.
- ROUJEAN, J. L., LEROY, M. & DESCHAMPS, P. Y. 1992. A bidirectional reflectance model of the Earth's surface for the correction of remote sensing data. *Journal of Geophysical Research*, 97, 20455-68.
- RUDDICK, K., DE CAUWER, V. & VAN MOL, B. Year. Use of the near infrared similarity reflectance spectrum for the quality control of remote sensing data. In: FROUIN, R. J., BABIN, M. & SATHYENDRANATH, S., eds., 2005 San Diego, CA, USA. SPIE, 588501-12.
- SCHAEPMAN-STRUB, G., SCHAEPMAN, M. E., PAINTER, T. H., DANGEL, S. & MARTONCHIK, J. V. 2006. Reflectance quantities in optical remote sensing-definitions and case studies. *Remote Sensing of Environment*, 103, 27-42.
- SCHILLER, S., HELDER, D., PAGNUTTI, M. & RYAN, R. n.d. *Implementation of Vicarious Calibration for High Spatial Resolution Sensors* [Online]. Available: http://www.commission1.isprs.org/isprs_ceos_workshop/Documents/Schiller/Schiller.ppt. [Accessed 20/09/ 2009].
- SCHILLER, S. J. Year. Technique for estimating uncertainties in top-of-atmosphere radiances derived by vicarious calibration. In: Earth Observing Systems VIII, August 3, 2003 - August 6, 2003, 2003 San Diego, CA, United states. SPIE, 502-516.
- SCOTT, K. P., THOME, K. J. & BROWNLEE, M. R. Year. Evaluation of Railroad Valley playa for use in vicarious calibration. In: HUBERTY, B., LURIE, J. B., CAYLOR, J. A., COPPIN, P. & ROBERT, P. C., eds., 1996 Denver, CO, USA. SPIE, 158-166.
- SELLERS, P. J. 1995. Remote sensing of the land surface for studies of global change: models - algorithms - experiments. *Remote Sensing of Environment*, 51, 3-26.
- SIX, D., FILY, M., ALVAIN, S., HENRY, P. & BENOIST, J.-P. 2004. Surface characterisation of the Dome Concordia area (Antarctica) as a potential satellite calibration site, using Spot 4/Vegetation instrument. *Remote Sensing of Environment*, 89, 83-94.
- SLATER, P. N. 1987. Reflectance- and radiance-based methods for the in-flight absolute calibration of multispectral sensors. *Remote Sensing of Environment*, 22, 11-37.
- SLATER, P. N., BIGGAR, S. F., HOLM, R. G., JACKSON, R. D., MAO, Y., MORAN, M. S., PALMER, J. M. & YUAN, B. 1987a. REFLECTANCE- AND RADIANCE-BASED METHODS FOR THE IN-FLIGHT ABSOLUTE CALIBRATION OF MULTISPECTRAL SENSORS. *Remote Sensing of Environment*, 22, 11-37.
- SLATER, P. N., BIGGAR, S. F., HOLM, R. G., JACKSON, R. D., MAO, Y., MORAN, M. S., PALMER, J. M. & YUAN, B. 1987b. REFLECTANCE- AND RADIANCE-BASED METHODS FOR THE IN-FLIGHT

- ABSOLUTE CALIBRATION OF MULTISPECTRAL SENSORS. *Remote Sensing of Environment*, 22, 11-37.
- SMITH, G. M. & MILTON, E. J. 1999. The use of the empirical line method to calibrate remotely sensed data to reflectance. *International Journal of Remote Sensing*, 20, 2653-2662.
- STRAHLER, A. H. 1997. Vegetation canopy reflectance modeling - recent developments and remote sensing perspectives. *Remote Sensing Reviews*, 15, 179-194.
- TEILLET, P. M., BARSI, J. A., CHANDER, G. & THOME, K. J. Year. Prime candidate Earth targets for the post-launch radiometric calibration of space-based optical imaging instruments. *In*, 2007 USA. SPIE - The International Society for Optical Engineering, 66770-1.
- TEILLET, P. M., FEDOSEJEVS, G., GAUTHIER, D., D'ORIO, M. A., RIVARD, B. & BUDKEWITSCH, P. Year. Initial examination of radar imagery of optical radiometric calibration sites. *In*, 1995 Paris, Fr. Society of Photo-Optical Instrumentation Engineers, 154-165.
- THOME, K. Year. Sampling and uncertainty issues in trending reflectance-based vicarious calibration results. *In*: BUTLER, J. J., ed., 2005 San Diego, CA, USA. SPIE, 588216-11.
- THOME, K., MARKHAM, B., BARKER, J., SLATER, P. & BIGGAR, S. 1997. Radiometric calibration of Landsat. *Photogrammetric Engineering and Remote Sensing*, 63, 853-858.
- THOME, K., SCHILLER, S., CONEL, J., ARAI, K. & TSUCHIDA, S. Year. Results of the 1996 Earth Observing System vicarious calibration joint campaign at Lunar Lake Playa, Nevada (USA). *In*: 6th International Conference on Radiometry. NEWRAD '97, 27-29 Oct. 1997, 1998 France. Bur. Int. Poids & Mesures, 631-8.
- THOME, K. J. 2001. Absolute radiometric calibration of Landsat 7 ETM+ using the reflectance-based method. *Remote Sensing of Environment*, 78, 27-38.
- THOME, K. J., BIGGAR, S. F., GELLMAN, D. L. & SLATER, P. N. Year. Absolute-radiometric calibration of Landsat-5 Thematic Mapper and the proposed calibration of the Advanced Spaceborne Thermal Emission and Reflection Radiometer. *In*, 1994 New York, NY, USA. IEEE, 2295-7.
- THOME, K. J., HELDER, D. L., AARON, D. & DEWALD, J. D. 2004. Landsat-5 TM and Landsat-7 ETM+ absolute radiometric calibration using the reflectance-based method. *IEEE Transactions on Geoscience and Remote Sensing*, 42, 2777-85.
- TWOMEY, S. A., BOHREN, C. F. & MERGENTHALER, J. L. 1986. Reflectance and albedo differences between wet and dry surfaces. *Applied Optics*, 25, 431-7.
- UNGAR, S., CAMPBELL, P., RAST, M. & CHANGYOUNG, C. Year. Data quality guidelines for GEOSS consideration-the CEOS Working Group on Calibration and Validation (WGCV). *In*, 2008 Barcelona, Spain. Institute of Electrical and Electronics Engineers Inc., 306-309.
- USGS 2009. Site Location: Tuz Golu.

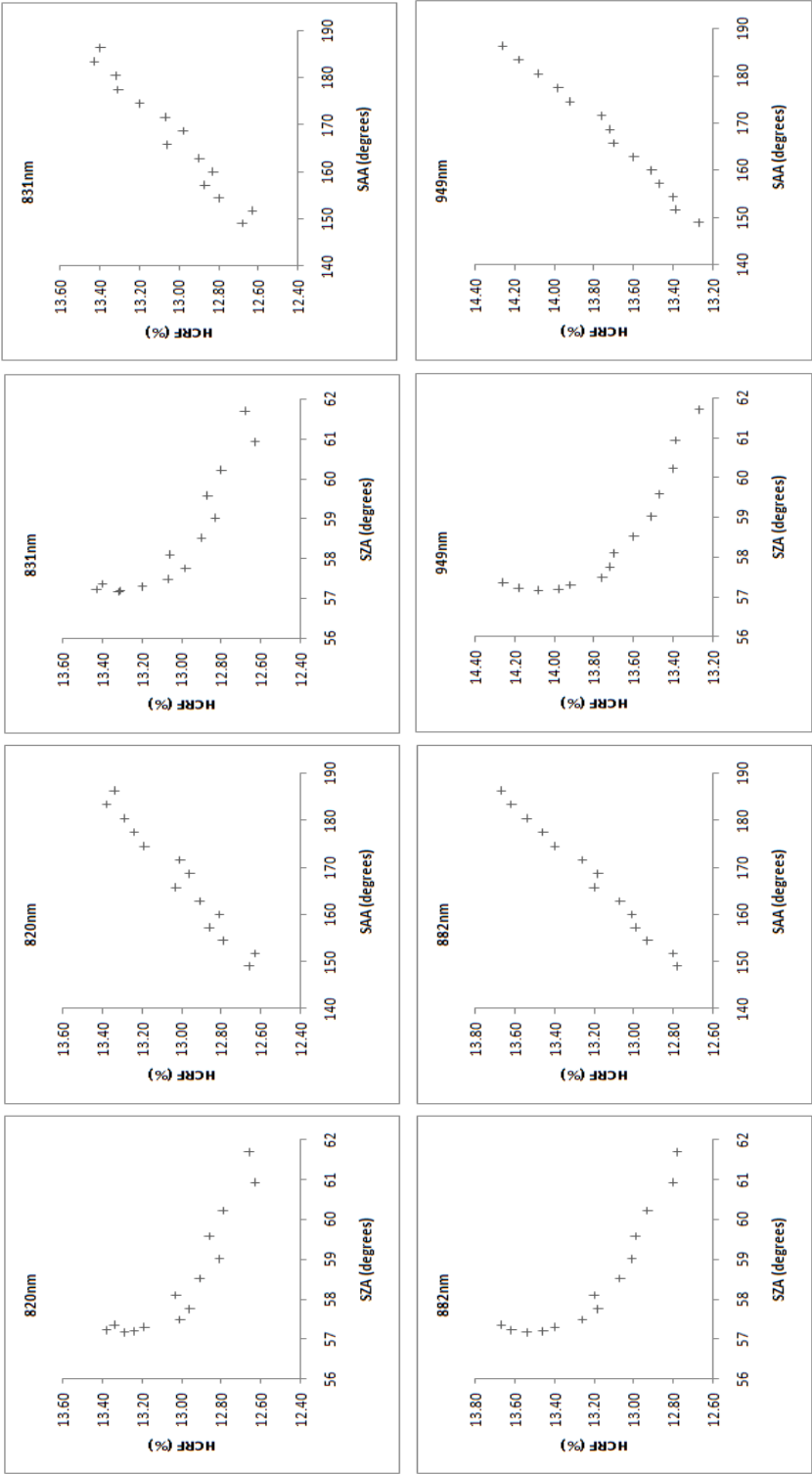
- WALTHALL, C. L., NORMAN, J. M., WELLES, J. M., CAMPBELL, G. & BLAD, B. L. 1985. Simple equation to approximate the bidirectional reflectance from vegetative canopies and bare soil surfaces. *In: Applied Optics*, 24(1985)3, pp. 383-387.
- WILLIAMS, T. & KELLEY, C. 1986-1993, 1998, 2004. Gnuplot.
- WILSON, R. T. 2009. RTWTools for ENVI, Version 0.5, Available at <http://rtwtools.googlecode.com>.
- WULDER, M. & BOOTS, B. 1998. Local spatial autocorrelation characteristics of remotely sensed imagery assessed with the Getis statistic. *International Journal of Remote Sensing*, 19, 2223-2231.

8. APPENDICES

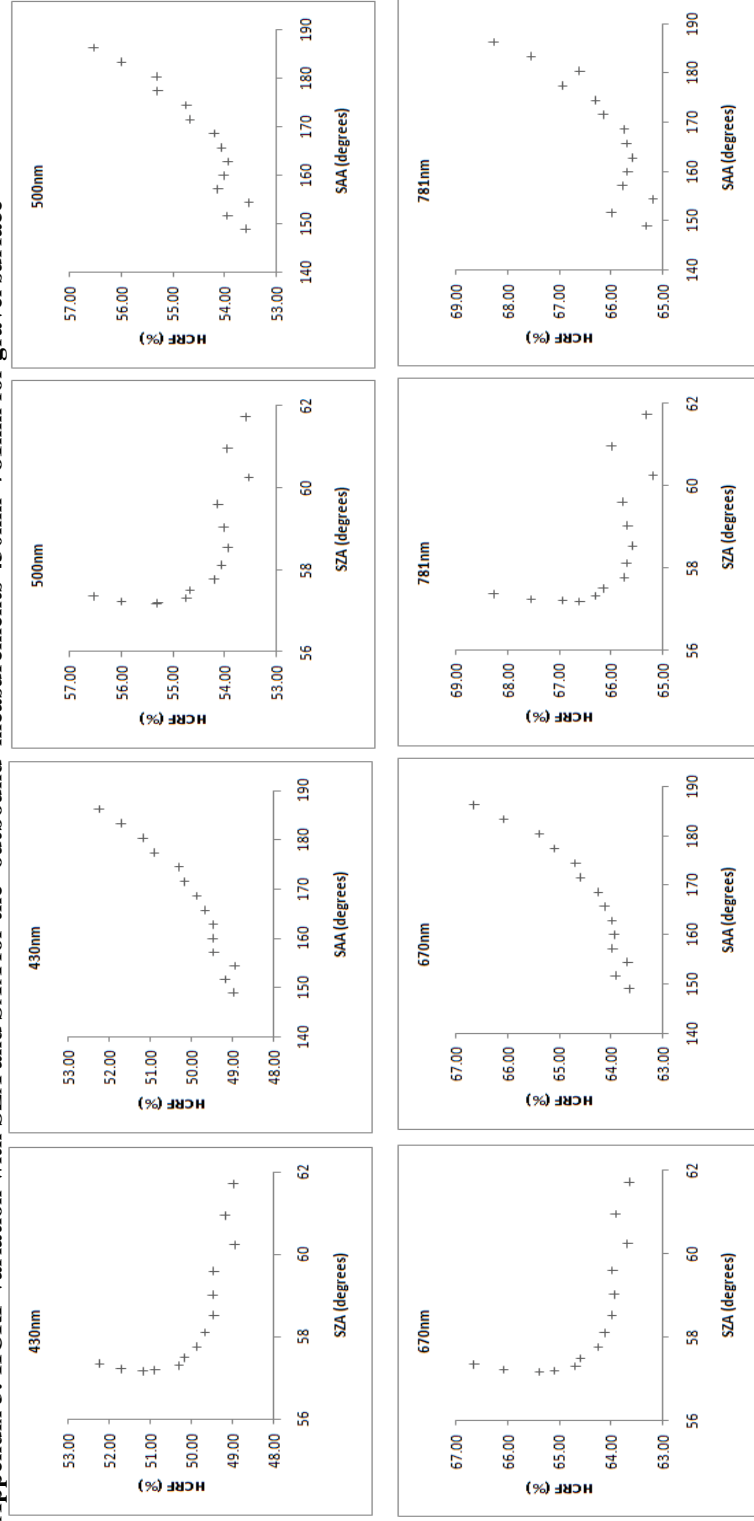
Appendix 1: HCRF variation with SZA and SAA for the ‘outbound’ measurements 430nm~781nm for sand surface



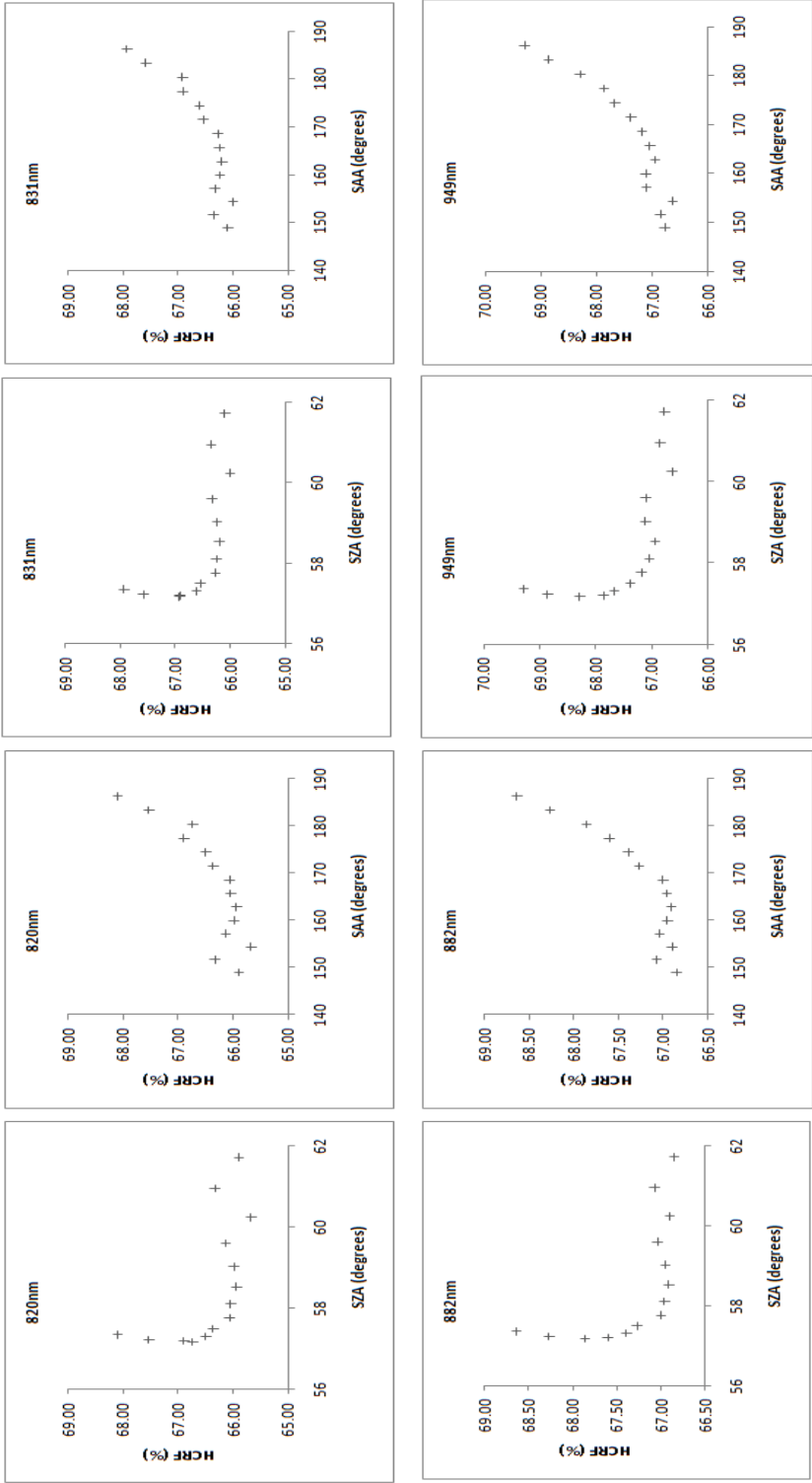
Appendix 2: HCRF variation with SZA and SAA for the ‘outbound’ measurements 820nm~949nm for sand surface



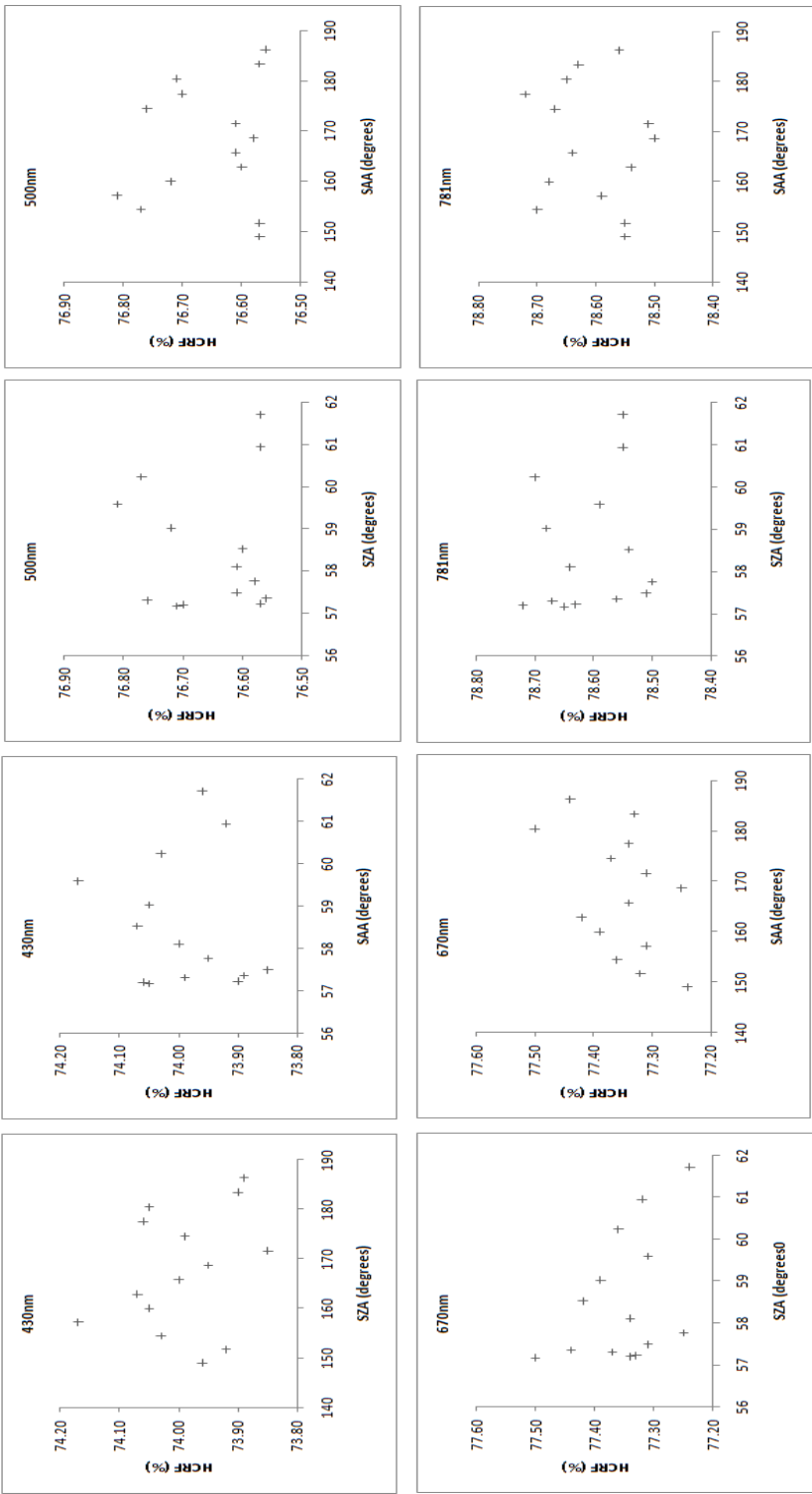
Appendix 3: HCRF variation with SZA and SAA for the ‘outbound’ measurements 430nm~781nm for gravel surface



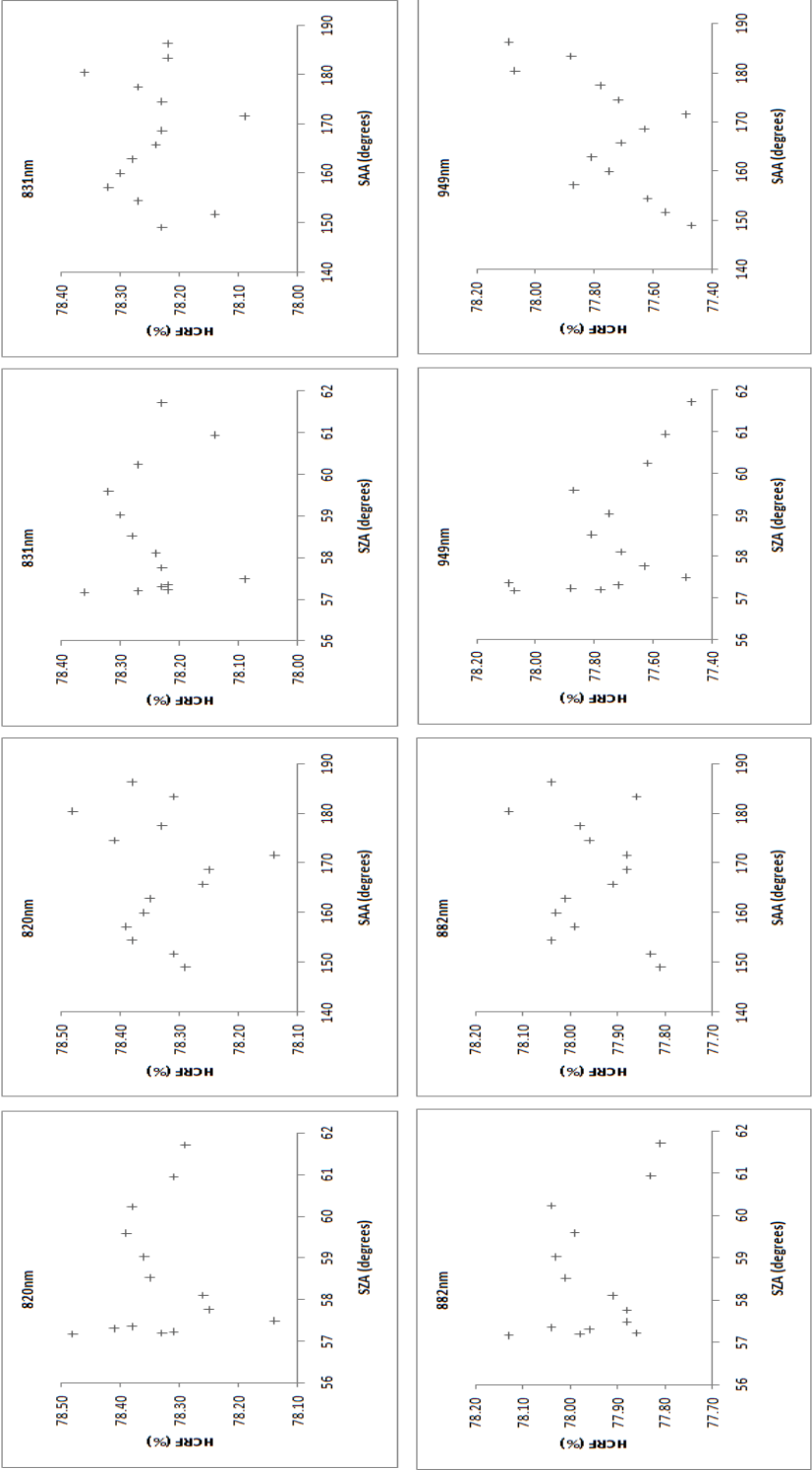
Appendix 4: HCRF variation with SZA and SAA for the ‘outbound’ measurements 820nm~949nm for gravel surface



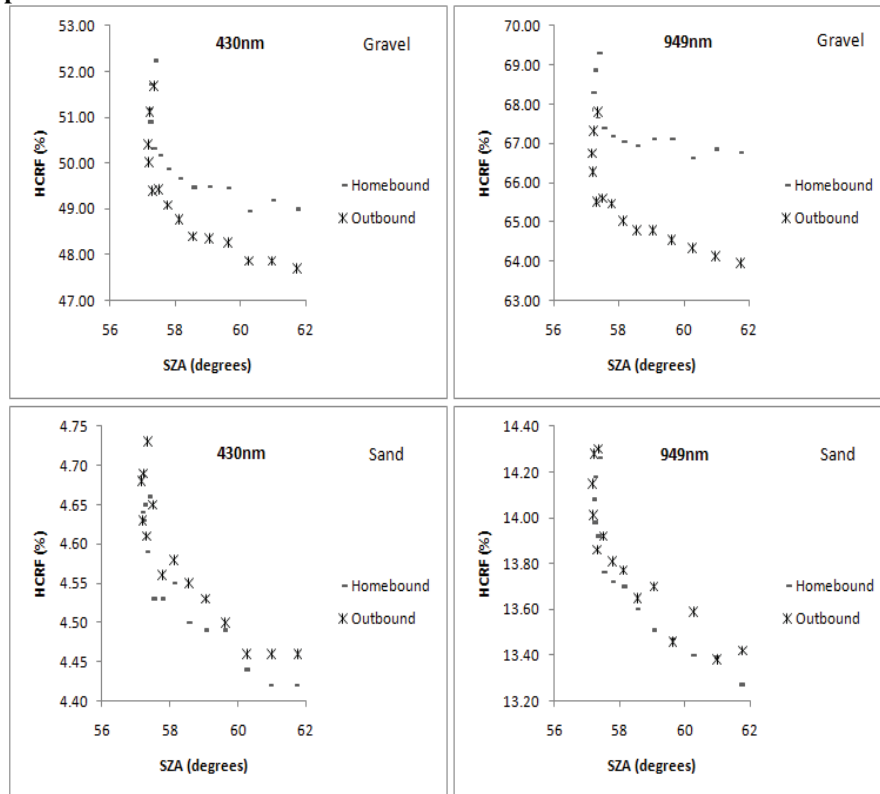
Appendix 5: HCRF variation with SZA and SAA for the ‘outbound’ measurements 430nm~781nm for the white tile surface



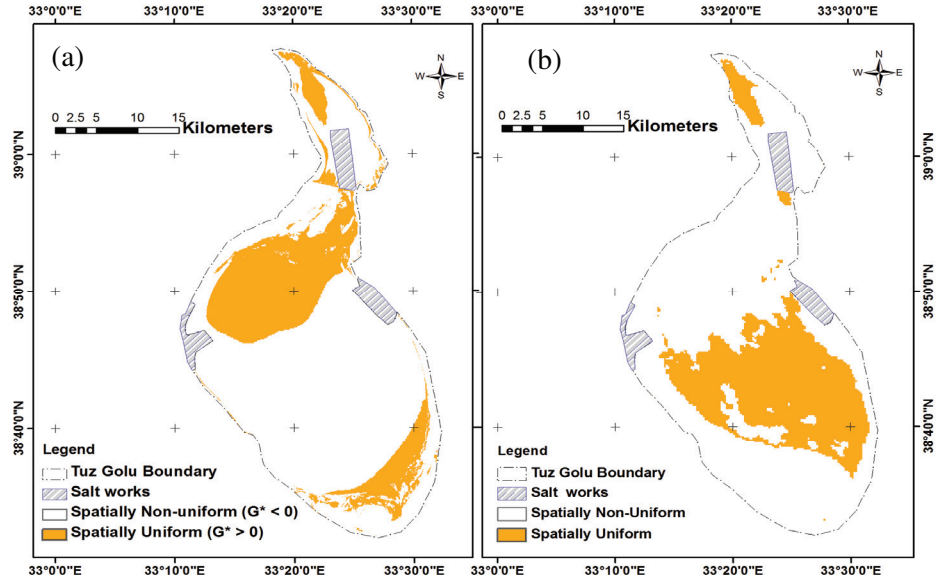
Appendix 6: HCRF variation with SZA and SAA for the ‘outbound’ measurements 820nm~949nm for the white tile surface



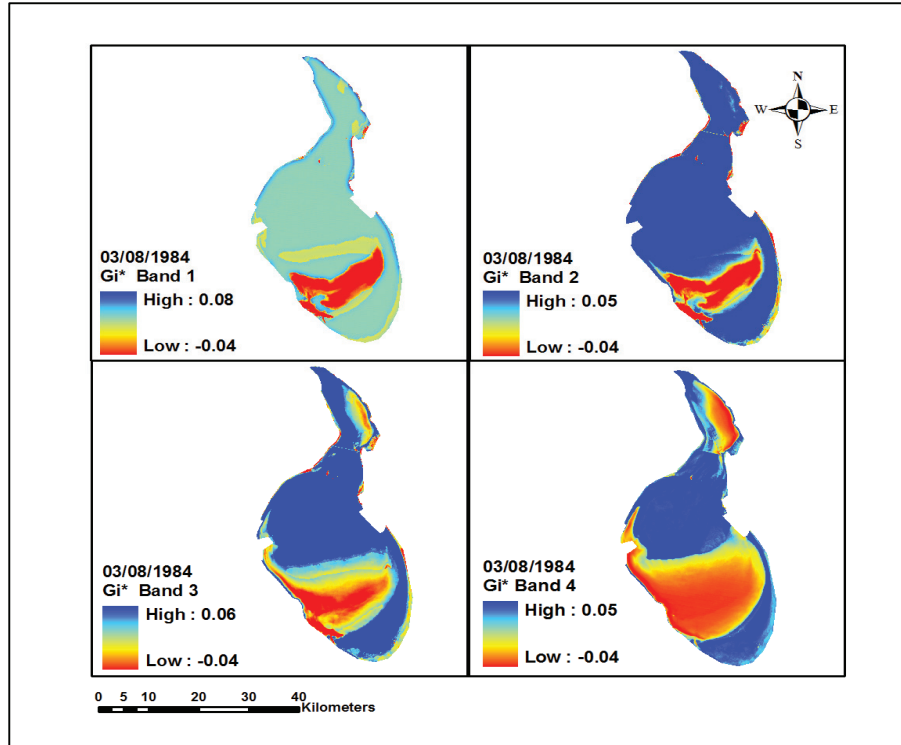
Appendix 7: ‘Outbound’ and ‘homebound’ HCRF measurement of the automated tramway spectro-radiometer. The difference in the two was due to positional drift of the instrument.



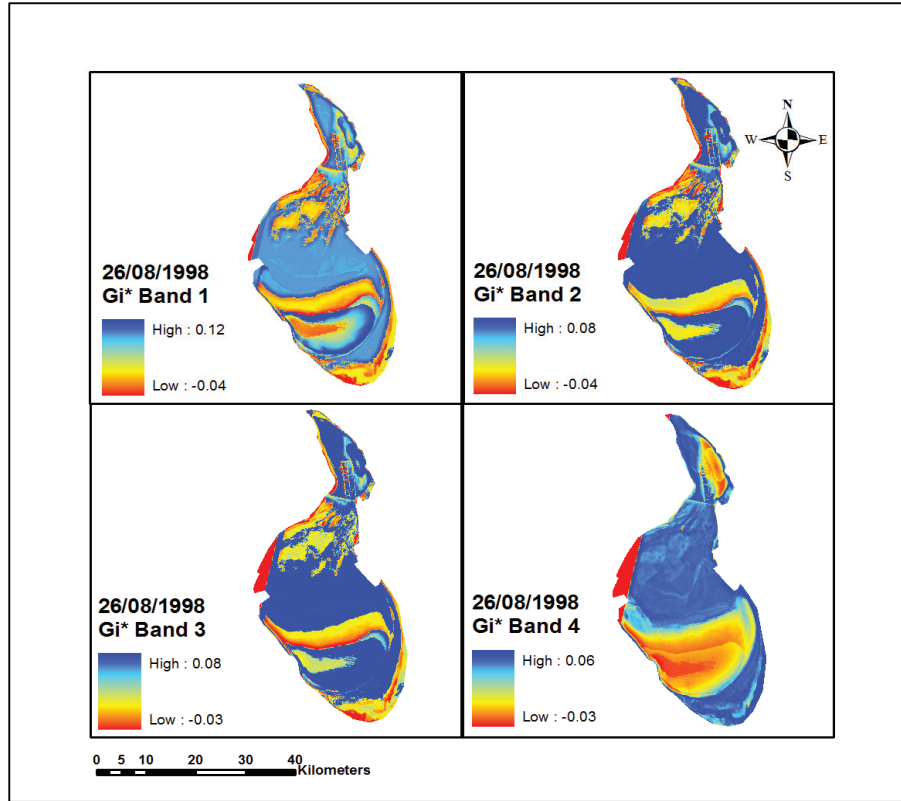
Appendix 8: (a) Spatial uniformity map of current study based on Landsat TM for the month of August for 1984, 1989 (2 images), 1998, 2000, 2003, 2006, 2009 (3 images) integrating bands 1, 2, 3, 4 (b) Spatial uniformity map of NPL based on MODIS (LPDAAC, 2007) satellite images of July and August (2004-2006) for using only red and near infra-red bands (adopted from Pegrum, 2008)



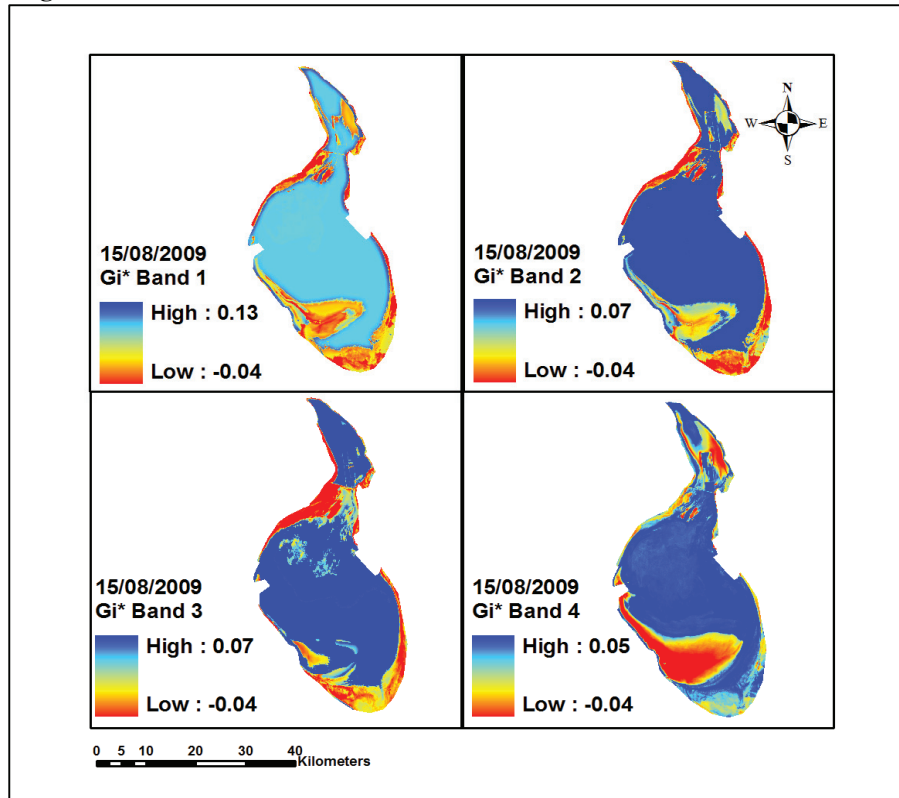
Appendix 9: Gi* index map of Tuz Gölü in bands 1, 2, 3 and 4 for the month of August 1984



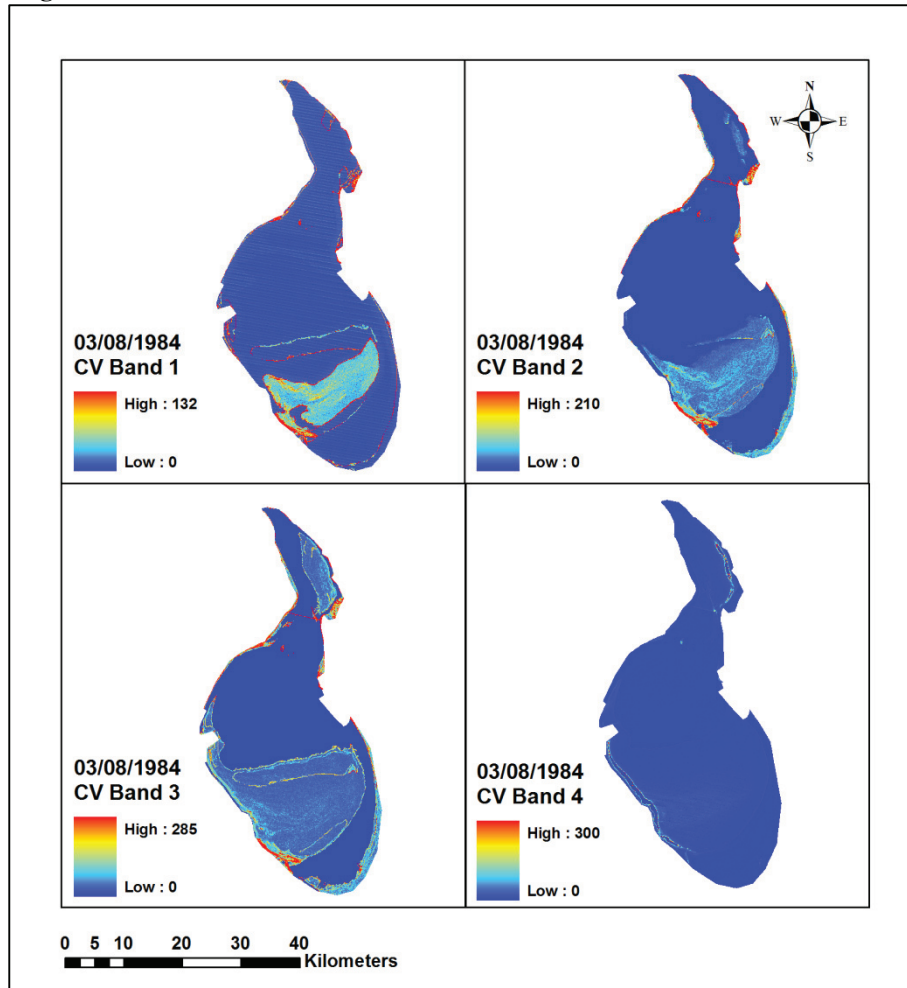
Appendix 10: Gi* index map of Tuz Gölü in bands 1, 2, 3 and 4 for the month of August 1998



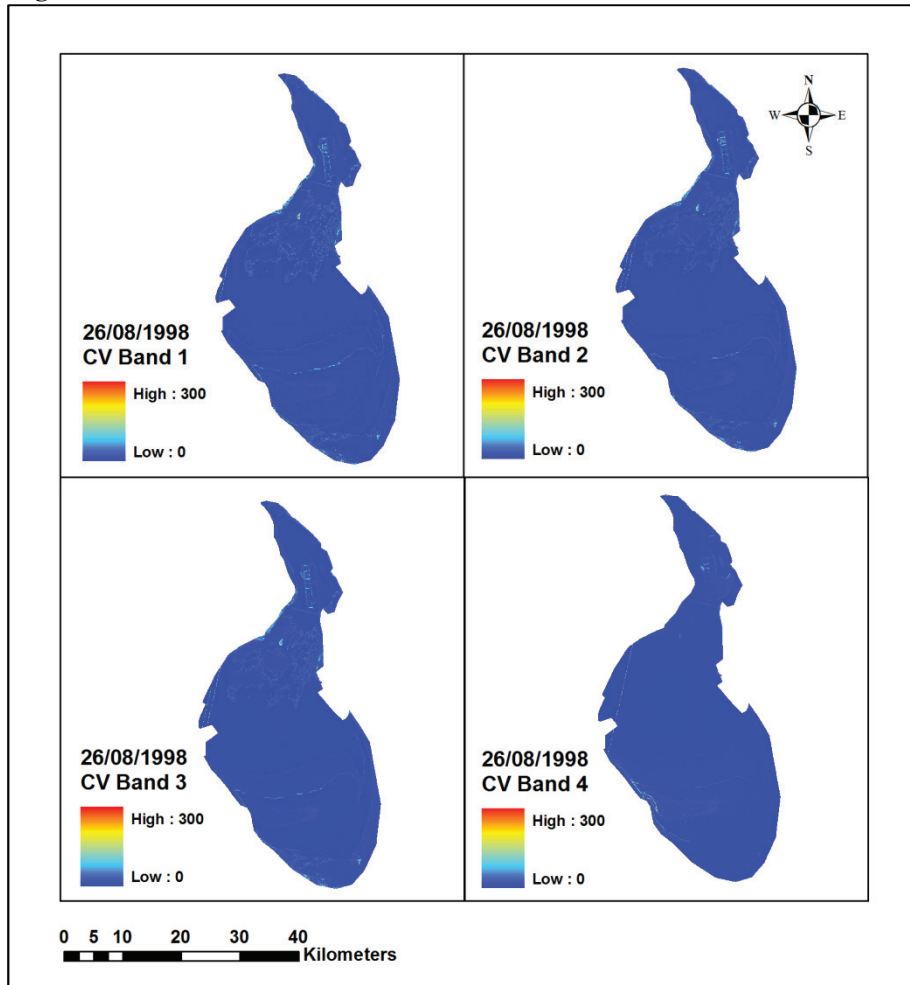
Appendix 11: Gi* index map of Tuz Gölü in bands 1, 2, 3 and 4 for the month of August 2009



Appendix 12: CV index map of Tuz Gölü in bands 1, 2, 3 and 4 for the month of August 1984



Appendix 13: CV index map of Tuz Gölü in bands 1, 2, 3 and 4 for the month of August 1998



Appendix 14: CV index map of Tuz Gölü in bands 1, 2, 3 and 4 for the month of August 2009

